To the Graduate Council:

I am submitting herewith a dissertation written by Kurt L. Nichol entitled "The Enhancement of Analytical Structural Models Including Consideration of Elastic Boundary Conditions". I have examined the final copy of this dissertation for form and content and recommend that it be accepted in partial fulfillment of the requirements for the degree of Doctor of Philosophy, with a major in Engineering Science and Mechanics.

R. Engels

Dr. Remi Engels, Major Professor

We have read this dissertation and recommend its acceptance:

John E. Caruthers

Dr. John Caruthers

Louis R. Deken

Dr. Louis Deken

Gary R. Flandro

Dr. Gary Flandro

Accepted for the Council:

Lew Winkel

Associate Vice Chancellor and
Dean of the Graduate School

The Enhancement of Analytical Structural Models Including Consideration of Elastic Boundary Conditions

A Dissertation

Presented for the

Doctor of Philosophy

Degree

The University of Tennessee, Knoxville

Kurt L. Nichol

December 1995

DEDICATION

This work is dedicated to the glory of God, His only Son, Jesus Christ, and the Holy Spirit, without whom, this work would be meaningless.

> ***"This is what the LORD says, He who made the earth, the LORD who formed it and established it--The LORD is His name: 'Call to me and I will answer you and tell you great and unsearchable things you do not know'."***
>
> Jeremiah 33:2-3 NIV

ACKNOWLEDGMENTS

I wish to thank all those who have been instrumental in the completion of this effort. First of all, I am grateful to my wife Linda who was steadfastly supportive, especially during the qualifying phase of the degree.. Thanks are also due to my parents, Karl and Joan Nichol and to my sister, Nancy, for their support. I would also like to express appreciation to Messrs. Jim Brown, Mark Anderson, Steve Carter, Ed Marquart, and Willy Wattenbarger of the MicroCraft Corporation for their support in conducting the experimental portion of this work and to Messrs. Terry Hayes and Tom Tibbals of Sverdrup Technology, Inc. for the use of the data processing and recording equipment also used during the experimental phase of this effort. Additionally, I would like to thank Mr. Tom Cromer for his assistance in the project management issues of this work and Mr. Woody Dorrell for his assistance with much of the computer programming needed to complete this effort. Special recognition is due my major professor, Dr. Remi Engels, for his continuous support, encouragement and representation on my behalf to the Graduate School. Additionally, his vision of an automated finite element-like model adjustment scheme led to the development of the perturbation finite elements presented in this dissertation. Finally, I wish to thank the United States Air Force and Sverdrup Technology, AEDC Group for their financial provision for the experimental and academic work and for awarding me the Resident Graduate Study Program which was extremely instrumental in completion of this degree.

ABSTRACT

Factors which produce differences between analytically computed modal characteristics, such as frequency and mode shape, and those derived experimentally are many. One area of significant uncertainty, both analytically and experimentally, are the physical boundary conditions between the component under consideration and the surrounding structure or test apparatus. This work was conducted to study the extent to which the elasticity of this interface can affect the modal characteristics of flat plates. Flat plates are studied as a first step in the understanding of boundary condition effects on the modal characteristics of compressor blade structures commonly found in gas turbine engines.

A new model adjustment scheme was developed, which uses *perturbation finite elements*, to compute adjustments at user specified locations of an analytical model to improve the agreement between analytical and experimental results. The scheme takes advantage of the users knowledge of where modeling uncertainties are highest, such as at the boundary, and computes adjustments to the model for only these locations. The technique not only permits changes in the elasticity of the boundary, but also permits the user to affect changes in stiffness at any specified location. Further, adjustments to the mass at specific locations are permitted to account for the mass of instrumentation, lead wires or distributions in mass density of the component itself.

The technique seeks to minimize the differences between analytical and experimental results within the constraints of the finite element formulation. Consequently, the agreement between analytical and experimental results are improved; the technique does not seek to match explicitly the experimental results. The reason for this is that experimental results typically have a measure of non-repeatability in them making "matching" of the data unrealistic. An example problem is presented for which intentionally introduced adjustments are correctly computed.

Analytical and experimental investigations of four flat plates with five different distributions of stiffness at the support in addition to the baseline were conducted to examine their effect on modal frequency, displacement and strain. Analytical results were computed using a commercially available finite element package and eight node,

isoparametric brick elements. Experimental accelerations and strains were measured on the plates as they were subjected to sinusoidal base excitation from a shaker table. Results were compared to quantify differences between analytical sensitivities to the various boundary stiffnesses and experimental sensitivities to the same boundary stiffnesses. The experimental method, data processing techniques, modeling techniques and other factors were evaluated to minimize potential for error. Elimination or reduction of these factors was then pursued so that the resulting experimental data and the analytical results were of the highest quality.

Results of the investigation showed that the modal characteristics of some modes of some plates were more sensitive to variations in boundary stiffness than others. This highlights the need for a model adjustment technique that can interrogate the boundary conditions to account for potential boundary stiffness influences. Further, significant differences between analytically computed sensitivities to boundary stiffness changes and those derived experimentally were present, although both sets of results identified the same plates and modes as having the highest sensitivities.

Adjustments to a representative analytical model using the newly developed *perturbation finite elements* were computed to investigate potential reasons for disagreements between analytical and experimental results. Adjustments to the stiffness of the elements at the boundary and the mass of elements at instrumentation locations were computed to determine if these could account for the observed differences. Up-front modeling of the instrumentation mass was not possible since precise measurement of the amount of mass added by the instrumentation adhesive as well as the mass of the instrumentation itself was not known. Computed adjustments were reasonable. Consequently, it was concluded that the observed differences between experimental and analytical results were attributable to the mass of the experimental instrumentation, and to difficulties with the experimental set-up at the boundary.

TABLE OF CONTENTS

	PAGE
1. INTRODUCTION	1
2. LITERATURE SURVEY	6
Turbine engine structural test and analysis history	6
Flat plate test and analysis work	8
Finite element error estimators	10
Modal testing error estimation	12
Combining finite element analysis and modal test data	13
3. CONCLUSIONS FROM THE LITERATURE SURVEY	15
4. OBJECTIVES OF THE PRESENT STUDY	17
5. DESCRIPTION OF EXPERIMENTAL AND ANALYTICAL DATA ACQUISITION	18
Description of the hardware	18
Experimental determination of plate modal characteristics	25
Experimental overview and set-up	25
Display and recording of experimental data	28
Post test data processing	29
Finite element analysis of the various plates	30
6. ANALYSIS OF RESULTS	37
Experimental results	37
Finite element analysis results	42
Comparison of experimental and analytical results	47
7. DYNAMIC FINITE ELEMENT MODEL IMPROVEMENT TECHNIQUE	50
Solution of the overdetermined system	53
Construction of **R**	54
Two dimensional axial bar perturbation finite element	58
Three dimensional eight node isoparametric perturbation finite element	59
Example application	63
Implementation using test data	63

8. CONCLUSIONS 77
9. RECOMMENDED FUTURE WORK 78
LIST OF REFERENCES 79
APPENDICES 92
APPENDIX 1 93
APPENDIX 2 100
APPENDIX 3 126
VITA 135

LIST OF TABLES

TABLE		PAGE
1.	Plate geometries	19
2.	Comparison of input material properties vs. solution	67
A1-1.	Tabulation of normalized displacement data	94
A1-2.	Tabulation of stress data	96

LIST OF FIGURES

FIGURE		PAGE
1.	Blade and disk attachment features	2
2.	Turbine engine disk schematic and nomenclature	3
3.	Effect of web axial position on disk radial displacement contours	5
4.	Experimental set up	20
5.	Test apparatus	21
6.	Boundary stiffness distributions	24
7.	Accelerometer locations	26
8.	Strain gage rosette locations	27
9.	Data filename code	29
10.	Effect of Hanning window on FFT	31
11.	Raw FFT output frequency vs. input frequency	32
12.	Raw FFT output amplitude vs. input frequency	32
13.	Parabolic interpolation on spectrum	33
14.	Output frequency with parabolic interpolation vs. input frequency	34
15.	Output FFT amplitude with parabolic interpolation vs. input frequency	34
16.	Example finite element model used in analyses	36
17.	Example of unexpected skewed node line	38
18.	Effect of constraint distribution on experimental displacements	40
19.	Effect of constraint distribution on experimental X-stress	41
20.	Experimental displacement data repeatability	43
21.	Experimental X-stress data repeatability	44
22.	Effect of constraint distribution on analytical displacements	45
23.	Effect of constraint distribution on analytical X-stress	46
24.	Difference between experimental and analytical displacements	48
25.	Difference between experimental and analytical X-stress	49
26.	Axial bar finite element model	55
27.	Assembly of **R**	58
28.	Two dimensional axial bar finite element	58

FIGURE PAGE

29. Adjustment technique demonstration model 64
30. Baseline mode shapes and frequencies 65
31. Perturbed mode shapes and frequencies 66
32. Model used with experimental data 69
33. Experimental Z-displacement contours 71
34. Baseline Z-displacement contours 72
35. Computed weight of instrumentation 73
36. Computed stiffness parameters of boundary constraint elements 74
37. Z-displacement contours of adjusted model 75
A2-1. Plate clamping 101
A2-2. 12 x 4 x 0.100 inch plate 102
A2-3. Strain gage rosette close up 103
A2-4. Second bending of 12.5 × 4 × 0.100 inch plate with stiffness distribution 1 104
A2-5. Second bending of 12.5 × 4 × 0.100 inch plate with stiffness distribution 2 105
A2-6. Second bending of 12.5 × 4 × 0.100 inch plate with stiffness distribution 3 106
A2-7. Second bending of 12.5 × 4 × 0.100 inch plate with stiffness distribution 4 107
A2-8. Second bending of 12.5 × 4 × 0.100 inch plate with stiffness distribution 5 108
A2-9. Second bending of 12.5 × 4 × 0.100 inch plate with stiffness distribution 6 109
A2-10. Third bending of 12.5 × 4 × 0.100 inch plate with stiffness distribution 1 110
A2-11. Third bending of 12.5 × 4 × 0.100 inch plate with stiffness distribution 2 111
A2-12. Third bending of 12.5 × 4 × 0.100 inch plate with stiffness distribution 3 112

FIGURE PAGE

A2-13. Third bending of 12.5 × 4 × 0.100 inch plate with stiffness distribution 4 113
A2-14. Third bending of 12.5 × 4 × 0.100 inch plate with stiffness distribution 5 114
A2-15. Third bending of 12.5 × 4 × 0.100 inch plate with stiffness distribution 6 115
A2-16. Second bending of 8.5 × 4 × 0.188 inch plate with stiffness distribution 1 116
A2-17. Second bending of 8.5 × 4 × 0.188 inch plate with stiffness distribution 2 117
A2-18. Second bending of 8.5 × 4 × 0.188 inch plate with stiffness distribution 3 118
A2-19. Second bending of 8.5 × 4 × 0.188 inch plate with stiffness distribution 4 119
A2-20. Second bending of 8.5 × 4 × 0.188 inch plate with stiffness distribution 5 120
A2-21. Third bending of 8.5 × 4 × 0.188 inch plate with stiffness distribution 1 121
A2-22. Third bending of 8.5 × 4 × 0.188 inch plate with stiffness distribution 2 122
A2-23. Third bending of 8.5 × 4 × 0.188 inch plate with stiffness distribution 3 123
A2-24. Third bending of 8.5 × 4 × 0.188 inch plate with stiffness distribution 4 124
A2-25. Third bending of 8.5 × 4 × 0.188 inch plate with stiffness distribution 5 125
A3-1. Analytical second bending mode shapes of 12.5 × 4 × 0.100 inch plate 127
A3-2. Analytical third bending mode shapes of 12.5 × 4 × 0.100 inch plate 128
A3-3. Analytical second bending mode shapes of 12.5 × 4 × 0.188 inch plate 129
A3-4. Analytical third bending mode shapes of 12.5 × 4 × 0.188 inch plate 130

FIGURE PAGE

A3-5. Analytical second bending mode shapes of 8.5 × 4 × 0.100 inch plate 131

A3-6. Analytical third bending mode shapes of 8.5 × 4 × 0.100 inch plate 132

A3-7. Analytical second bending mode shapes of 8.5 × 4 × 0.188 inch plate 133

A3-8. Analytical third bending mode shapes of 8.5 × 4 × 0.188 inch plate 134

1. INTRODUCTION

Designing structures to operate in a dynamic force environment presents many challenges to the structural dynamics engineer. Methods used to design, analyze and test these structures seek to produce a structure capable of operating in the dynamic environment without serious durability or performance deficiencies. Attempts are made to keep natural frequencies away from known excitation frequencies, provide adequate structural damping, and/or simply make the structure strong enough to withstand the dynamic forces. In order to facilitate analysis of a proposed design, assumptions are made about a host of variables, such as material properties, geometric tolerances, boundary conditions and the like. The degree of uncertainty in these variables differs and is generally unquantified. Upon making these assumptions, an analytical model is constructed to compute natural frequencies and mode shapes. However, uncertainties in the assumptions used to construct the analytical model can affect the accuracy of the computed frequencies and mode shapes. This could lead to an inadequate design.

Modal testing is often conducted to indirectly verify design assumptions used in the analysis by measuring the resulting modal characteristics. Test results are compared with analytical results to assess the adequacy of the analytical model. If results agree to within a predetermined amount, the analytical model is used for additional studies. If not, some enhancement is usually made to the analytical model so that it reflects the modal test data. Experimental results are infrequently questioned or assessed for accuracy.

In the case of the gas turbine engine, significant effort is aimed at insuring the structural dynamic capability of the blading. Gas turbine blades are generally cantilevered plate-like structures and are attached to rotating disks via a so-called "dovetail" attachment (Figure 1) which is designed to be loose when the engine is not operating to permit easy assembly and replacement. Blade retainers are used to insure that the blades remain in place. When the engine is operating, centrifugal loading forces the dovetail into radial contact with the mating structure on the disk. Because of this, the boundary condition at the interface of the blade and disk can change each time the engine is started or rotational speed is changed. Further, the geometry of the disk, Figure 2, and

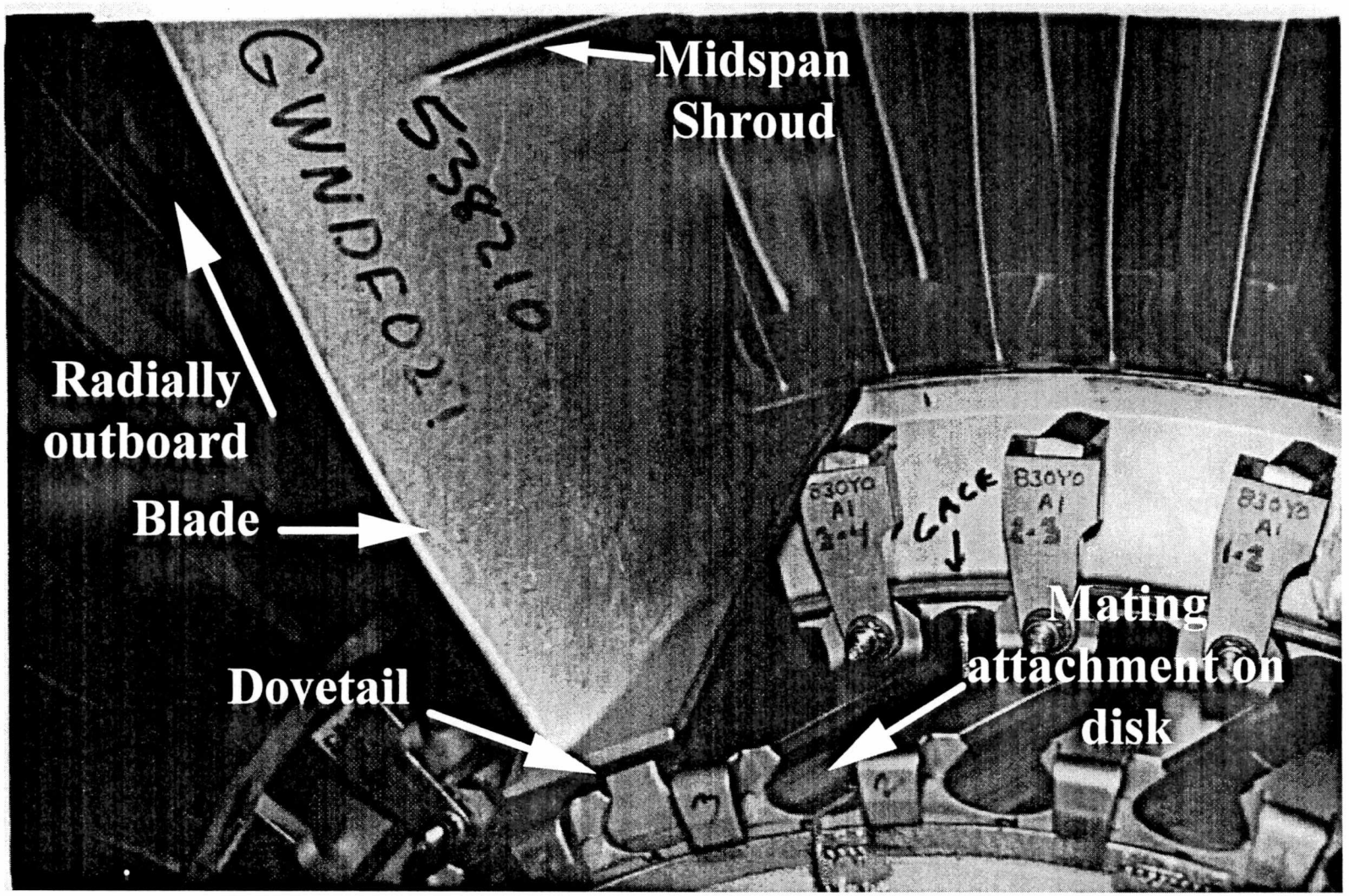


Figure 1. Blade and disk attachment features.

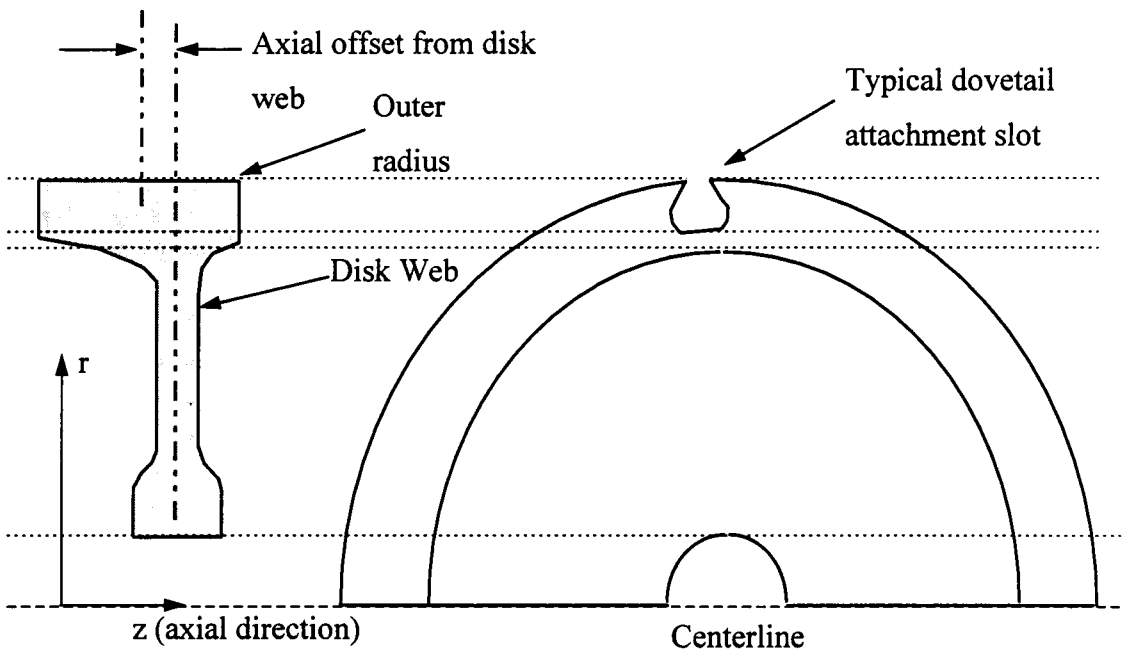


Figure 2. Turbine engine disk schematic and nomenclature.

blade can produce load distributions along the mating parts that can further complicate the boundary description in an analytical model. This effect is shown graphically in Figure 3. Contours in Figure 3 are of radial displacement. As shown, introduction of an axially offset web skews the contours and reveals the variation in stiffness along the attachment. An additional complication present in gas turbine blading is shown in Figure 1 and is identified as the "mid-span shroud". This feature is an interblade friction damping device which introduces an additional boundary condition that is mode shape dependent. All of these features complicate the analytical modeling of the blades and introduce non-repeatability in the experimental modal data. Determining the adequacy of the analytical model by comparing analytical results to experimental results can, therefore, be quite difficult. Consequently, a technique that interrogates the boundary conditions when assessing the commonality between analytical and experimental results would be quite useful.

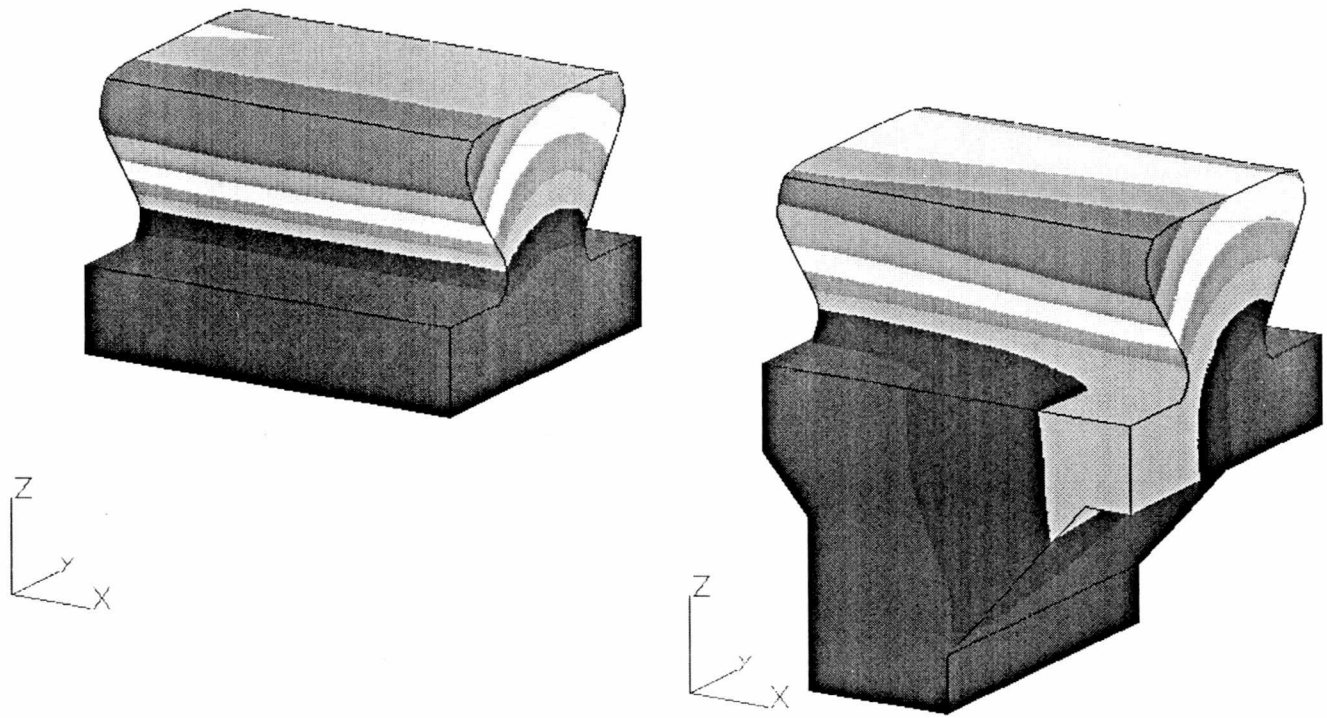


Figure 3. Effect of web axial position on disk radial displacement contours.

2. LITERATURE SURVEY

A survey of the open literature was conducted to review work done in areas pertaining to structural dynamics and, more specifically, to structural dynamics of gas turbine blading. The goal of the survey was primarily to establish the state of the art in finite element model adjustment techniques based on experimental data. Further, since application will ultimately be made to gas turbine blade-type structures, a survey of relevant work in that area was warranted as well. Areas reviewed were:

1) Turbine engine structural test and analysis history
2) Flat plate test and analysis history
3) Finite element error estimation
4) Modal testing error estimation
5) Model adjustment using modal test data.

Detailed results of the literature survey for each of these areas follows. Conclusions pertaining to the literature survey are presented and used as a basis for establishing the present work.

Turbine engine structural test and analysis history

By virtue of the fact that the gas turbine engine is composed of a series of rotating blades in close proximity to rows of non-rotating blades, there exists potential for vibration. As rotating blades pass through the aerodynamic wake of upstream blades, regular disturbances in the flow field produce a periodic forcing function. Also, bow waves from downstream rows of blades can likewise create regular impulses. Consequently, the frequency of excitation is linearly related to the rotational speed of the rotor and the number of up and downstream blades. The gas turbine engine has many other sources of excitation, as well. As the benefits of the turbine engine became increasingly popular to aircraft designers, more effort was devoted to uncovering some of

these sources of excitation [1-4]* . These efforts were experimentally based because analytical tools to evaluate complex geometries and flow fields were lacking. Because of the relatively small size of the blades and the relatively harsh environment, test engineers relied heavily on strain gage measurements to acquire the needed data. Experimental methods were developed, as needed, along with experimental hardware, particularly with respect to the strain gage [5-16].

Early analytical efforts relied on simple beam theory for computation of blade frequencies and modes [17-20]. These techniques were limited, however, since compressor blading became more plate-like with each new design. Analysis efforts were greatly enhanced in the early 1960's with the introduction of the finite element method. Application of the method to plates was begun in the late 1960's [21] and early 1970's [22]. With the method, data could be generated at any number of generalized coordinates. The only limitations were the computing capability of the computer and memory requirements. Nearly all dynamic evaluations since have utilized the finite element method. Combining finite element data and experimental data was proposed as early as 1977 [23].

Other analytical methods have been, and continue to be used for evaluation of relatively simple flat plates. Among these are the Rayleigh Ritz method [24-25] and the boundary integral method [26]. The advantage of these methods is that they do not depend on discretization of the structure, as the finite element method does, and therefore produce continuous results for all points on the structure. A disadvantage is that the related equations quickly become impractical to solve as geometric complexities increase. A more in-depth presentation of the historical aspects of experimental and analytical methods for turbine engines can be found in [27].

---

* Numbers in brackets refer to listed references in the bibliography.

Flat plate test and analysis work

Because of the complexities involved with working on actual gas turbine blading and the significant variability among designs, much of the basic research work in gas turbine blading is conducted on various types of plates and beams. A review of historical work in this area was, therefore, in order.

One of the earlier efforts in the literature by Dalley and Ripperger [28] sought to develop accurate ways to determine the resonant frequency of flat rectangular and skew rectangular plates. They found that variations of up to 5% in frequency were encountered between reassemblies of the same hardware. This was attributed to differences in bolt torque on the plate clamping fixture; an obvious boundary condition variability. This was not investigated as a test variable, however. Instead, a bolt torque specification above that which produced repeatable results was specified. Reports of difficulty with the boundary are common occurrences in most all of the experimental literature reviewed.

Dalley and Ripperger determined the mode shapes for their plates by sprinkling soap powder on the plates while they were vibrating in resonance. The soap powder "heaped-up" at the plate node lines thereby identifying the mode. This technique is only useful for flat plates.

At about the same time, Grinsted [29] was conducting experiments to study the relationships between modal frequencies and mode shapes. His premise was that complex, high frequency modes observed on impeller blades must be of the same character as lower order modes. He concluded that there existed a relationship between families of modes (with varying numbers of node lines) and the modal frequency. Further, the engineer could use this information to determine the mode shape of a frequency of interest as a combination of regular nodal patterns. These experiments were conducted on a variety of plate geometries and were also conducted on a turbine blade and an impeller blade. This work was virtually repeated in 1988 using slightly more sophisticated techniques by Chapman and Wang [30].

In the late 1960's Leissa [31], under a NASA grant, conducted an comprehensive literature search which documented significant work done on various types of plates. The

great majority of the work reported in the document includes both analytical and experimental results. All combinations of classical edge constraints are included as well as constant elastic, discontinuous and point supports. No work was found in the open literature with respect to distributed elastic supports. This seems unusual since many of the experimental accounts cite proper simulation of desired boundary conditions as a difficulty. The only work found that considered the elasticity of the support outside of that reported in [31] was that of O'Donnell [32] and MacBain and Genin [33]. Each of these papers considers only two dimensional beams and both showed that the effect could be significant.

Point masses are also considered in the formulations for natural frequencies and modes in Leissa's work [31]. Additional work on the effect of point masses on plate vibration has been done as late as 1993 by Boày [25] in the design of circuit boards.

In the mid 1980's an effort was initiated to document differences in analysis procedures and to compare analytical and experimental results for twisted cantilevered plates [34-37]. The effort was a joint government/industry/university study. It highlighted the variability that can occur between different analysis methods and even within the same method, including finite elements. Analysis results were compared to experimental data that was generated under carefully controlled conditions. Mode shapes and resonant frequencies were identified using holography techniques [36]. Comparisons between analytical and experimental mode shapes were based on general similarity, however, and not by precise comparison of displacement data.

One area which is noticeably lacking in the literature is a controlled study comparing analytical and experimental strain distributions in vibrating plates. The only effort dedicated to this found in the literature was work done by Lyle, Leatherwood and Daniels [24]. Their work studied the strain distributions in flat isotropic plates and compared experimental results to analytical results generated using the Ritz method. The equations of motion were solved, using experimentally inferred values of damping, to determine the strain distributions. Differences between analytical and experimental results were as high as twenty percent and were attributed to "uncertainties in the experimentally determined damping values and the inability to obtain ideal clamped

boundary conditions." It is interesting that more basic research has not been documented that considers strain distributions, particularly in light of the fact that numerous examples of the use of strain gages for stress determination on gas turbine blades can be found ([38-45] for example).

Finite element error estimators

One of the greatest drawbacks of the finite element method (FEM) is a direct consequence of the concept that makes it so powerful; discretization of a continuous structure. Obviously, as more and more elements are used, the solution will approach that of the continuous structure. This is accompanied by an increase in computing cost, however. The question of element density is highly subjective since it depends on the desired fidelity of the results and the computing power available. Articles have appeared in various engineering magazines [46-48] in recent years which have attempted to point out some of the limitations and assumptions involved with the FEM. These do not provide in-depth methodologies to maximize results.

When attempting to assess how much "error" there is in a given finite element analysis there is a need for a benchmark to determine what the correct answer is. Ideally, this benchmark would be the "real" answer associated with the continuous structure. This implies that "errors" in the finite element analysis arise from the discretization process. One of the most commonly referenced and earliest efforts to assess the quality of the finite element mesh was done by Zienkiewicz and Zhu [49]. Their work is based on computation of an energy norm and requires that the value of this norm be less than a user specified value. Output from the process, highlights elements in the mesh exceeding the prescribed error value. The user must then refine the mesh in the highlighted area manually or through some adaptive meshing process. This method does not compare discretized results to the continuous results, but instead compares them to a "smoothed" approximation of the discretized results. Consequently, the method has received some criticism. Similar results for a given mesh were generated using a finite difference

method by Dow, et al , [50] which, they said, independently validated the Zienkiewicz-Zhu method.

The methods outlined in references [49] and [50] are both for use with static solutions and rely on the computation of stresses from finite element (or finite difference) derived displacements. Neither is directly concerned with dynamic analysis although extension could be easily made. One technique applicable to dynamic analysis was presented by Cook [51] which attempts to estimate errors in the computation of the eigenvalues during dynamic analysis. Cook's premise was that eigenvalues computed with a lumped mass matrix tend to converge to the actual values from below and that consistent mass matrices tend to produce eigenvalues which converge to the actual values from above. The method proposes to solve the eigenvalue problem using either of these two mass matrix types in the standard fashion. Eigenvalues are then estimated using the Rayleigh quotient and the other, not used, type of mass matrix. This will theoretically bound the real eigenvalues and provide a measure of the error in the finite element formulation. It does not, however, provide a means of identifying where the mesh is deficient.

Realizing that the best way to determine deficiencies in a discretized solution is by comparison to the real, continuous solution, a novel approach has been developed called recontinuization. This approach utilizes finite element output along with the equations of equilibrium and continuity to derive a continuous solution that replaces the descretized solution. The form of the recontinuization is a differentiable, double Fourier sine series describing the displacements. Strains are easily computed by differentiating displacement results. Recontinuized results are compared to finite element results to establish the error measure. This technique has shown remarkable results when applied to plate elements [52-56]. No work on other element types was found in the literature.

Each of the techniques presented above consider errors introduced by the discretization process. However, inaccurate representations of continuous structures can also result from statistically variable parameters of the object being analyzed, such as geometric variations, variations in material properties, etc. To address these types of "inaccuracies", eigensensitivity analysis has been proposed. These procedures seek to

compute the rates of change in eigenvalues and eigenvectors with respect to changes in design variables; so-called *eigenderivatives*, or *eigensensitivities*. Large eigensensitivities would indicate which aspects of the analytical model would have potential for error. Much significant work has been published on this subject, most recently by Lin, Du and Ong [57]. An obvious benefit from the approach is that specific parameters, such as beam cross section or moment of inertia, which produce significant variations in vibratory characteristics of the structure are identified. This gives physical relevance to any modifications made in the analytical model. Most of the techniques are complex, iterative and computationally intensive, however. An overview of other related work is provided by Ibrahim [58]. Other, perhaps more fundamental, work on the subject is found in [59-61]. This approach is also used for identifying parameters in a finite element model that could be changed to bring about agreement between experimental and analytical data.

Modal testing error estimation

Most (if not all) literature which seeks to compare analytical and experimental results make an assumption that the experimental data is "correct", e.g., devoid of errors or variability, and then proceed to adjust the analytical model to bring about agreement. Simply by virtue of the fact that statistical methods have been used for years, [62-64] for example, tends to bring this assumption into question. All experimentally generated data is simply not completely repeatable. Similarly, much effort has been expended in the writing of many books on experimental modal testing all of which seek to produce the "best" data possible [65-68]. Obviously, if an experiment is conducted under the highest measure of control possible, the data will be correspondingly free from errors (variability). Unfortunately, to a large extent, the quality of the data is unquantifiable. Experimentation is still largely an art.

There was not much material found in the literature that dealt with ways to quantify experimental errors *a posteriori*. Some relevant work has been done by Adibi in the power industries [69-70] which rely on measurement redundancies to construct

functions relating the measurements to their attending errors. The functions are then minimized to yield corrective coefficients. Work done by Gutenberger [71] and Soucy and Deering [72] sought to define the extent to which experimental errors were related to experimental technique. No means of correcting results are proposed; only cautions. Fessler [73] simply expressed the importance of conscientious experimental methods based on experience (art). Nichol [74] introduced a technique to account for and correct variability in strain data resulting from strain gage mislocation and misorientation.

Most commercially available transducers, data conditioning systems, recorders and display systems list data uncertainties as part of the component specification. Uncertainties induced in a given data system could then, in theory, be accounted for.

Combining finite element analysis and modal test data

The last area of significance in the literature survey was that of combining analytical and experimental data. As stated earlier, in most of the literature on the subject, it was assumed, *a priori*, that the experimental data was devoid of errors. Under this premise, the goal of all the techniques was to *minimally* modify an existing, "reasonably" accurate analytical model so that it duplicated experimental results at measurement locations. All of the experimental data used for this purpose and described in the literature was accelerometer data.

In a technique described by Wei [75], the objective was to simultaneously modify existing analytical stiffness and mass matrices so that they will reproduce the experimental data. The technique uses Lagrangian multipliers. Constraints are the basic eigenvalue problem statement, orthogonality condition, and matrix symmetries. The paper represents a conclusion of much other work done with this technique [76-83]. The technique can also be used when the damping matrix is included in the problem formulation [84]. Minimization of the Lagrangian function is done with respect to each individual element in the mass and stiffness matrix. Minimization does not consider parameters used in the construction of the elements of the matrices. The process is non-iterative and computationally straightforward. However, changes must be "small".

Another approach by Tong, et al, [85] utilizes the damping matrix to establish so-called "correct correspondence" between analytical and experimental modes. Their process operates iteratively and seeks to minimize a cost, or error function which describes the differences between analytical and experimental eigenvalues and eigenvectors. Errors in test data can be accounted for by the introduction of error scaling factors in the formulation of the error function. These values are arbitrarily selected, however, and can affect the number of iterations required for convergence.

Glaser, et al, [86] isolate "errors" in the analytical model of a space structure by testing the structure with variations on the supporting boundary conditions. The approach is termed MBCT or Multiple Boundary Condition Testing. An error function is formulated using the eigenvalues and eigenvectors which are normalized to make the function dimensionless. The normalization constants are arbitrarily chosen as with Tong, et al, and can be used to account for experimental data errors. The error function consists of the sum of the squares of the individual differences between test results and analytical results. This is expanded in the form of a truncated Taylor series, giving rise to sensitivity coefficients, $\frac{\partial f}{\partial k}, \frac{\partial f}{\partial m}, \frac{\partial \varphi}{\partial k}, \frac{\partial \varphi}{\partial m}$, where f refers to frequency, k and m are stiffness and mass matrix elements, and φ refers to eigenvector elements. These are minimized in a least squares sense. The authors point out that this is really a nonlinear generalized least squares problem since the error function is composed of elements of differing units (hence the need for normalization). A covariance matrix is constructed which is used to solve the generalized nonlinear least squares problem. Construction of the covariance matrix is generally required at each iteration and must, according to the authors, be inverted to obtain the solution at each iteration. This is computationally intensive. Various options are presented which can ease some of the computational effort but, the authors have themselves expressed that the technique may not be practical in "real" situations.

3. CONCLUSIONS FROM THE LITERATURE SURVEY

Turbine engine testing will continue to be an area of emphasis since analytical tools, although advancing, are still inadequate for complete evaluation of actual systems. Many of the fundamental questions related to the vibratory behavior of gas turbine blading are still being addressed by laboratory testing of flat and twisted plates. Most of this work, however, is focused on accurate prediction of frequencies and similarity of mode shapes. Few efforts were documented which sought to rigorously match up actual displacement data. Additionally, little experimental work has been done to investigate strain distributions in vibrating flat plates or airfoil structures. Work that has been done is in poor agreement with predicted strain distributions [24] and highlights a potential for error in testing of more complex geometries.

All of the literature with respect to plate testing clearly identified nonrepeatability of boundary conditions as a source of nonrepeatability in frequency results. No experimental investigations were found, however, that studied the effect of boundary stiffness distributions on resonant frequencies, mode shapes or strain distributions. This is potentially a source of variability in frequencies and strain measurements in gas turbine engine testing since blade attachments can produce variations in boundary conditions. The issue of blade-to-blade variations are discussed in the literature ([40] for example) which indicate that rotor response can be affected by the circumferential position of a given set of blades in a disk.

Improvements in computer technology have made the finite element method available to nearly every engineer. Because of this, model fidelity can be addressed by simple "brute force" trial and error. However, in situations where one is provided an analytical model for follow-on use, it is important to have methodologies for evaluating model fidelity. Error estimators such as that of Zienkiewicz and Zhu [49] and Dow, et al, [50] are useful for this purpose. Each of these methods require substantial computation since they both manipulate the finite element output files, but each effectively highlight locations where mesh is inadequate.

Recontinuization of finite element results is interesting, especially since it addresses the fundamental requirements of equilibrium and continuity. Additionally, it "corrects" many of the extrapolation-to-surface (nodes) problems associated with the finite element method. The resulting differentiable displacement functions can be used to generate strains at any point on or in the structure. They can also be used to generate visualizations of the component displacements, strains, and stresses without having to manipulate large finite element output files.

The test enhanced model improvement techniques which seek to find the minimum changes to a given analytical mass and stiffness matrix are advantageous from a computational standpoint since they are non-iterative. However, they do not attempt to insure that any of the modifications make physical sense. Additionally, they are restricted by assumptions that the changes need to be "small". They also produce changes in the mass and stiffness matrices which may destroy the consistency of the matrices, i.e., the distributions of stiffness and mass within a particular element may no longer be consistent with the original element formulation.

Test enhanced model improvement techniques based on eigensensitivies, such as that of Lin, Du, and Ong [57], are advantageous since they attempt to find changes that make physical sense. These methods are iterative and tend to be complex and computationally intensive. Additional research is needed to find ways to reduce the computational effort required. Also, many of them use a truncated Taylor series in the formulation which requires that the changes are "small".

None of the methods for enhancing analytical models based on test used strain data for the enhancements. This is interesting since strain gages are used almost exclusively in gas turbine blading tests. Additionally, only one case was found which formally used analytical data and test data to derive fatigue information [23]. Finally, while some of the methods used to derive test enhanced analytical models determined sensitivities of responses to design variables, none of the techniques considered the variabilities in response resulting from environmentally induced differences in design variables such as thermally induced variations in Young's Modulus.

4. OBJECTIVES OF THE PRESENT STUDY

While many areas of potential research were highlighted in the literature survey, the present study sought to determine the effect of elastic boundary conditions on modal frequencies, mode shapes and strain distributions of vibrating plates. Specifically the research included the following:

- Experimental investigation of elastic boundary conditions of cantilevered flat plates.
- Analytical investigation of elastic boundary conditions of cantilevered flat plates.
- Comparison of experimental boundary stiffness distribution results.
- Comparison of analytical boundary stiffness distribution results.
- Comparison of results from the experimental and analytical investigations.
- Demonstration of adjustment of finite element model mass and stiffness matrices using experimental data.

Completion of these areas of research were to lead to understanding of the relative importance of the stiffness of the surrounding structure in experimental and analytical determination of the modal characteristics of plate-like structures. Assuming this to be significant, the research would then go on to develop a technique by which adjustments could be made that would improve agreement between experimental and analytical results. The technique should have the capability to "focus" adjustments to regions of the model where uncertainties were greatest and to either mass or stiffness parameters or both. Further, the adjustments should make physical sense and should produce mass and stiffness matrices consistent with the structure of the original finite element matrices.

5. DESCRIPTION OF EXPERIMENTAL AND ANALYTICAL DATA ACQUISITION

Description of the hardware

The choice of hardware to use for this investigation was selected with several considerations in mind. First, it was decided that cantilevered plates would be the type of structure to be examined. This was due primarily to the fact that results from the investigation would be applied to gas turbine blading, which are fundamentally cantilevered plate-like structures. Also, since limited resources were available to generate the experimental data, flat plates were selected so that mode shapes could be identified using the "soap powder" technique [28] thereby avoiding costly holography type methods. The soap powder technique could not be used with twisted or cambered airfoil structures since the powder would simply vibrate off the test article.

The geometric configuration of the plates were defined so that each plate had two to three fundamental bending modes below 3000 Hz which was the maximum frequency attainable with the shaker table that was available for the experimental portion of the investigation. Additionally, the shaker table had a force limitation which set the maximum weight for the test article below five pounds, including mounting hardware. This limitation drove selection of the plate material. Finally, four plate geometries were selected to provide an overview of geometrical effects on plate strain and displacement distributions. The plate geometries (of the cantilevered portions of the plates) are listed in Table 1. The plates were constructed from 0.100 inch and 0.188 inch, 6061-T6 aluminum plate stock. No specific surface finish was specified.

The control variable of the experimental portion of the investigation was the stiffness distribution along the width, or chord, of the plate, so a means of controlling the stiffness distribution was required. The approach taken was to fabricate 1/4 inch cubic blocks of three different materials, and consequently with differing Young's modulii, and to use these to clamp the plate to the mounting structure at the cantilevered interface.

Table 1. Plate Geometries

Plate Number	Nominal Cantilevered Length (inches)	Nominal Plate Width (inches)	Nominal Plate Thickness (inches)
1	12.50	4.0	0.188
2	12.50	4.0	0.100
3	8.50	4.0	0.188
4	8.50	4.0	0.100

Mild steel, copper and aluminum were selected as materials for the support blocks. A steel clamping fixture was fabricated to contain the blocks and to secure the assembly to the shaker table. The experimental set up is shown in Figure 4 to illustrate the concept. As shown in Figure 4, the plate was held in a "diving board" fashion between two supports; one at the aft end of the plate and the other at the cantilevered interface. The aft support blocks were single bars of 1/4 inch-square mild steel bar stock. Additionally, the cantilevered interface baseline configuration also used two 1/4 inch-square mild steel bars. Stiffness variations along the chord were then introduced by taking combinations of the various blocks at the cantilevered interface. Since the plate was nominally four inches wide, sixteen blocks were required along the top and bottom of the plate (32 total) to secure the plate at the interface. The design drawings are provided in Figure 5 for completeness in documentation.

Selection of the stiffness distributions was based loosely on potential axial stiffness distributions of compressor disks as described earlier (cf. Figures 2 and 3). Five stiffness distributions and a baseline were selected for investigation. Since each of the 1/4 inch cubes had the same geometry and differed only by Young's modulus, the stiffness of each cube was directly related to Young's modulus. Plots of Young's modulus vs. chord position are shown in Figure 6 to illustrate the variations examined. No attempt was made to reproduce actual stiffnesses of disk attachments. The goal was simply to produce chordwise stiffness distributions which were of a realistic order of

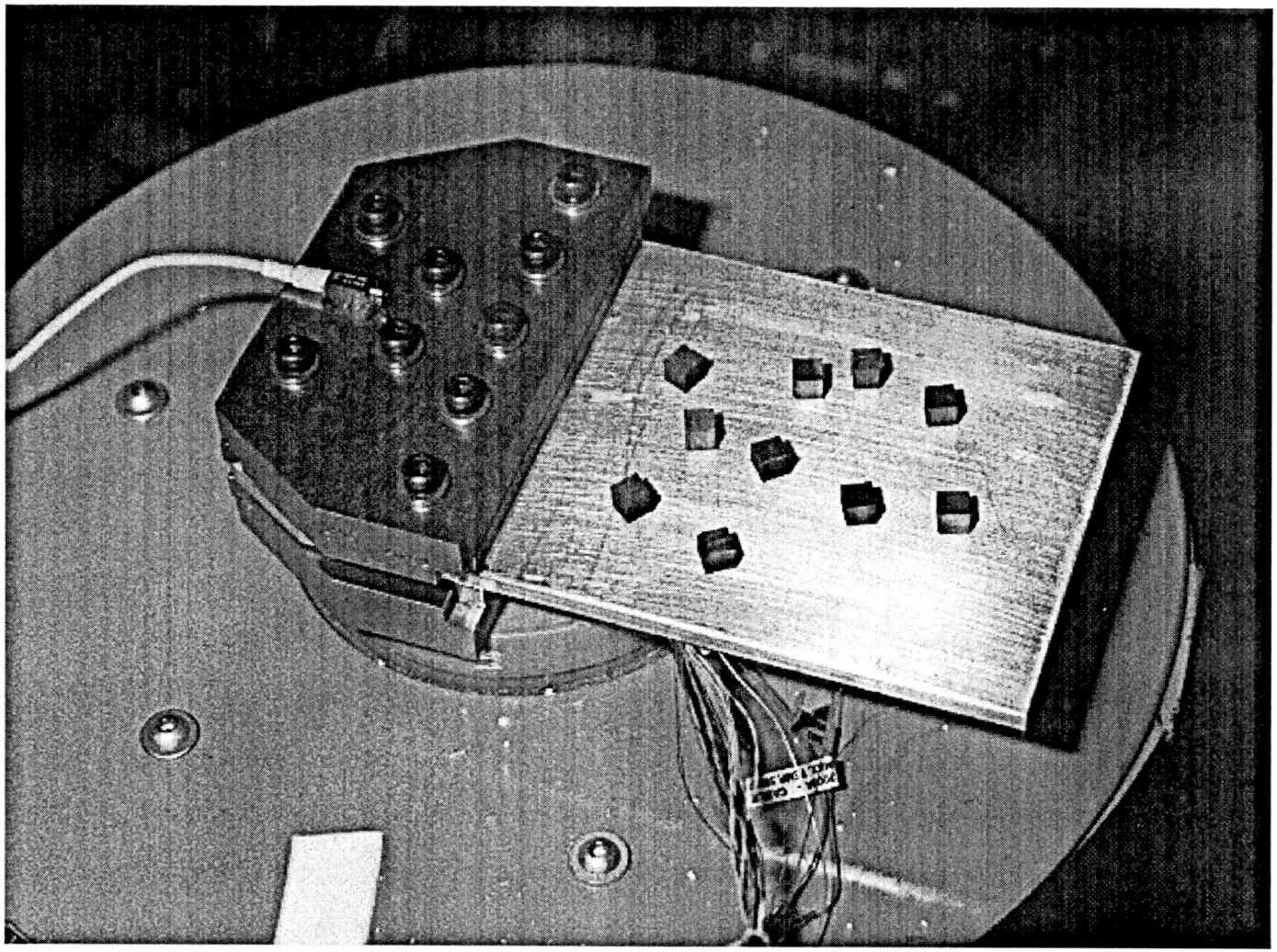


Figure 4. Experimental set up.

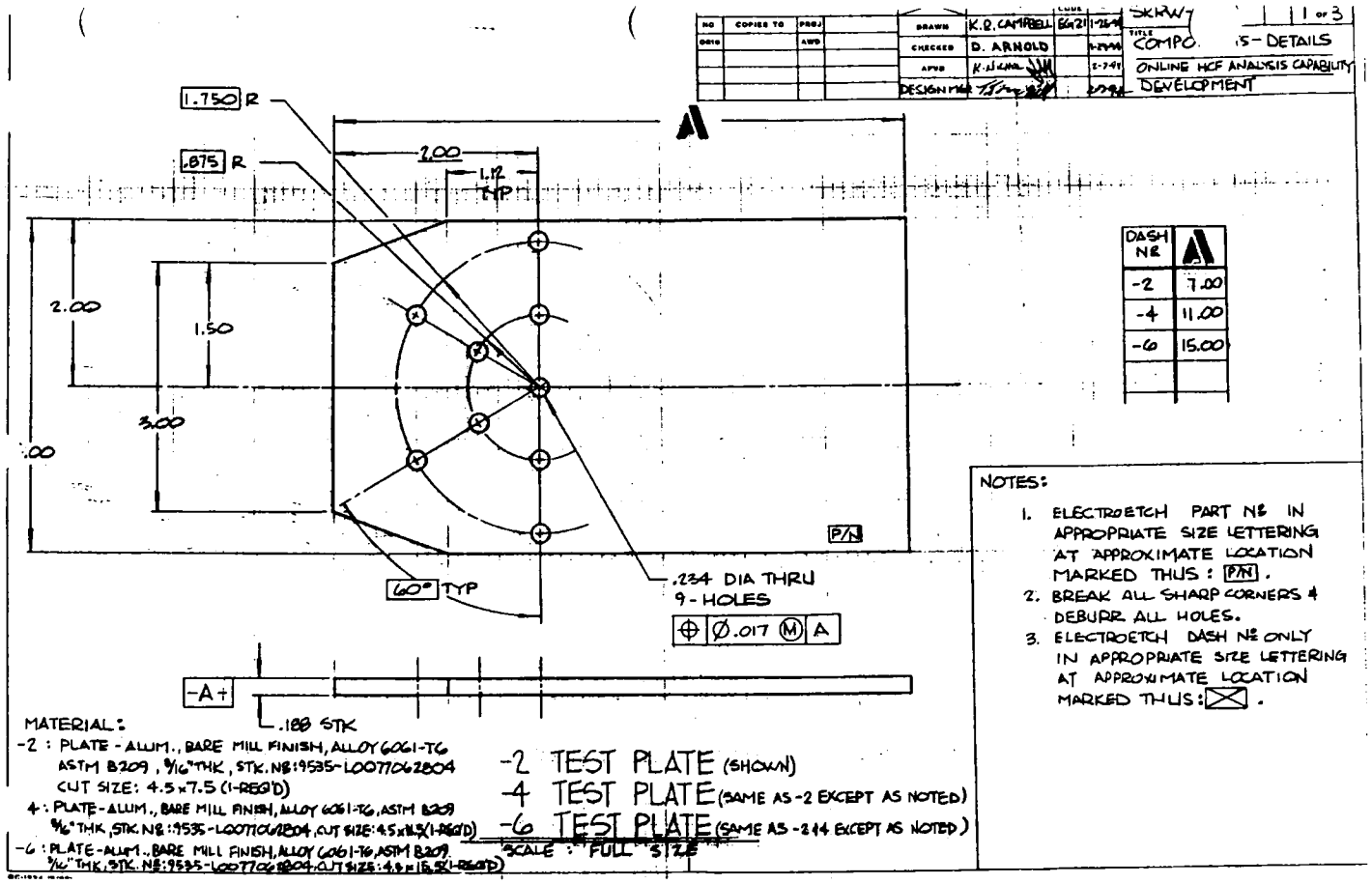


Figure 5. Test apparatus.

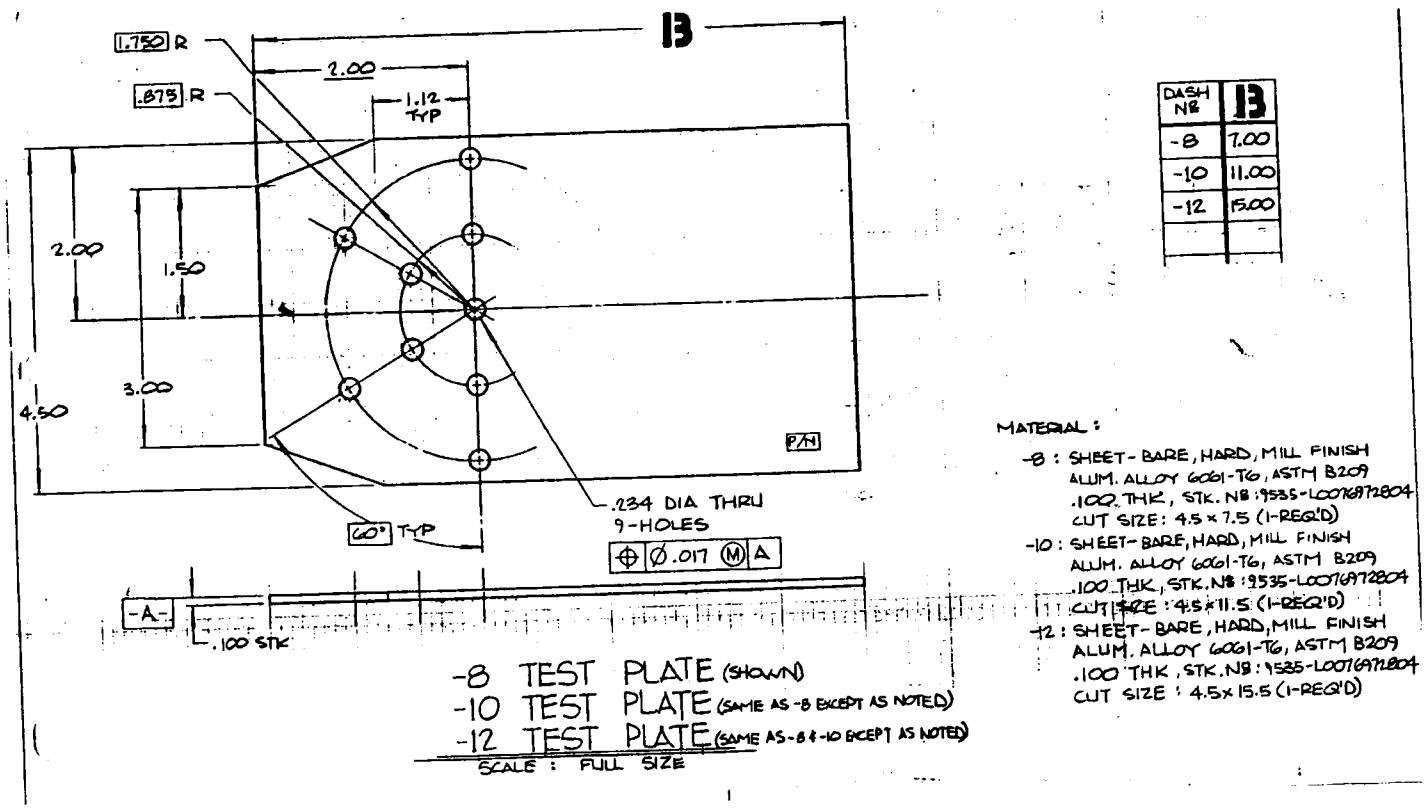


Figure 5 (continued). Test apparatus.

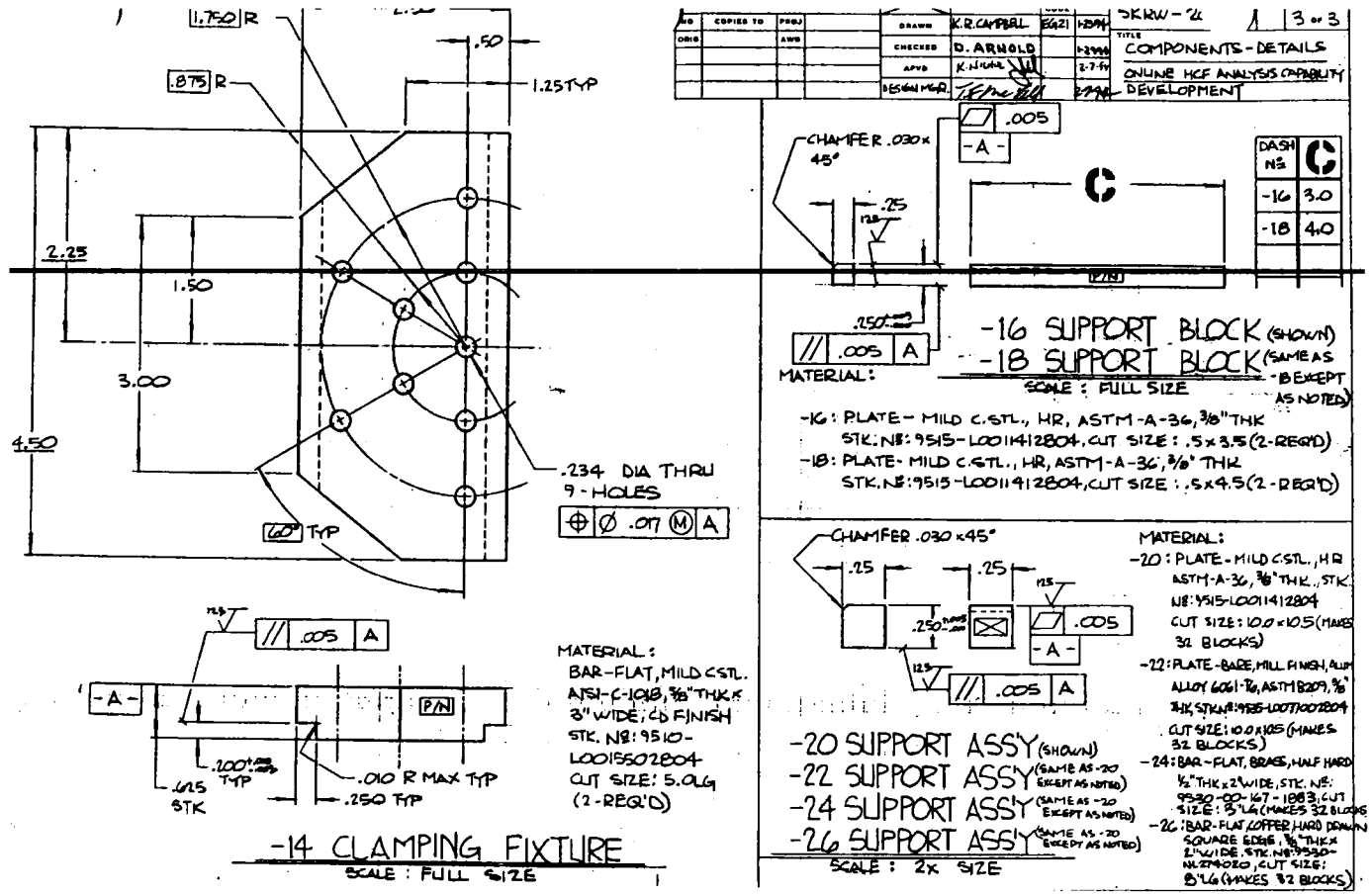


Figure 5 (concluded). Test apparatus.

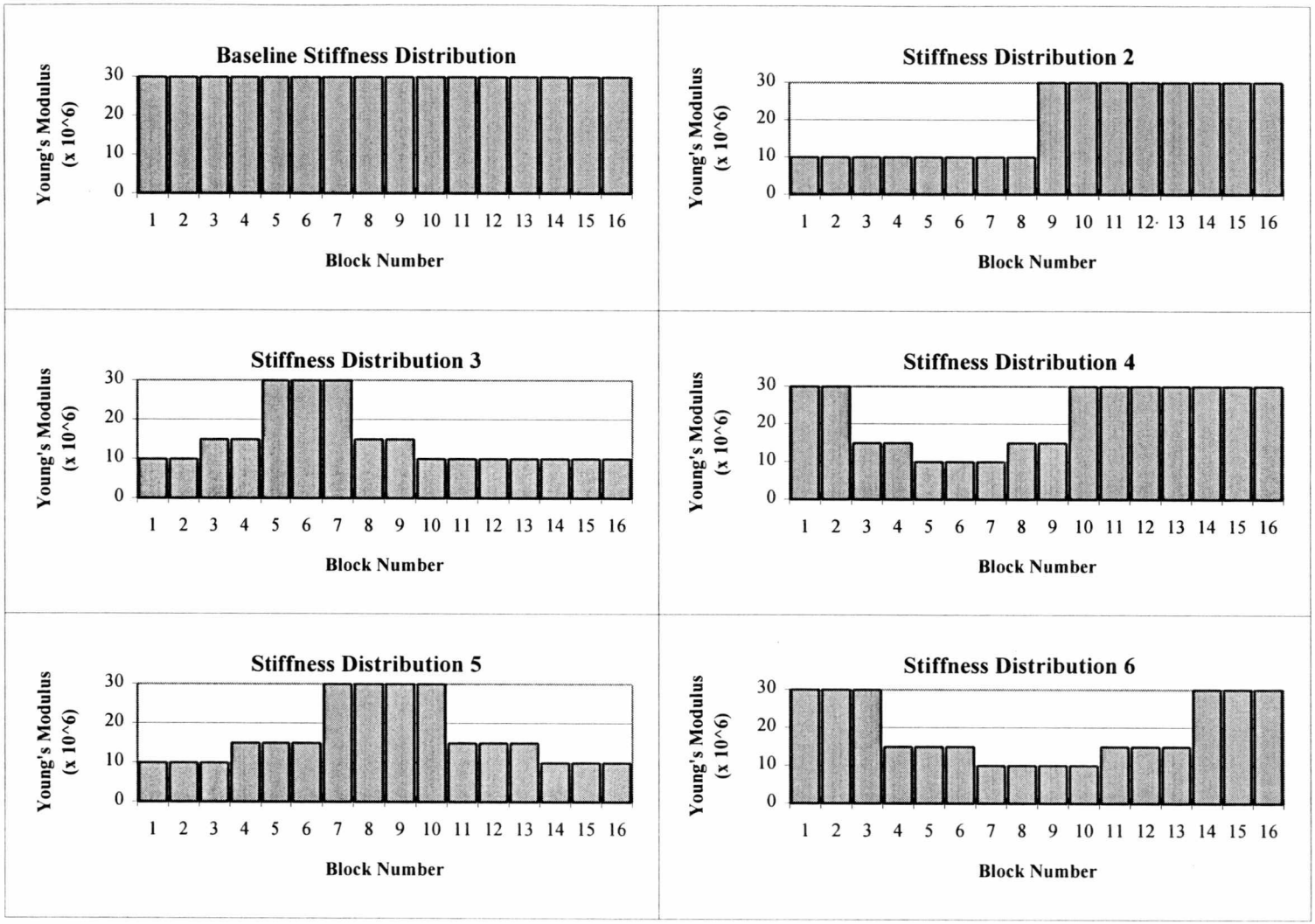


Figure 6. Boundary stiffness distributions.

magnitude. The total maximum variation in stiffness along the chord was approximately 3:1. Values of Young's modulus used for all components were obtained from Mil-Handbook 5 [87]. The Young's modulii were not independently verified.

Experimental determination of plate modal characteristics

Experimental overview and set-up

Each of the four plates were instrumented using strain gage rosettes and accelerometers. Six rosette locations were selected based on percentage of the cantilevered plate length and the plate width. Rosette locations were identified by color corresponding the colors of the instrumentation lead wires. The "x-direction" was defined along the span of the plate. Five accelerometer locations were also selected based on percentage of span. Twenty four dynamic data channels, in all, were used. Instrumentation locations are shown in Figures 7 and 8. Instrumentation was applied to the bottom of the plate so that data could be recorded while mode shapes were determined with the soap powder. The general procedure used was to mount the plate to the shaker table using the appropriate constraint stiffness distribution, sweep the base excitation frequency until resonance had been established in the mode of interest, record the data, and then sprinkle soap powder on the plate to identify the mode. Photographs were taken of most of the mode shapes. The process was then repeated for each mode of interest. Only fundamental bending modes were considered. Once testing of all modes of interest for a given plate and constraint distribution were completed, the assembly was untorqued from the shaker table mounting head and then retorqued and selective repeat data was acquired. The next constraint distribution was then tested and, upon completing all six distributions, the next plate was mounted.

Several difficulties with the experimental set up were encountered. First, because the support blocks were dimensionally specified as 0.250, +.005/-.000 inch cubes (cf. Figure 5), slight deviations in actual dimensions were encountered. Because of this, there was an occasional block that was somewhat thicker than the others resulting in the

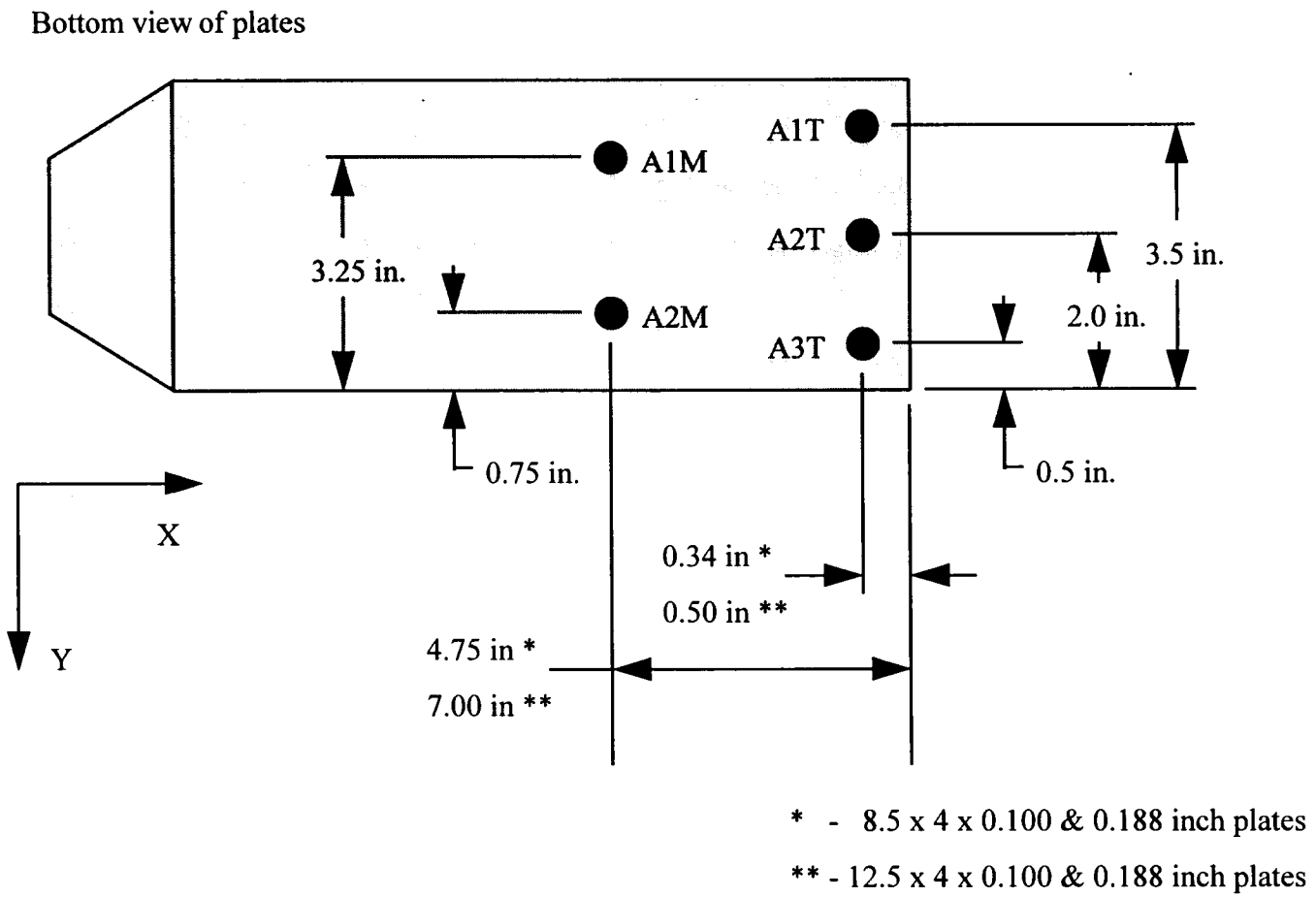


Figure 7. Accelerometer locations.

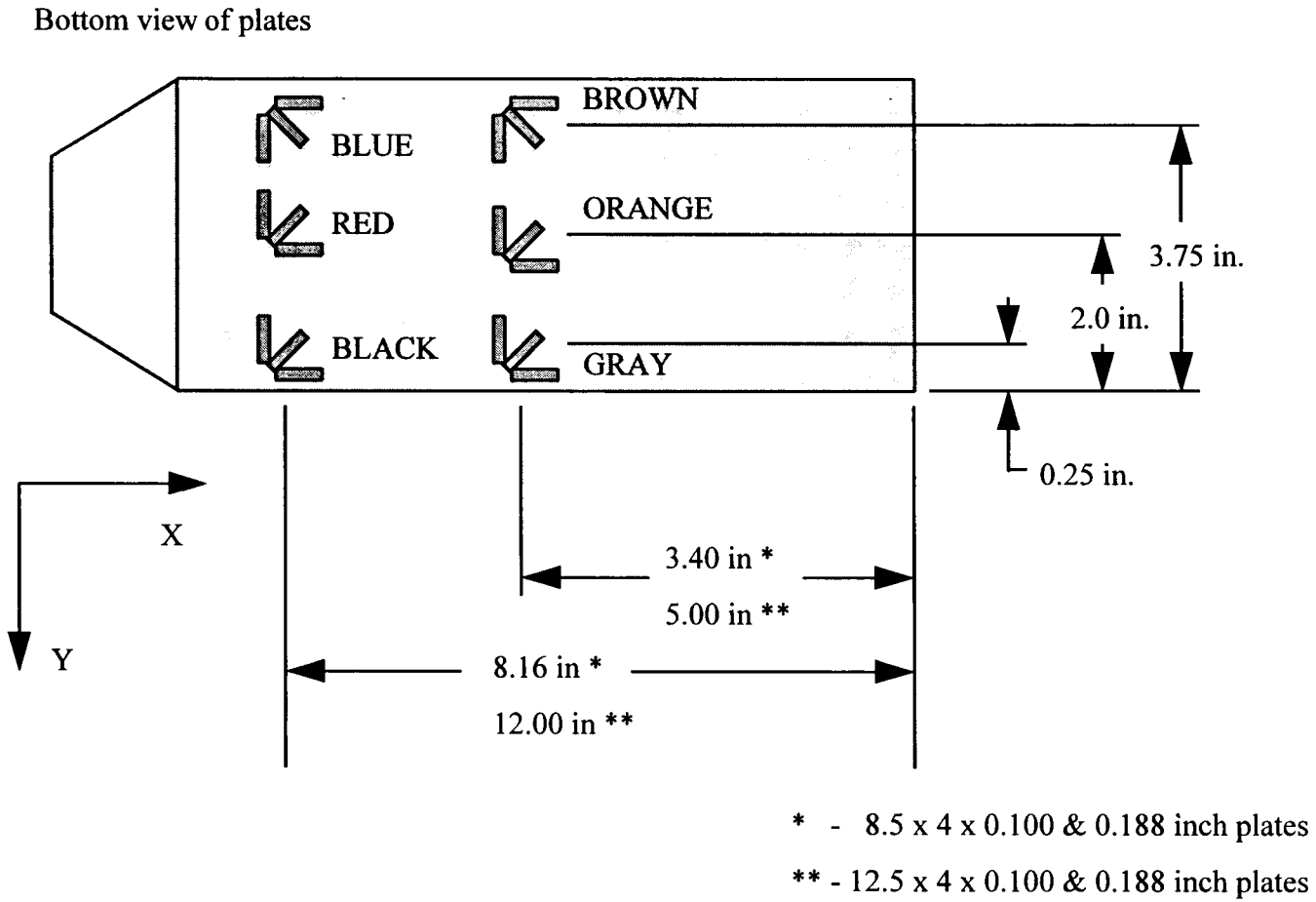


Figure 8. Strain gage rosette locations.

adjacent blocks being loose. Judicious choice of the blocks used provided a work around to this problem. Additionally, a strip of paper was inserted between the blocks and the steel support fixture which provided a small dimensional "cushion" which helped to hold the blocks in place. Consequently, desired stiffness distributions were not ideally implemented. Secondly, the plate, fixture, and support blocks had no design feature that would hold the assembly in place prior to final bolting which made assembly difficult. This also reduced consistency in assembly between plates. Thirdly, because the shaker table head used 3/16 inch bolts, the amount of torque that could be applied to hold the assembly in place was limited. Bolt torque was carefully controlled and held to forty inch-pounds, which was low by comparison to other experimental set-ups described in the literature. A bolt torque sequence was carefully adhered to insure consistent assembly of the test article. However, because of the relatively low torque used to secure the assembly to the shaker table, small excitation amplitudes had to be used. The excitation force was not held to a specified value since the data was to be normalized for comparison to the analytical results. Instead, input amplitude was varied to provide a reasonable response amplitude in resonance for each test case.

Display and recording of the experimental data

Dynamic strains and accelerations were monitored on a dynamic data monitoring and recording system. Data were sampled and then recorded on the internal disk drive of a personal computer at a rate of 7324.219 samples per second per channel which provided a recording frequency range of approximately 3600 cycles per second (Hz). The associated bandwidth, or monitoring frequency resolution, using a 1024 ensemble fast Fourier transform (FFT) was therefore, ≈3.6 Hz. Three ensembles (3072 samples total) were collected for each channel of instrumentation. Channels were simultaneously sampled in groups of three until all twenty four channels were recorded. Strain gage rosette channels were grouped together for simultaneous sampling so that conversion from recorded digital *counts* to stress units could be directly accomplished without having to consider phase angle differences resulting from sampling time differentials. In other words, the signal of each leg of a given rosette were in time phase by sampling each

signal simultaneously. Recorded data from each mode was assigned a unique filename describing the plate geometry, constraint distribution, whether the data point was a repeat or not, and what the mode was. An example of the filename code is shown in Figure 9.

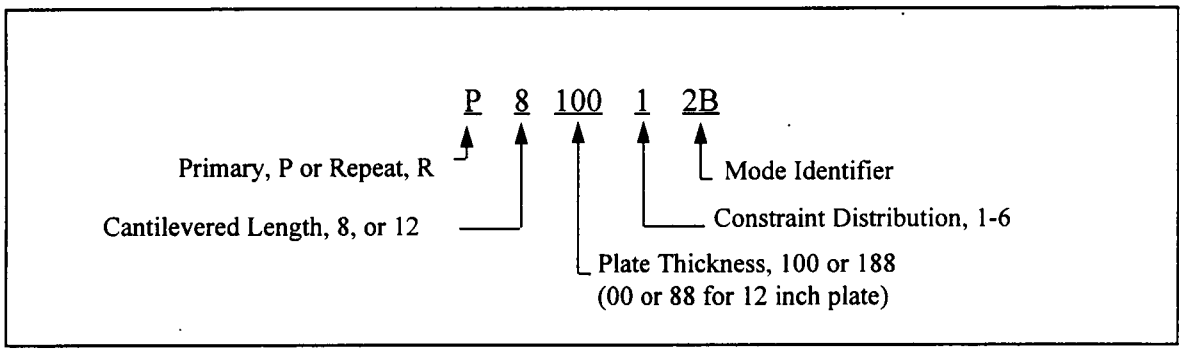


Figure 9. Data filename code

Plots of amplitude in counts versus frequency were displayed on computer screens for all of the data channels simultaneously. These plots were monitored as the frequency generator was slowly swept until the amplitude peaked. Once the amplitude was peaked, the data were recorded and the mode shape was photographed.

Post test data processing

Recorded data were processed after the test using equipment different from that used for monitoring so that better control over data quality could be provided. A program was written which first read the data from the disk and then determined the average value over the data block. Two thousand forty eight samples were processed per block in preparation for computation of the FFT (Fast Fourier Transform). The data were then transformed to engineering units. Accelerometer data was converted from counts to inches x 10^{-3} or "mils" via scaling and double integration. Strain gage data were scaled from counts to strain units, inches/inch, and then to stress units using values of Young's

modulus and Poisson's ratio from Mil Handbook 5 [87]. Final units were pounds-force per square inch, psi. Average values from each channel were then subtracted from all data values to "zero" the data. This left only the a.c. portion of the signal in engineering units and subtracted out the d.c. "drift" from the conditioning equipment.

Fast Fourier Transform (FFT) data processing was accomplished using the FFT algorithm in MATLAB™. Blocks of 2048 data samples were used so that frequency resolution would be doubled from that used for the monitoring. Frequency resolution of the processed data was therefore, 1.8 Hz. A Hanning window [88] was used to improve signal leakage, Figure 10, and the corresponding amplitude of the FFT. Validation of the FFT algorithm as coded in a MATLAB™ ".m" file was accomplished using an input sinusoidal signal generated in MATLAB™ of a range of specified frequencies and unit amplitude. The frequency of the sine wave was then varied over several frequency ranges using a frequency step much smaller than the bandwidth. As expected, the resulting plot of input frequency vs. output frequency, Figure 11, showed step increases at each spectral line. A plot of output amplitude vs. input frequency, Figure 12, produced a periodic, parabolic-like function with maxima, equal to one, directly on each spectral line (no attenuation due to processing) and the minima, equal to 0.85 directly between spectral lines (15% attenuation due to processing). To improve frequency and amplitude resolution, a parabola was "fit" between spectral lines of each FFT around amplitude peaks, Figure 13. This "parabolic interpolation" had the effect of improving frequency resolution to ≈0.1 Hz from 1.8 Hz and maximum amplitude attenuation from -15% to ≈-6.5% as shown in Figures 14 and 15. All data was processed using this processing strategy. Peak data was then transferred to a Microsoft EXCEL™ spreadsheet for later analysis.

Finite element analysis of the various plates

Finite element analyses of each of the plates were conducted to compute the natural frequencies, mode shapes and normalized unit strain distributions. The finite

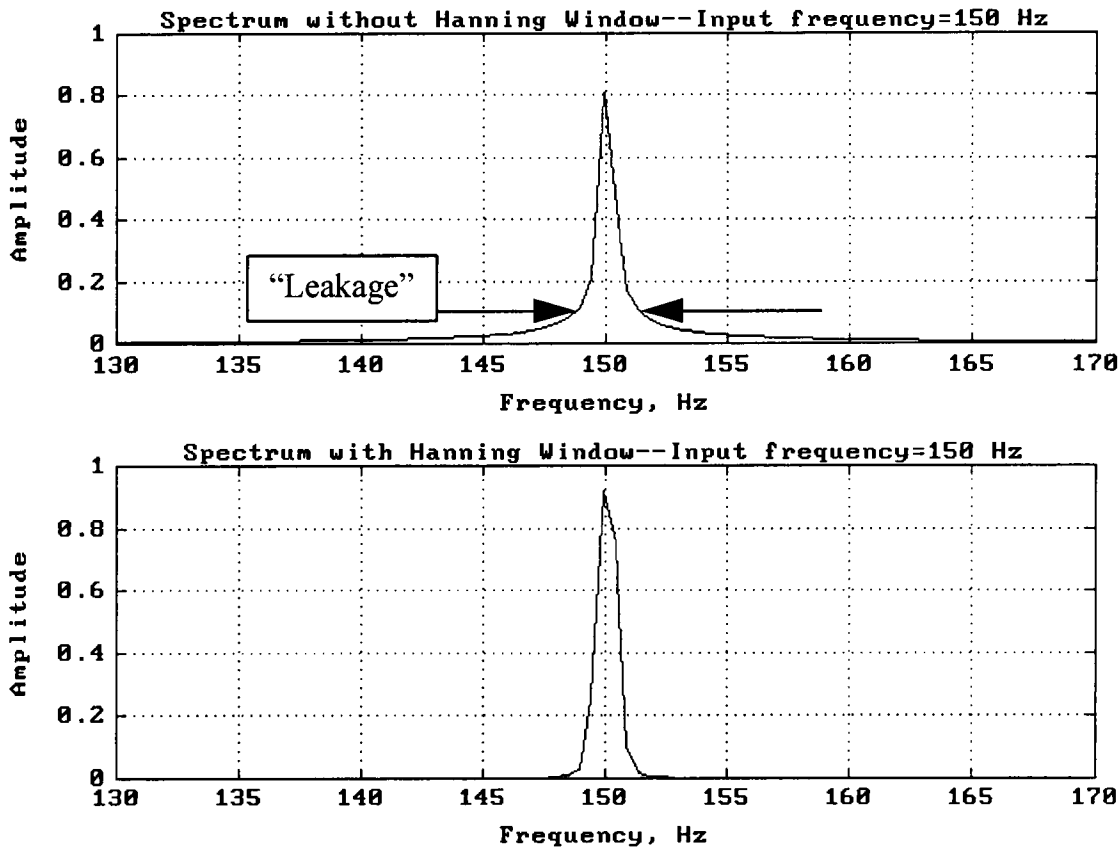


Figure 10. Effect of Hanning window on FFT.

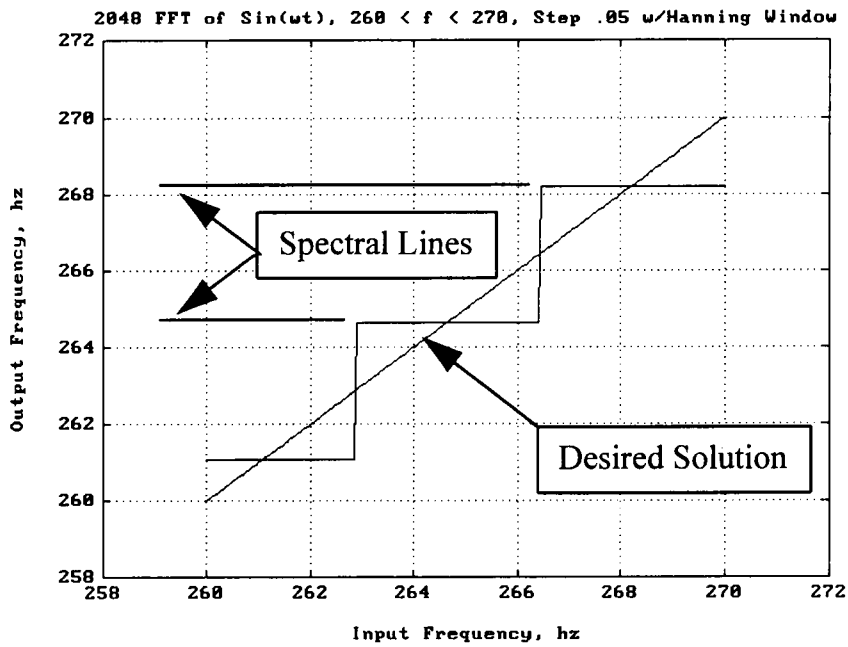


Figure 11. Raw FFT output frequency vs. input frequency

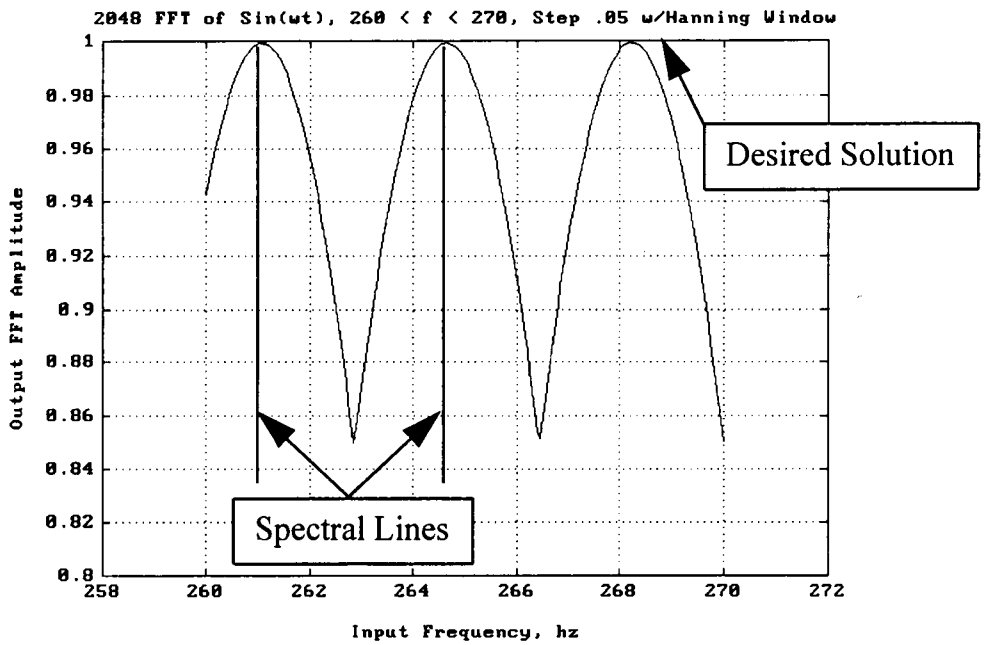


Figure 12. Raw FFT output amplitude vs. input frequency.

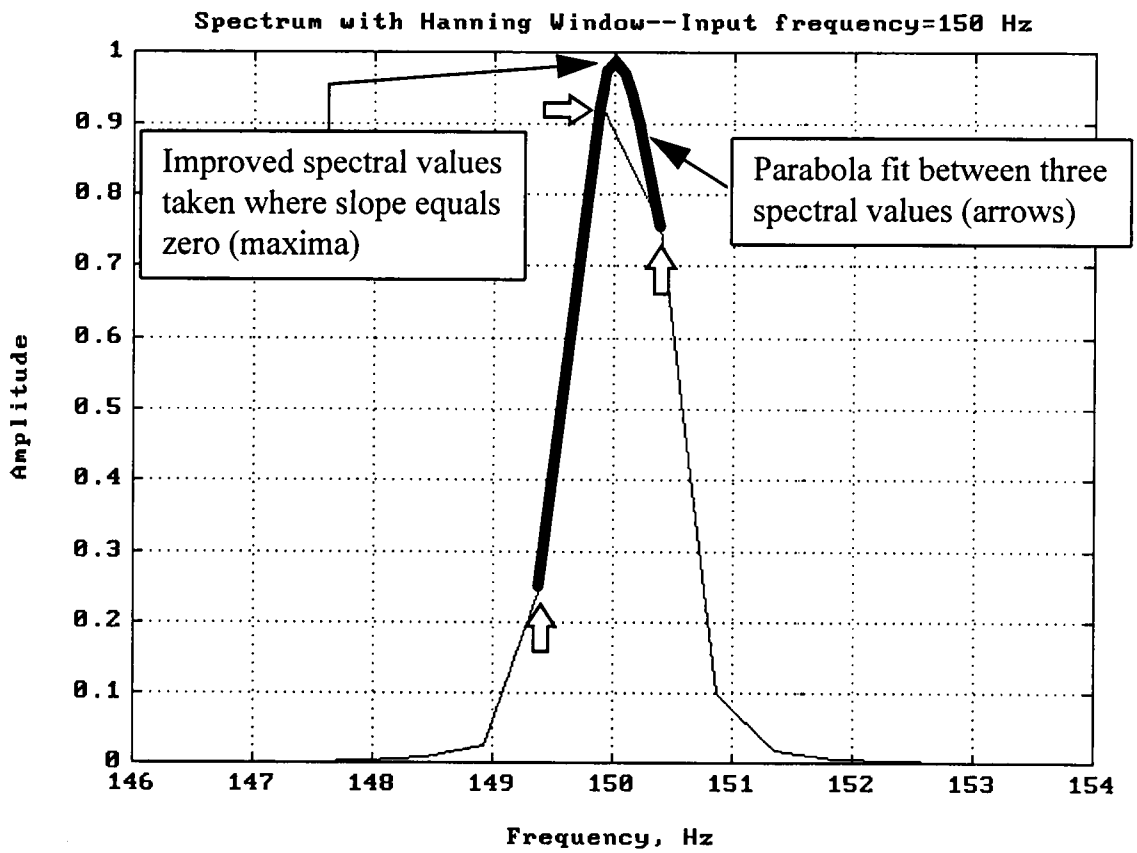


Figure 13. Parabolic interpolation on spectrum.

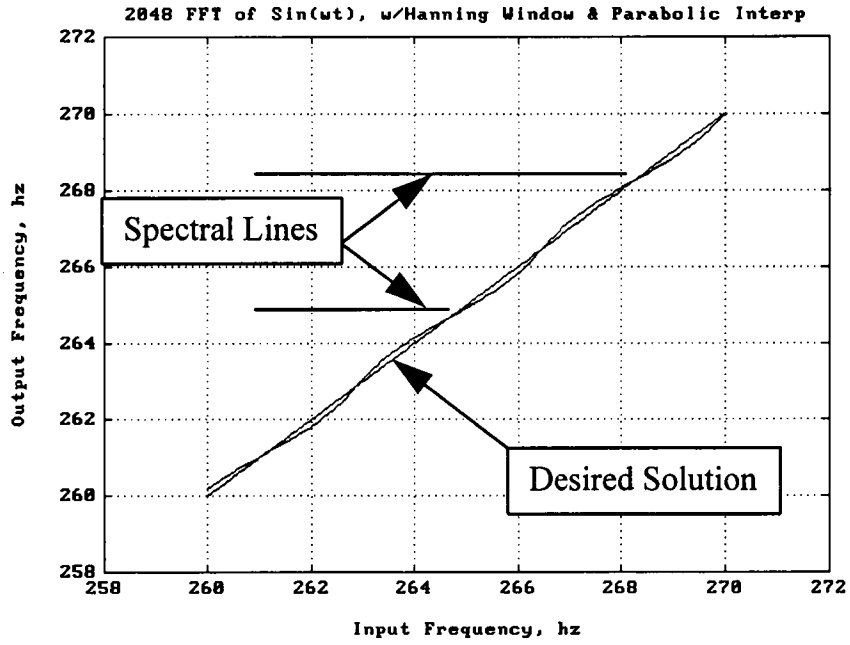


Figure 14. Output frequency with parabolic interpolation vs. input frequency.

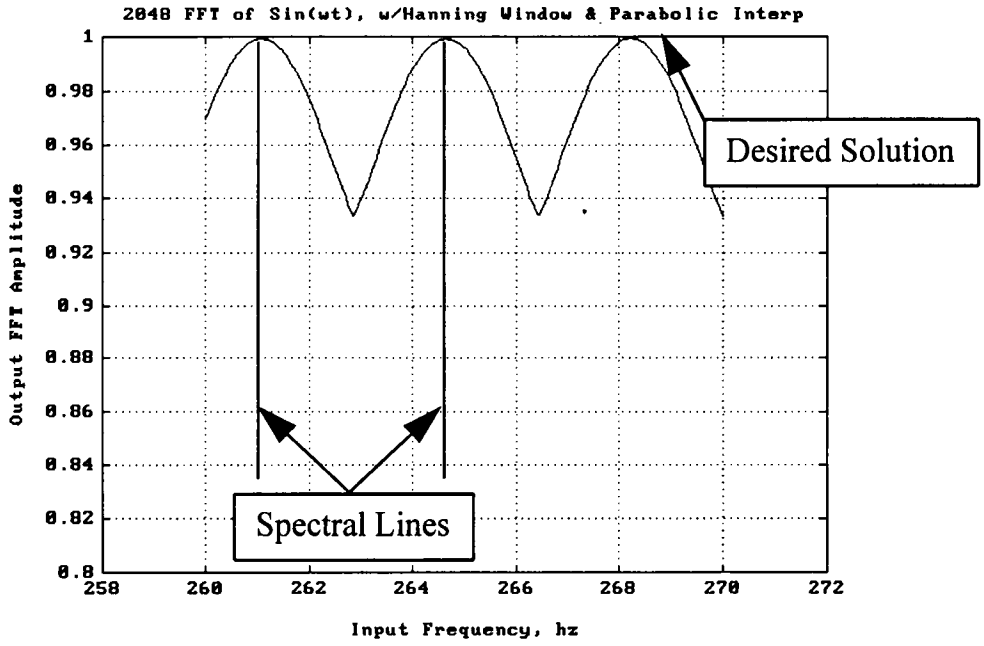


Figure 15. Output FFT amplitude with parabolic interpolation vs. input frequency.

element analysis was run on a personal computer using ALGOR™, a commercially available finite element package. Normal modes analysis was conducted. No attempt at computation of responses to base excitation were made since damping characteristics were unknown. Further, other research efforts underway are attempting to utilize the mode summation method, [89] for example, for describing response vectors as a function of time. Consequently, only the eigenvalues and eigenvectors were needed. Eight node isoparametric "brick" elements were used exclusively. A single element was used through the thickness. Each of the four plates were similarly descretized. Support blocks at the cantilevered interface were modeled using a single element. Only one row of support cubes were modeled since the elements are connected to the plate at the interface and, therefore, produce the same stiffness in compression and tension. The experimental set up clamped the plate between two rows of cubes. Each row, therefore, provided only compressive restraint. An example of one of the finite element models used is provided in Figure 16. The others were similar. Nodal displacement and strain data for each of the modes and plates were stored for later comparison with the experimental data. Instrumentation mass was not modeled.

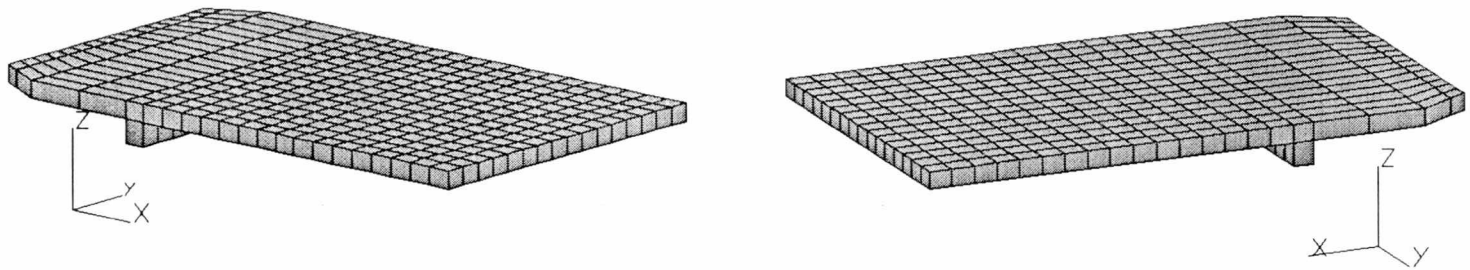


Figure 16. Example finite element model used in analyses.

6. ANALYSIS OF RESULTS

A detailed tabular listing of experimental and analytical results are provided in Appendix 1. Additionally, photographs of many of the experimental modes are provided in Appendix 2. The frequencies shown in the photographs are taken from the input frequency generator. Analytical mode shape contours are presented in Appendix 3.

Experimental results

Analysis of all experimental data began by normalizing each channel to a unit displacement ($\times 10^{-3}$) at the "A3T" location (ref. Figure 7) to provide a common reference between plates and constraint distributions since input excitation values were not held constant during the experiment. Units for comparative data were then mils/mil-@-A3T and psi/mil-@-A3T. This step was also necessary for subsequent comparison to the finite element analysis results since only eigenvectors were computed. These units are used in the table of Appendix 1.

Baselines for each plate and mode were obtained with the one piece steel bars at the clamping interface. This configuration should have produced classical cantilevered plate bending modes (cf. [31]) with node lines symmetric with respect to the chord of the plate. These results were not always obtained, however, as shown in Figure 17, for example, drawn from Appendix 2. Reasons for the discrepancy were unknown but were later partially attributed to the mass of the instrumentation and, to a lesser extent, the instrumentation lead wires which were dangling from below the plate. This demonstrates that differences between experimental results and analytical results can be introduced by the instrumentation itself and must either be accounted for in the analysis or in any subsequent model correction scheme.

The objective of the analysis was to determine how much variation in modal frequency, displacement and strain could be attributed to variations in stiffness at the boundary. Comparisons of the various constraint stiffness distributions are, therefore,

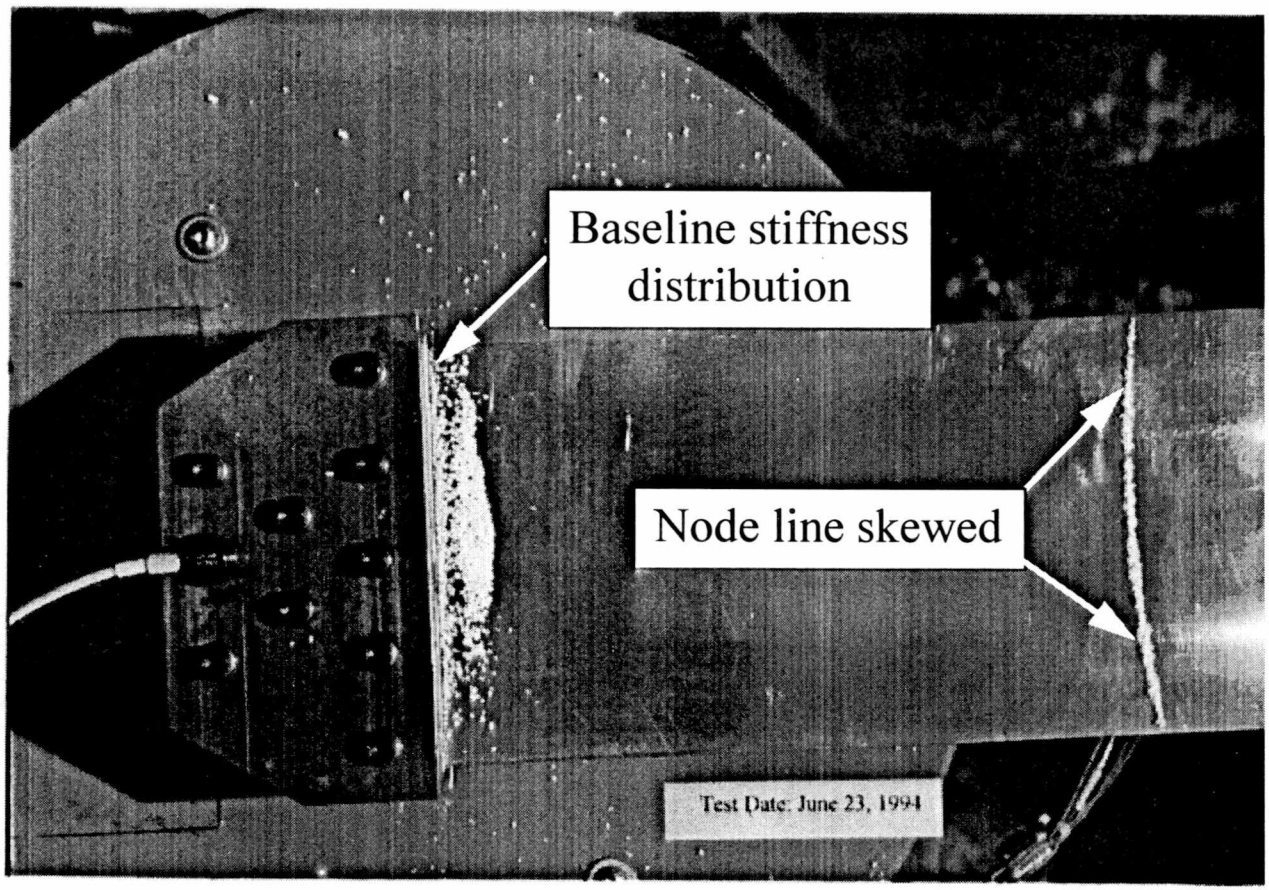


Figure 17. Example of unexpected skewed node line

made with the baseline, or constraint distribution 1 (CD 1). Figure 18 presents summary normalized accelerometer data for each of the five variable constraint distributions as a percentage difference from the baseline, CD 1. Positive percent deviation means that the displacement amplitude was larger than the baseline. Conversely, negative percent deviation corresponds to displacements less than the baseline. As shown in Figure 18, there was generally less than ten percent variation in displacement at measurement locations for most of the test conditions as a result of changes in the constraint stiffness distribution. Less than five percent variation in modal frequencies were measured for all the plates and modes tested. Some combinations of plate and boundary stiffness distribution produced significant differences in modal response amplitudes in some modes. Maximum deviation from the baseline occurred while testing the second constraint distribution on the 12.5 × 4.0 × 0.188 inch plate in the second bending mode. Nearly fifty five percent deviation was recorded. Further examination of results from the A2M accelerometer, to be discussed later, tended to discount data measured using that transducer. Setting data from A2M aside, the maximum displacement deviation from the baseline was still nearly 35% and was measured on A1T while testing the fifth constraint distribution on the 12.5 × 4.0 × 0.188 inch plate in the second bending mode. The longest plates tended to be most sensitive to changes in the constraint distribution. This is to be expected when considering the fact that longer plates produce larger bending moments at the cantilevered interface.

Strain data acquired on each plate were converted to stress units and then normalized to unit stress values using displacement data from A3T. Stress in the longitudinal, or spanwise direction were analyzed since only bending modes were considered in the investigation. This component of the stress tensor is labeled as "X-stress" in subsequent figures. Summary of the strain gage results are presented in Figure 19. Results presented in Figure 19 agree with accelerometer results, in that, generally less than ten percent variation as a function of constraint distribution was generated. Results also indicate that the 12.5 × 4.0 × 0.188 inch plate in the second bending mode was again most sensitive to changes in the constraint stiffness distribution.

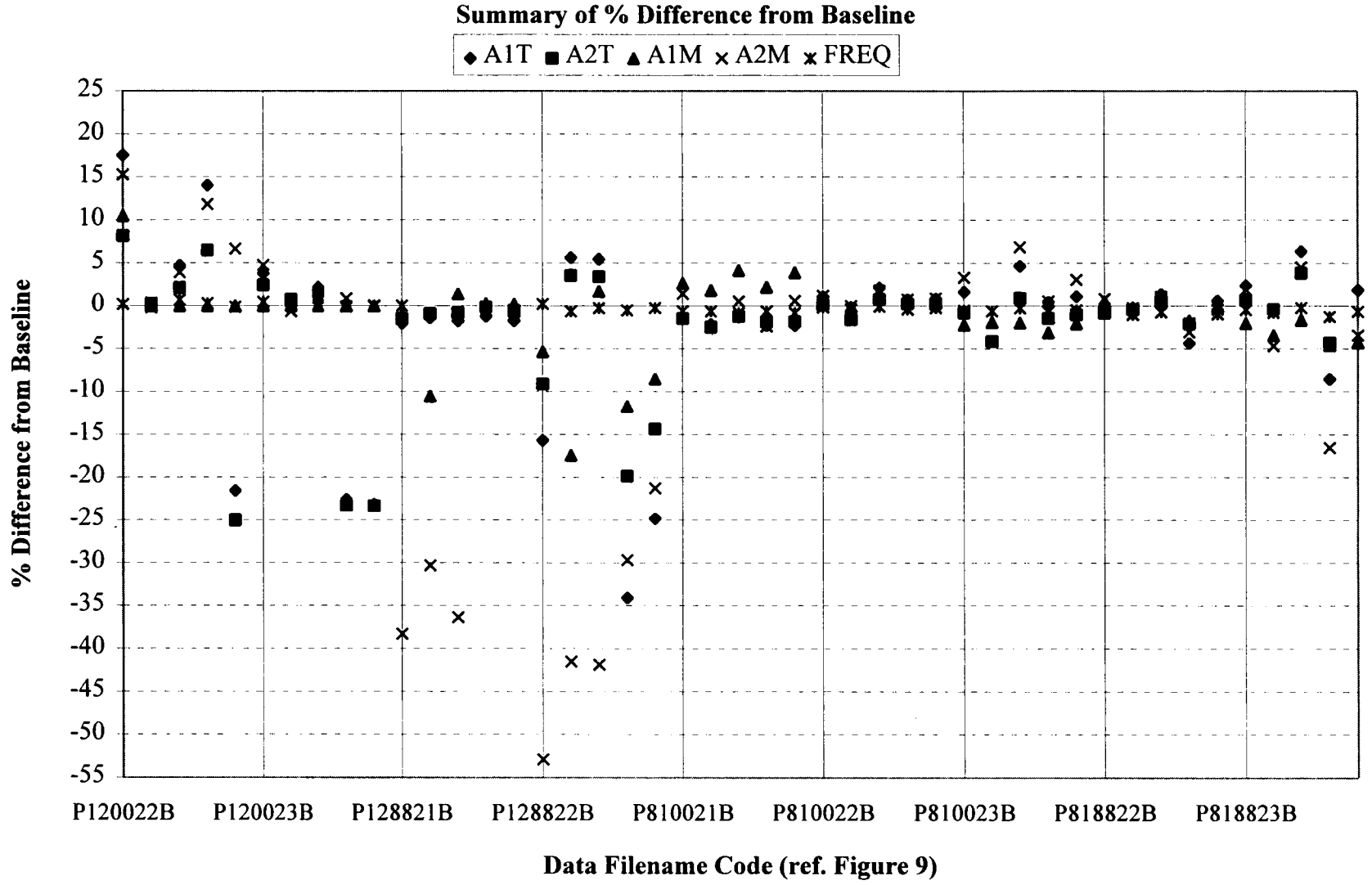


Figure 18. Effect of constraint distribution on experimental displacements.

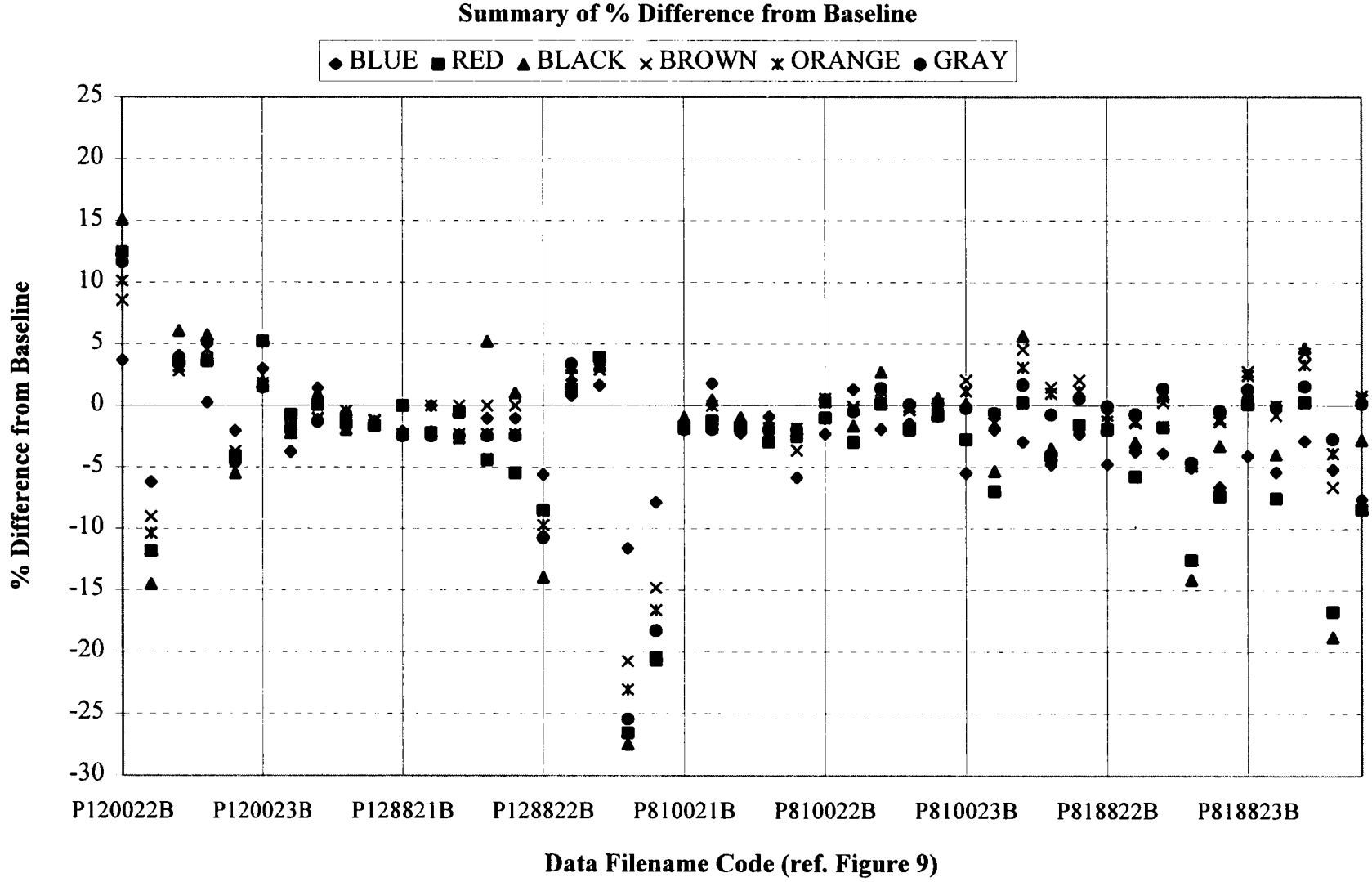


Figure 19. Effect of constraint distribution on experimental X-stress.

Maximum percent deviation from the baseline stress was nearly 30% and occurred while testing the fourth constraint distribution.

As shown, strain gage data were more consistent than the accelerometer data, in that, no particular strain gage rosette showed significantly different results from any other. This is in sharp contrast to the accelerometer data particularly with respect to the A2M accelerometer. Since the data from that accelerometer was significantly different from much of the other data, it would stand to reason that significant inconsistencies would also be present in at least one of the strain gage rosettes. Since this was not encountered, results from the A2M accelerometer are considered to be invalid.

The experimental results were "spot checked" for repeatability as described earlier. Results of the repeatability checks are presented in Figures 20 and 21. As shown, experimental data generally repeated within ±2%. Frequency repeatability, shown in Figure 20, was better than ±0.25%. Experimental amplitudes, therefore, repeated within the FFT data processing uncertainty (c.f. Figure 15). Experimental frequency repeatability was similar to FFT data processing uncertainties (c.f. Figure 14).

Finite element analysis results

Analysis of all finite element data began by normalizing each channel to a unit displacement ($\times 10^{-3}$) at the A3T location in the same fashion as the experimental data. This provided a common reference between experimental data and analytical data. Units for the analytical data were then mils/mil-@-A3T and psi/mil-@-A3T.

The strategy used for analysis of the finite element data was the same as for the experimental data. Consequently, plots similar to Figures 17 and 18 were generated for the finite element data. These data are presented in Figures 22 and 23. Both Figures show that again the 12.5 × 4.0 × 0.188 inch plate was most sensitive to changes in boundary stiffness distribution with variations in displacement relative to the baseline of up to 28% generated. Again, most of the analysis conditions produced less than 2% variation as a function of boundary constraint distribution.

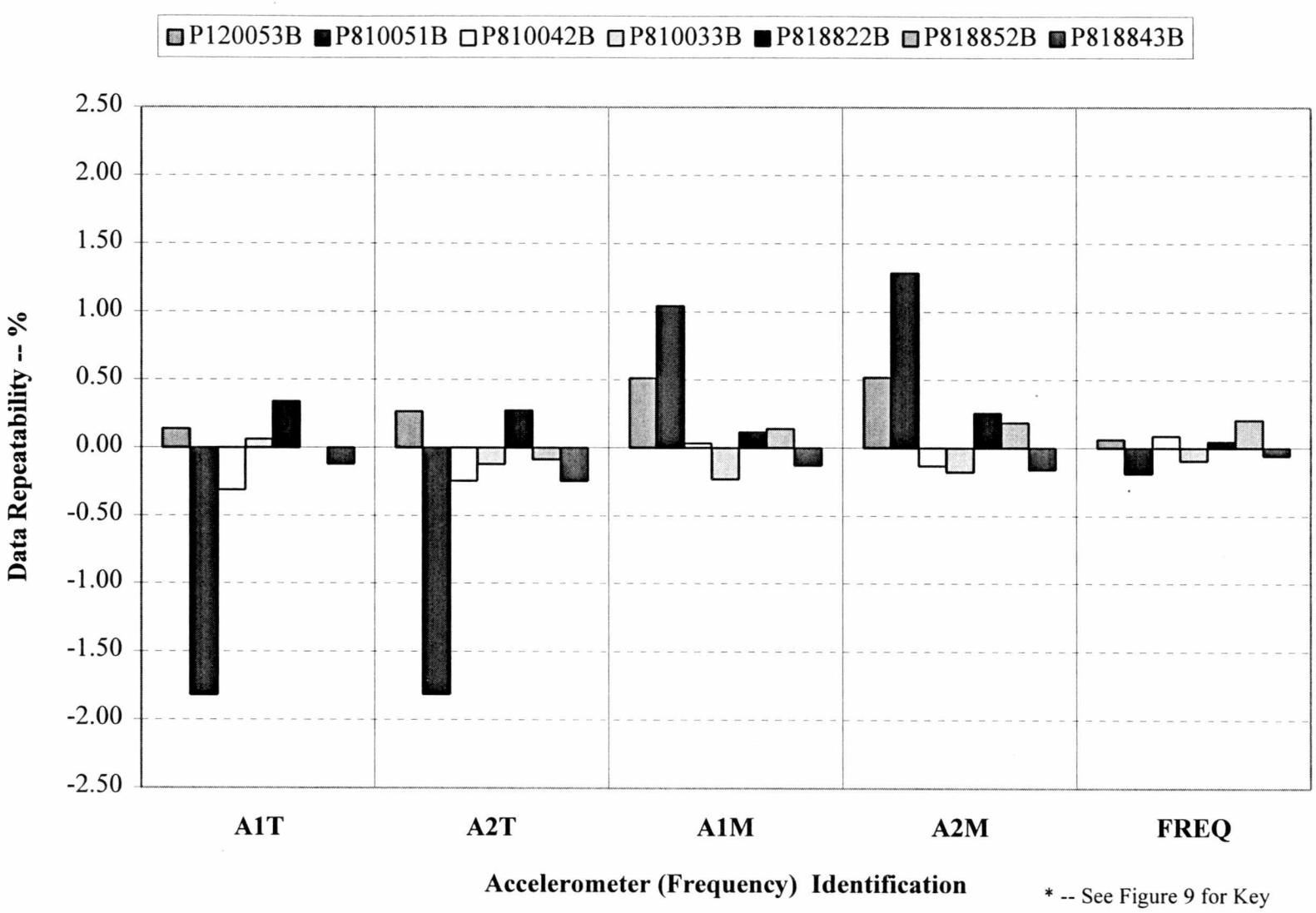


Figure 20. Experimental displacement data repeatability.

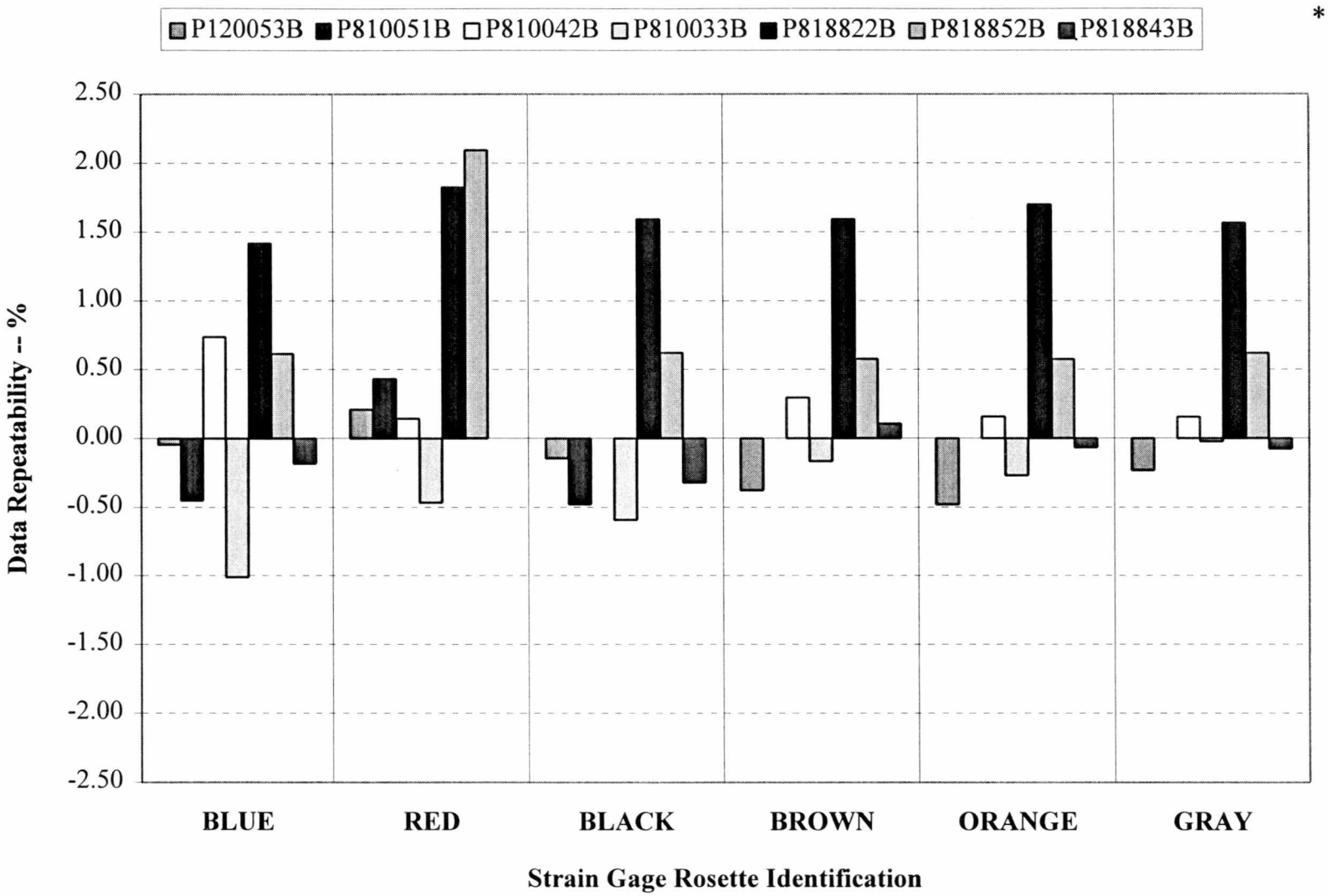


Figure 21. Experimental X-stress data repeatability.

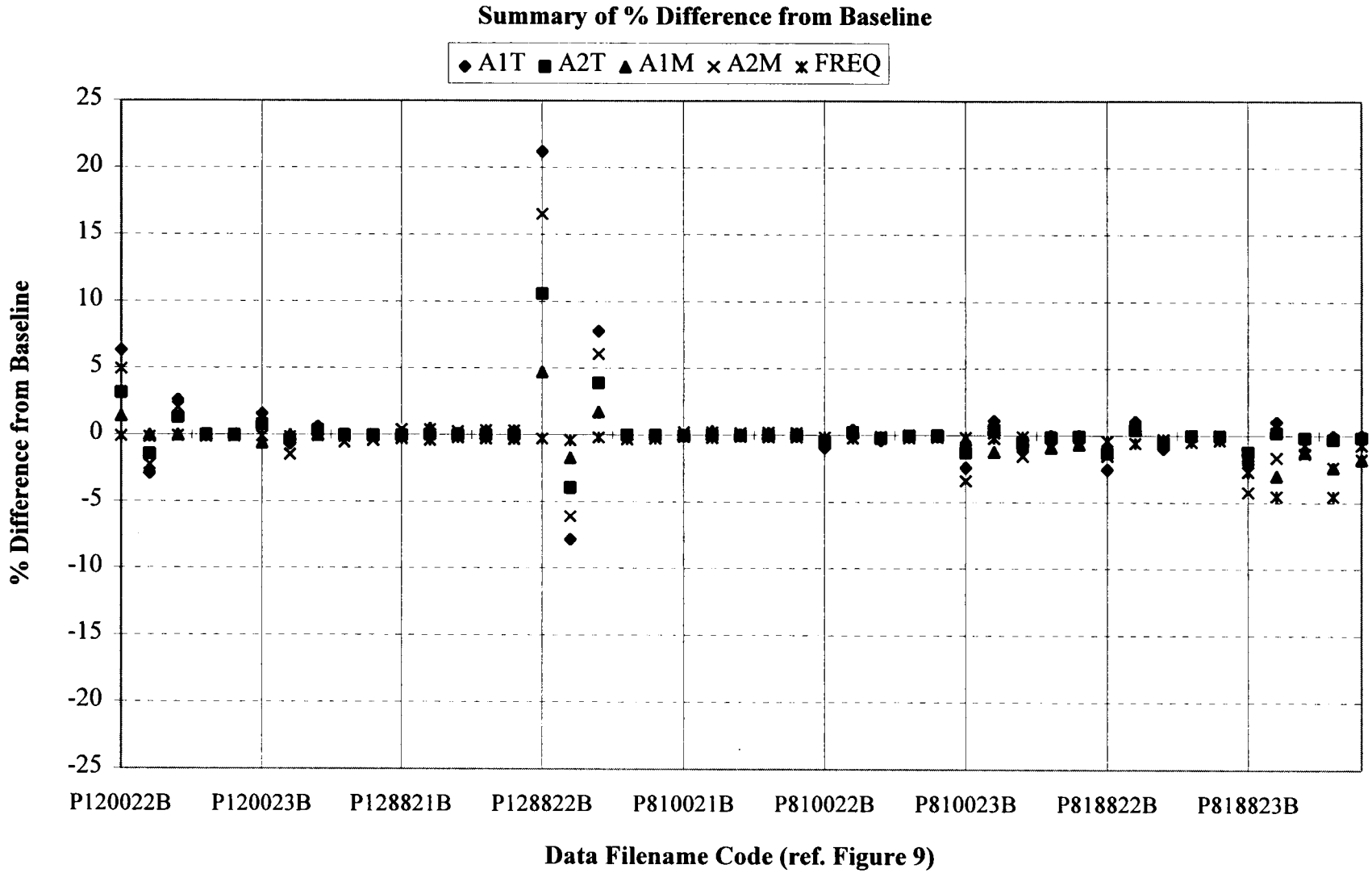


Figure 22. Effect of constraint distribution on analytical displacements

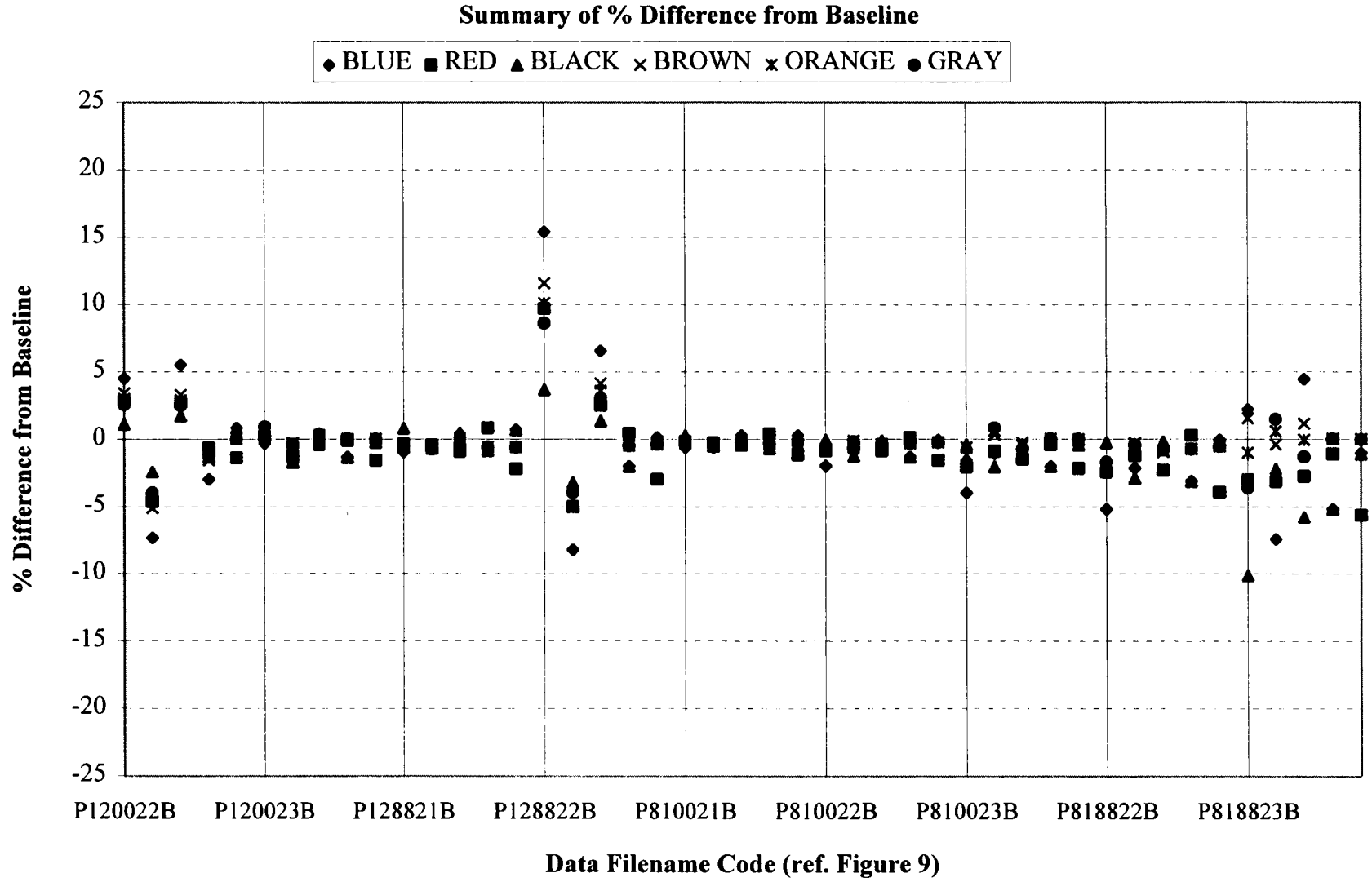


Figure 23. Effect of constraint distribution on analytical X-stress

Both the experimental and analytical data showed clearly that the modal response of some plates in particular modes could be significantly affected by the elasticity of the support. Both sets of data identified the same plates and the same modes as being most sensitive although actual sensitivities were different. This is in complete agreement with findings in the literature that cited clamping torques as a consideration in repeatability of modal data. However, it is not as clear from the data why specific modes of specific plates are more sensitive to this effect than others.

Comparison of experimental and analytical results

Ideally, the experimental and analytical results would produce identical variations in modal response for each of the boundary constraint distributions tested. This would indicate, among other things, that the analytical model correctly described the physical system that was tested; including variations in boundary constraint stiffness distributions. Comparisons between analytical and experimental results are presented in Figures 24 and 25 for the Z-displacement and X-stress data respectively. As shown, significant differences were indeed present that were unexpected. Differences were remarkably repeatable between experimental and analytical results indicating that a single parameter is likely biasing the data. Because the mass of the instrumentation was not modeled in the analysis, this was suspected of causing the discrepancy. Other sources of potential modeling difficulties could lie in the use of a single element throughthe plate thickness. The ability to address these areas was given significant consideration in subsequent development of the model adjustment scheme.

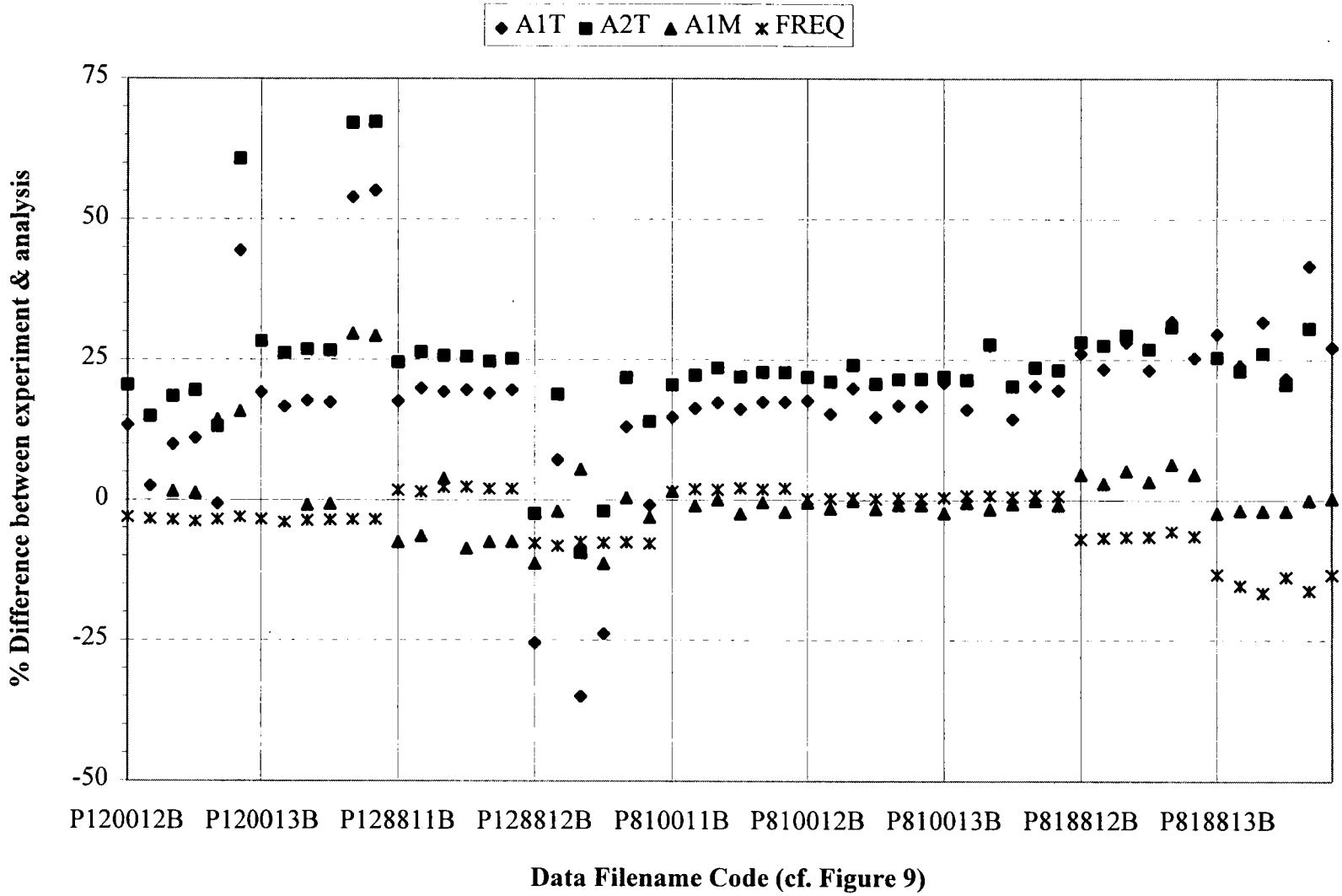


Figure 24. Difference between experimental and analytical displacements.

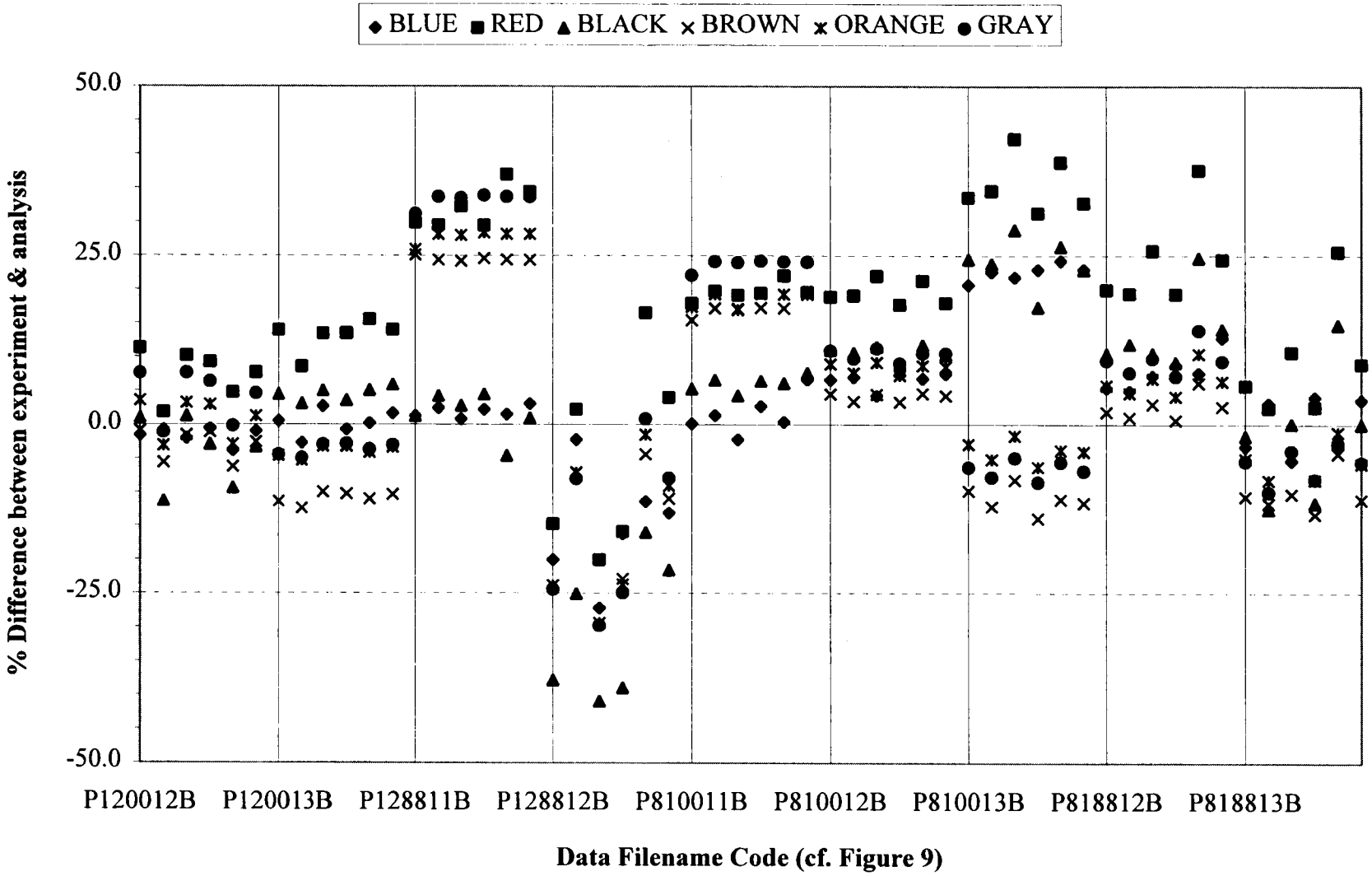


Figure 25. Difference between experimental and analytical X-stress.

7. DYNAMIC FINITE ELEMENT MODEL ADJUSTMENT TECHNIQUE

The goal in developing a technique for adjusting a finite element model was to provide an ability to "focus" adjustments to specific areas of the model where the potential for modeling errors might be highest. Additionally, the approach would be able to specify adjustments to only mass or stiffness if this information were known up front. Adjustments must make physical sense, i.e. be changes to physical parameters, not just elements of the stiffness and mass matrices, and maintain the overall structure and consistency of the stiffness and mass matrices. Examples of how this may be useful are adjustment of the stiffness distribution at the boundary and taking into account the mass of the instrumentation.

Some of the techniques in the literature, e.g. [75]-[84], seek to find minimum changes to the elements of the mass and stiffness matrix that bring about a match with experimental data. Matching experimental data has little physical significance since it is never 100% repeatable. Consequently, to "correct" an analytical model to match a set of data will not produce a model that will match *all* the data. Also, because only a few modes of vibration are tested experimentally, many models could be generated that match the first few modes. Finally, finding the "minimum" changes to the elements of the mass and stiffness matrix destroys the structure of the matrices themselves so that they no longer reflect the physical system.

Other techniques in the literature, e.g., [57]-[59] and [61], set out to find changes in physical parameters that will account for differences between experimental and analytical results. Unfortunately, parameters found in the finite element formulation generally occur in groups, e.g. AE/L for an axial bar element where A is the cross sectional area, E is Young's modulus and L is the length of the element. As a result, there exists an infinite number of combinations that will "match" the experimental data. While they seek to find physically meaningful adjustments, they have no ability to take

advantage of information about where the model might be deficient. They are also numerically intensive and iterative.

Some approaches seek to maintain the structure of the matrices and make adjustments to "groups" of parameters such as that by Lim [90] and Farhat and Hemez [91]. These approaches are linked to the finite elements themselves and consequently make adjustments that are consistent with the connectivity and structure of the elements. Neither approach has the capability to focus adjustments. They do, however, provide a good basis for the present approach.

Credit for the concept of the present technique is due my major professor, Dr. Remi Engels. Given an analytical finite element stiffness matrix, $\mathbf{K}_A$ and mass matrix, $\mathbf{M}_A$, and a number of test frequencies, Ω_t and mode shapes, $\vec{\varphi}_t$, compute a set of meaningful perturbations, $\Delta\mathbf{K}$ and $\Delta\mathbf{M}$ which satisfy the following relation

$$\left(\mathbf{K}_A + \Delta\mathbf{K} - \Omega_t\left(\mathbf{M}_A + \Delta\mathbf{M}\right)\right)\vec{\varphi}_t = \vec{0}\,. \tag{1}$$

Measurements in $\vec{\varphi}_t$ are initially assumed to be displacements and all elements are known. Ω_t has units of (radians/sec)^2. Equation (1) is rearranged as

$$\left(\Delta\mathbf{K} - \Omega_t\Delta\mathbf{M}\right)\vec{\varphi}_t = -\left(\mathbf{K}_A - \Omega_t\mathbf{M}_A\right)\vec{\varphi}_t \stackrel{\Delta}{=} \vec{\beta} \tag{2}$$

from which it is apparent that if $\vec{\beta} = \vec{0}$ for all modes, Ω_t and $\vec{\varphi}_t$ are the eigenvalues and eigenvectors of the analytical, two-matrix eigenproblem. Further, this implies that $\Delta\mathbf{K}$ and $\Delta\mathbf{M}$ are both zero and that no adjustments are needed.

The present approach seeks to find a set of adjustments to parameters inherent in the finite element formulation. As an example of the paramaterization of a finite element, consider the stiffness matrix of the axial bar element,

$$\mathbf{k}^e = \frac{A^e E^e}{L^e}\begin{pmatrix} 1 & -1 \\ -1 & 1 \end{pmatrix} \tag{3}$$

where the superscript, e, denotes the element number. Parameterization is accomplished by setting $A^eE^e/L^e=P^e$. Changes to the stiffness matrix are then simply reflected as changes in this parameter. The mass matrix can be similarly described.

The goal is to construct $\Delta\mathbf{K}$ and $\Delta\mathbf{M}$ as changes in fundamental parameters, ΔP^i's. Having done this, the left hand side of equation (2) can be rewritten

$$\left(\Delta\mathbf{K} - \Omega_t\Delta\mathbf{M}\right)\vec{\varphi}_t = \mathbf{R}\Delta\vec{P} \tag{4}$$

where $\mathbf{R}$ is a matrix containing available Ω_t's and appropriate combinations of the eigenvector elements in $\vec{\varphi}_t$. Note, therefore, that $\mathbf{R}$ is mode dependent and is partitioned row-wise by mode for as many sets of modal data as are available. $\vec{\beta}$ is similarly partitioned. Algebraically, this appears as

$$\mathbf{R} = \begin{bmatrix} \mathbf{R}_{\text{mode 1}} \\ \cdots \\ \mathbf{R}_{\text{mode 2}} \\ \cdots \\ \mathbf{R}_{\text{mode } n} \end{bmatrix} \quad \text{and} \quad \vec{\beta} = \begin{Bmatrix} \left(\mathbf{K}_A - \Omega_{t\,\text{mode 1}}\mathbf{M}_A\right)\vec{\varphi}_{t\,\text{mode 1}} \\ \cdots \\ \left(\mathbf{K}_A - \Omega_{t\,\text{mode 2}}\mathbf{M}_A\right)\vec{\varphi}_{t\,\text{mode 2}} \\ \cdots \\ \left(\mathbf{K}_A - \Omega_{t\,\text{mode } n}\mathbf{M}_A\right)\vec{\varphi}_{t\,\text{mode } n} \end{Bmatrix}. \tag{5}$$

Substituting the result of equation (4) into equation (2) yields

$$\mathbf{R}\Delta\vec{P} = \vec{\beta}\,. \tag{6}$$

Equation (6) is generally overdetermined which requires that the vector of adjustments, $\Delta\vec{P}$,be determined by a least squares, singular value decomposition or similar technique. Having solved for $\Delta\vec{P}$, corrections are made to $\mathbf{M}_A$ and $\mathbf{K}_A$ which produces the adjusted analytical model.

Solution of the overdetermined system

Solution of equation (6) is accomplished in the present work using the singular value decomposition, or SVD. The SVD of **R** produces a diagonal matrix σ, of dimension ($m \times n$), with $m > n$, a set of left hand orthogonal singular vectors, **U**, of dimension ($m \times m$), and a set of right hand orthogonal singular vectors, $\mathbf{V}^{\mathrm{T}}$, of dimension ($n \times n$), such that

$$\mathbf{R} = \mathbf{U}\sigma\mathbf{V}^{T}. \tag{7}$$

The solution of (6) is then,

$$\Delta\vec{P} = \mathbf{V}\sigma^{+}\mathbf{U}^{T}\vec{\beta}, \tag{8}$$

where

$$\sigma^{+} = \begin{bmatrix} \frac{1}{\sigma_1} & 0 & \cdots & \cdots & \cdots & 0 \\ 0 & \frac{1}{\sigma_2} & & & & \vdots \\ \vdots & & \frac{1}{\sigma_3} & & & \vdots \\ \vdots & & & \ddots & & \vdots \\ \vdots & & & & \frac{1}{\sigma_{n-1}} & 0 \\ 0 & \cdots & \cdots & \cdots & 0 & \frac{1}{\sigma_n} \\ \cdots & \cdots & \cdots & \cdots & \cdots & \cdots \\ & & & 0 & & \end{bmatrix} \tag{9}$$

and $\sigma_1 > \sigma_2 > \sigma_3 > \ldots > \sigma_n$. What this technique effectively does is prescribe a specific linear combination of the right singular vectors, $\mathbf{V}^{T}$, to construct the solution vector. Since these left singular vectors are orthogonal, they span the space of the

solution vector. Linear combinations of these vectors therefore produce unique solutions to the problem, equation (6). The magnitude of the singular values, σ_j, relative to the maximum value, σ_1, are an indication of how "ill-conditioned" **R** is. Ill-conditioning can arise from model symmetries or attempts to adjust excessive numbers of parameters. This problem is flagged, however, by use of the present scheme. "Small" singular values are not inverted in (9). Instead a zero is put in place of the quotient. This effectively zero's out the corresponding right singular vector from the linear combination comprising the solution vector. Note that the resulting solution is no longer unique, however. This clearly shows that the criteria used to select the linear combination of right singular vectors can significantly affect the solution vector. Some criteria used for selecting linear combinations of the singular vectors are documented by Hemez and Farhat [92] and Golub and VanLoan [93]. Experience with the present technique has shown that **R**, as formulated in the following sections, is well conditioned in most cases and insertion of zero's in (9) is unnecessary.

Construction of R

As already mentioned, the present model adjustment technique seeks to find adjustments to parameters of elements inherent in the finite element formulation. Because of this, there is opportunity to adjust only those elements for which the parameters have a measure of uncertainty. These elements may be near some geometric feature, such as a boundary or have some mass uncertainty such as may arise from the application of instrumentation. Element types and associated degree's of freedom are therefore known. Explanation of the construction of **R** best proceeds by example. Consider the two element model of an axial rod shown in Figure 26. Element one is on the left and element two is on the right. Nodes are numbered as shown.

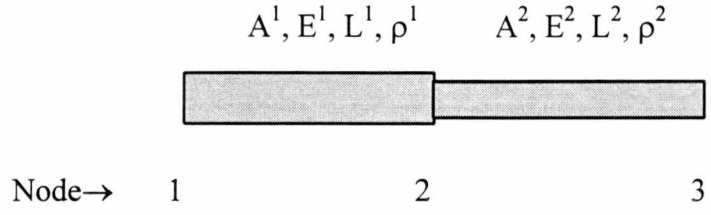


Figure 26. Axial bar finite element model

The element stiffness and mass matrices for each of the two elements are

$$\mathbf{k}^e = \frac{A^e E^e}{L^e}\begin{pmatrix} 1 & -1 \\ -1 & 1 \end{pmatrix} = P_1^e\left(\bar{\mathbf{k}}\right), \quad \mathbf{m}^e = \frac{\rho^e A^e L^e}{2}\begin{pmatrix} 1 & 0 \\ 0 & 1 \end{pmatrix} = P_2^e\left(\delta_{ij}\right), \tag{10}$$

where the superscript, e, identifies the element and has values of 1 and 2, A^e is the cross sectional area of the element, E^e is Young's modulus for the element, L^e is the length of the element, ρ^e is the mass density and δ_{ij} is the Kronecker delta. Perturbations in each of these expressions are made by perturbations in the two parameters,

$$\Delta\mathbf{k}^e = \Delta\frac{A^e E^e}{L^e}\begin{pmatrix} 1 & -1 \\ -1 & 1 \end{pmatrix} = \Delta P_1^e\left(\bar{\mathbf{k}}\right), \quad \Delta\mathbf{m}^e = \Delta\frac{\rho^e A^e L^e}{2}\begin{pmatrix} 1 & 0 \\ 0 & 1 \end{pmatrix} = \Delta P_2^e\left(\delta_{ij}\right), \tag{11}$$

Formally writing out equation (2) using equations (10) and (11) results in

$$\begin{pmatrix} \Delta P_1^1 & -\Delta P_1^1 & 0 \\ -\Delta P_1^1 & \Delta P_1^1 + \Delta P_1^2 & -\Delta P_1^2 \\ 0 & -\Delta P_1^2 & \Delta P_1^2 \end{pmatrix}\begin{Bmatrix} \varphi_{t1} \\ \varphi_{t2} \\ \varphi_{t3} \end{Bmatrix} - \Omega_t\begin{pmatrix} \Delta P_2^1 & 0 & 0 \\ 0 & \Delta P_2^1 + \Delta P_2^2 & 0 \\ 0 & 0 & \Delta P_2^2 \end{pmatrix}\begin{Bmatrix} \varphi_{t1} \\ \varphi_{t2} \\ \varphi_{t3} \end{Bmatrix} =$$

$$-\begin{pmatrix} P_1^1 & -P_1^1 & 0 \\ -P_1^1 & P_1^1 + P_1^2 & -P_1^2 \\ 0 & -P_1^2 & P_1^2 \end{pmatrix}\begin{Bmatrix} \varphi_{t1} \\ \varphi_{t2} \\ \varphi_{t3} \end{Bmatrix} + \Omega_t\begin{pmatrix} P_2^1 & 0 & 0 \\ 0 & P_2^1 + \Delta P_2^2 & 0 \\ 0 & 0 & P_2^2 \end{pmatrix}\begin{Bmatrix} \varphi_{t1} \\ \varphi_{t2} \\ \varphi_{t3} \end{Bmatrix} = \vec{\beta}. \tag{12}$$

Carrying out the multiplications on the left hand side of equation (12) and factoring out the ΔP's results in

$$\begin{pmatrix} \varphi_{i1}-\varphi_{i2} & 0 & -\Omega_i\varphi_{i1} & 0 \\ -(\varphi_{i1}-\varphi_{i2}) & \varphi_{i2}-\varphi_{i3} & -\Omega_i\varphi_{i2} & -\Omega_i\varphi_{i2} \\ 0 & -(\varphi_{i2}-\varphi_{i3}) & 0 & -\Omega_i\varphi_{i3} \end{pmatrix} \begin{Bmatrix} \Delta P_1^1 \\ \Delta P_1^2 \\ \Delta P_2^1 \\ \Delta P_2^2 \end{Bmatrix} = \bar{\beta} . \qquad (13)$$

The matrix in equation (13) is defined as the **R** matrix (for only one mode, c.f. equation (6)). Note that if it is known *apriori* that certain elements do not need modification then all ΔP's associated with these elements are zero and the corresponding columns of **R** can be deleted. Further, the columns of **R** are associated with either stiffness or mass parameters. Consequently, if only stiffness adjustments are sought, the mass parameter change is zero and the corresponding column of **R** is deleted and *vise-versa*. In cases where parameters, and consequently the perturbations in parameters, are the same for several elements, column entries corresponding to those elements in **R** add. This can be seen by requiring that entries in $\Delta\bar{P}$ are equal for each of these elements.

The matrix **R** will only contain rows corresponding to the degrees of freedom (DOF's) of the elements being modified. This can be seen by consideration of equation (2). Partitioning the $\Delta\mathbf{K}$ and $\Delta\mathbf{M}$ matrices according to the DOF's of the elements to be modified, it is apparent that non-zero entries are confined to these DOF's. Further, in order to maintain the equality in (2) it is evident that the only non-zero entries in $\bar{\beta}$ also correspond to these DOF's. Consequently, only the corresponding rows of $\bar{\beta}$ are retained. This dramatically reduces the size of the matrices involved and improves the computational efficiency of the present method.

Equation (13) will now be regenerated using *perturbation finite elements*, which will be defined directly, to demonstrate the required construction technique for computer implementation. For each element, an elemental part of the eigenproblem is formulated as follows:

$$\left(\Delta\mathbf{k}^e - \Omega_t \Delta\mathbf{m}^e\right)\vec{\varphi}_{t\,local} = \left[\Delta P_1^e\left(\bar{\mathbf{k}}\right) - \Omega_t \Delta P_2^e\left(\delta_{ij}\right)\right]\vec{\varphi}_{t\,local} \tag{14}$$

where each part of equation (14) is as defined previously and $\vec{\varphi}_{t\,local}$ are the modal displacements associated with the degrees of freedom of element, e (e.g., $\vec{\varphi}_{t\,local}$ has two elements for the axial bar). Locator vectors, $\bar{L}$, are defined which locate each of the $\vec{\varphi}_{t\,local}$ in $\vec{\varphi}_t$. $\bar{L}$, therefore, has the identification numbers of the global degrees of freedom as entries. For example, element 1 of the model shown in Figure 26 has locator vector, $\bar{L} = \lfloor 1,\ 2 \rfloor$, and for element 2, $\bar{L} = \lfloor 2,\ 3 \rfloor$. Continuing the development and considering element 2 of Figure 26,

$$\Delta P_1^2 \begin{pmatrix} 1 & -1 \\ -1 & 1 \end{pmatrix} \begin{Bmatrix} \varphi_{t2} \\ \varphi_{t3} \end{Bmatrix} - \Omega_t \Delta P_2^2 \begin{pmatrix} 1 & 0 \\ 0 & 1 \end{pmatrix} \begin{Bmatrix} \varphi_{t2} \\ \varphi_{t3} \end{Bmatrix} = \begin{Bmatrix} \varphi_{t2} - \varphi_{t3} \\ -\left(\varphi_{t2} - \varphi_{t3}\right) \end{Bmatrix} \Delta P_1^2 - \Omega_t \begin{Bmatrix} \varphi_{t2} \\ \varphi_{t3} \end{Bmatrix} \Delta P_2^2 \tag{15}$$

or

$$\begin{pmatrix} \varphi_{t2} - \varphi_{t3} & -\Omega_t \varphi_{t2} \\ -\left(\varphi_{t2} - \varphi_{t3}\right) & -\Omega_t \varphi_{t3} \end{pmatrix} \begin{Bmatrix} \Delta P_1^2 \\ \Delta P_2^2 \end{Bmatrix} \text{ or } \left(\left[\bar{\mathbf{k}}\right] \begin{Bmatrix} \varphi_{t2} \\ \varphi_{t3} \end{Bmatrix} \ \vdots\ -\Omega_t \begin{Bmatrix} \varphi_{t2} \\ \varphi_{t3} \end{Bmatrix} \right) \begin{Bmatrix} \Delta P_1^2 \\ \Delta P_2^2 \end{Bmatrix}. \tag{16}$$

The matrix to the left of $\Delta\vec{P}$ in equation (16) is defined as the *perturbation finite element* for the one dimensional axial bar element. Similar results can be generated for the first element in Figure 26 except that the subscripts associated with the φ_t's would be 1 and 2 rather than 2 and 3 and the superscripts on the parameters would be 1's. This structure is used assemble **R**. To do this, it is necessary to define a second locator vector, $\vec{Q}$, which locates the element $\Delta\vec{P}$ vectors in the overall $\Delta\vec{P}$ vector from equation (6). $\vec{Q}$, in effect, keeps track of the superscripts associated with each of the individual parameters. Considering again, element 2 from the example, the elements in **R** would be located row-wise by $\bar{L}$ and column-wise by $\vec{Q}$ as shown in Figure 27.

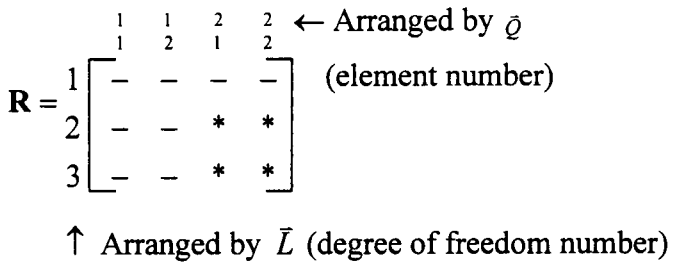


Figure 27. Assembly of **R**.

Two dimensional axial bar perturbation finite element

Since the technique described in the previous sections is based largely on the finite element method, it is extendable to other types of elements as well. The two dimensional axial bar perturbation finite element is derived in a similar manner to the one dimensional case already given. Consider now the two dimensional axial beam element shown in Figure 28.

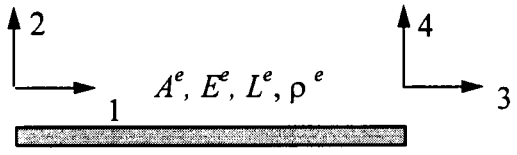


Figure 28. Two dimensional axial bar finite element.

The stiffness and mass matrices for this element are [94]

$$\mathbf{k}^e = \frac{A^e E^e}{L^e}\begin{pmatrix} l^2 & lm & -l^2 & -lm \\ lm & m^2 & -lm & -m^2 \\ -l^2 & -lm & l^2 & lm \\ -lm & -m^2 & lm & m^2 \end{pmatrix} \stackrel{\Delta}{=} P_1^e(\bar{\mathbf{k}}),$$

$$\mathbf{m}^e = \frac{\rho^e A^e L^e}{2}\begin{pmatrix} 1 & 0 & 0 & 0 \\ 0 & 1 & 0 & 0 \\ 0 & 0 & 1 & 0 \\ 0 & 0 & 0 & 1 \end{pmatrix} \stackrel{\Delta}{=} P_2^e(\delta_{ij}), \text{ i, j = 1 to 4,} \tag{17}$$

where $l=x_2-x_1/L^e$ and $m=y_2-y_1/L^e$. Perturbations are again introduced in terms of the parameters as $\Delta\mathbf{k}^e = \Delta P_1^e(\bar{\mathbf{k}})$ and $\Delta\mathbf{m}^e = \Delta P_2^e(\delta_{ij})$ and the elemental eigenproblem is formulated as in equation (14) resulting in (after rearranging)

$$\begin{pmatrix} l^2\varphi_{t1} + lm\varphi_{t2} - l^2\varphi_{t3} - lm\varphi_{t4} & -\Omega_t\varphi_{t1} \\ lm\varphi_{t1} + m^2\varphi_{t2} - lm\varphi_{t3} - m^2\varphi_{t4} & -\Omega_t\varphi_{t2} \\ -l^2\varphi_{t1} - lm\varphi_{t2} + l^2\varphi_{t3} + lm\varphi_{t4} & -\Omega_t\varphi_{t3} \\ -lm\varphi_{t1} - m^2\varphi_{t2} + lm\varphi_{t3} + m^2\varphi_{t4} & -\Omega_t\varphi_{t4} \end{pmatrix} \begin{Bmatrix} \Delta P_1^e \\ \Delta P_2^e \end{Bmatrix} \stackrel{\Delta}{=}$$

$$\left([\bar{\mathbf{k}}]\bar{\varphi}_{t\ local} \;\vdots\; -\Omega_t\bar{\varphi}_{t\ local}\right)\{\Delta P^e\}. \tag{18}$$

The matrix in equation (18) defines the perturbation finite element for the two dimensional axial rod. Note that it is the same as the one dimensional rod element except for the change in $[\bar{\mathbf{k}}]$ and $\bar{\varphi}_{t\ local}$ now has dimension 4.

Three dimensional eight node isoparametric perturbation finite element

Extension of the technique to more complex three dimensional elements proceeds naturally. Consider the definition of the element stiffness matrix of the 8-node isoparametric brick element [95],

$$\mathbf{k}^e = \int_{-1}^{1}\int_{-1}^{1}\int_{-1}^{1} \mathbf{B}^T \mathbf{C} \mathbf{B} |\det \mathbf{J}| d\xi d\eta d\zeta, \tag{19}$$

where **B** is the 6 x 24 matrix given by,

$$\mathbf{B} = \begin{pmatrix} \frac{\partial N_1}{\partial x} & 0 & 0 & \cdots & \frac{\partial N_8}{\partial x} & 0 & 0 \\ 0 & \frac{\partial N_1}{\partial y} & 0 & \cdots & 0 & \frac{\partial N_8}{\partial y} & 0 \\ 0 & 0 & \frac{\partial N_1}{\partial z} & \cdots & 0 & 0 & \frac{\partial N_8}{\partial z} \\ \frac{\partial N_1}{\partial y} & \frac{\partial N_1}{\partial x} & 0 & \cdots & \frac{\partial N_8}{\partial y} & \frac{\partial N_8}{\partial x} & 0 \\ 0 & \frac{\partial N_1}{\partial z} & \frac{\partial N_1}{\partial y} & \cdots & 0 & \frac{\partial N_8}{\partial z} & \frac{\partial N_8}{\partial y} \\ \frac{\partial N_1}{\partial z} & 0 & \frac{\partial N_1}{\partial x} & \cdots & \frac{\partial N_8}{\partial z} & 0 & \frac{\partial N_8}{\partial x} \end{pmatrix}. \tag{20}$$

In equation (20), the N_i are the element shape functions, **J** is the Jacobian relating the derivatives of the shape functions in global coordinates to the natural coordinates, ξ, η, and ζ, |det **J**| is the determinant of the Jacobian, and **C** is the material matrix given by

$$\mathbf{C} = \frac{E}{(1+\nu)(1-2\nu)} \begin{pmatrix} 1-\nu & \nu & \nu & 0 & 0 & 0 \\ \nu & 1-\nu & \nu & 0 & 0 & 0 \\ \nu & \nu & 1-\nu & 0 & 0 & 0 \\ 0 & 0 & 0 & \frac{1}{2}-\nu & 0 & 0 \\ 0 & 0 & 0 & 0 & \frac{1}{2}-\nu & 0 \\ 0 & 0 & 0 & 0 & 0 & \frac{1}{2}-\nu \end{pmatrix}. \tag{21}$$

Two stiffness parameters are now defined with respect to the material matrix, **C**:

$$P_1^e = \frac{E}{(1+\nu)(1-2\nu)} \quad , \quad P_2^e = P_1^e \nu \, . \tag{22}$$

Substituting (22) into (21) results in

$$\mathbf{C}^e = \begin{pmatrix} P_1^e - P_2^e & P_2^e & P_2^e & 0 & 0 & 0 \\ P_2^e & P_1^e - P_2^e & P_2^e & 0 & 0 & 0 \\ P_2^e & P_2^e & P_1^e - P_2^e & 0 & 0 & 0 \\ 0 & 0 & 0 & \frac{P_1^e}{2} - P_2^e & 0 & 0 \\ 0 & 0 & 0 & 0 & \frac{P_1^e}{2} - P_2^e & 0 \\ 0 & 0 & 0 & 0 & 0 & \frac{P_1^e}{2} - P_2^e \end{pmatrix} . \tag{23}$$

Equation (23) can be rearranged to produce

$$\mathbf{C}^e = P_1^e \begin{pmatrix} 1 & 0 & 0 & 0 & 0 & 0 \\ 0 & 1 & 0 & 0 & 0 & 0 \\ 0 & 0 & 1 & 0 & 0 & 0 \\ 0 & 0 & 0 & \frac{1}{2} & 0 & 0 \\ 0 & 0 & 0 & 0 & \frac{1}{2} & 0 \\ 0 & 0 & 0 & 0 & 0 & \frac{1}{2} \end{pmatrix} + P_2^e \begin{pmatrix} -1 & 1 & 1 & 0 & 0 & 0 \\ 1 & -1 & 1 & 0 & 0 & 0 \\ 1 & 1 & -1 & 0 & 0 & 0 \\ 0 & 0 & 0 & -1 & 0 & 0 \\ 0 & 0 & 0 & 0 & -1 & 0 \\ 0 & 0 & 0 & 0 & 0 & -1 \end{pmatrix}$$

$$= P_1^e \mathbf{D}_1 + P_2^e \mathbf{D}_2 \, . \tag{24}$$

Substituting equation (24) into (19) yields

$$\mathbf{k}^e = P_1^e \int_{-1}^{1}\int_{-1}^{1}\int_{-1}^{1} \mathbf{B}^T \mathbf{D}_1 \mathbf{B} |\det \mathbf{J}| d\xi d\eta d\zeta + P_2^e \int_{-1}^{1}\int_{-1}^{1}\int_{-1}^{1} \mathbf{B}^T \mathbf{D}_2 \mathbf{B} |\det \mathbf{J}| d\xi d\eta d\zeta \tag{25}$$

with P_1^e and P_2^e factored out of the integrations since they are constants.

The lumped mass matrix for the 8-node isoparamatric element is:

$$\mathbf{m}^e = P_3^e \frac{\delta_{ij}}{8} \int_{-1}^{1}\int_{-1}^{1}\int_{-1}^{1} |\det \mathbf{J}|\, d\xi\, d\eta\, d\zeta \quad i,j = 1,2,\ldots 24, \tag{26}$$

where $P_3^e = \rho^e$, the mass density of the material and the integral represents the volume of the element.

Perturbations in the element stiffness and mass representations are now introduced in the parameters as before;

$$\Delta\mathbf{k}^e = \Delta P_1^e \int_{-1}^{1}\int_{-1}^{1}\int_{-1}^{1} \mathbf{B}^T\mathbf{D}_1\mathbf{B}|\det \mathbf{J}|d\xi d\eta d\zeta + \Delta P_2^e \int_{-1}^{1}\int_{-1}^{1}\int_{-1}^{1} \mathbf{B}^T\mathbf{D}_2\mathbf{B}|\det \mathbf{J}|d\xi d\eta d\zeta$$

$$= \Delta P_1^e \mathbf{S}_1 + \Delta P_2^e \mathbf{S}_2 \tag{27}$$

and

$$\Delta\mathbf{m}^e = \Delta P_3^e \frac{\delta_{ij}}{8} \int_{-1}^{1}\int_{-1}^{1}\int_{-1}^{1} |\det \mathbf{J}|\, d\xi\, d\eta\, d\zeta \quad i,j = 1,2,\ldots 24,$$

$$= \Delta P_3^e \mathbf{S}_3. \tag{28}$$

Note that changes in the geometry of the element are not permitted. Substituting equations (28) and (27) into (14) and factoring out the ΔP_i^e's produces

$$\left[\mathbf{S}_1\bar{\varphi}_{t\,local} \;\vdots\; \mathbf{S}_2\bar{\varphi}_{t\,local} \;\vdots\; -\Omega_t\mathbf{S}_3\bar{\varphi}_{t\,local}\right]\begin{Bmatrix}\Delta P_1^e \\ \Delta P_2^e \\ \Delta P_3^e\end{Bmatrix} \tag{29}$$

with $\mathbf{S}_1$, $\mathbf{S}_2$, and $\mathbf{S}_3$ defined in equations (27) and (28). The bracketed portion of equation (29) is now defined as the *perturbation finite element* for the eight node isoparametric brick element, and is assembled into **R** row-wise according to degree of freedom and column-wise by element number and parameter as before.

Example application

The technique just described for the eight node isoparametric brick element was programmed for computer implementation to investigate its effectiveness. Numerical data (eigenvalues and eigenvectors) used for the check-out were generated using ALGOR™. All integrations within the computer implementation were carried out using two-point Gaussian quadrature [95]. The SVD routine was taken from LINPACK, a set of industry standard routines.

The model used for the check-out is shown in Figure 29. The baseline model was constructed using the same material properties for all the elements. The same model was then run with the perturbations noted in the figure. "Test data" consisted of the eigenvalues and eigenvectors obtained from the solution with the perturbed material properties. The three baseline modes and the three modes resulting from the perturbations are shown in Figures 30 and 31 respectively. Since it was known up-front that only elements 8, 38, and 56 were perturbed from the baseline, these elements were selected for adjustment. In addition, two other elements, 10 and 59 were included in the solution even though no adjustments were needed. Computed parameters for these two elements should then have been unchanged. Results of the solution are compared in Table 2 with the expected values. As shown, the algorithm produced excellent results and correctly "focused" the adjustments to only the elements requiring adjustment.

Implementation using test data

The technique presented for adjusting analytical models is based on knowledge of the mode shape at each degree of freedom in the analytical model. Rarely, however, are that many measurements made during a test. More often, a significantly smaller number of measurements are made. Two options are, therefore, available to define $\vec{\varphi}_t$. First, the analytical model can be reduced to the number of degrees of freedom that are

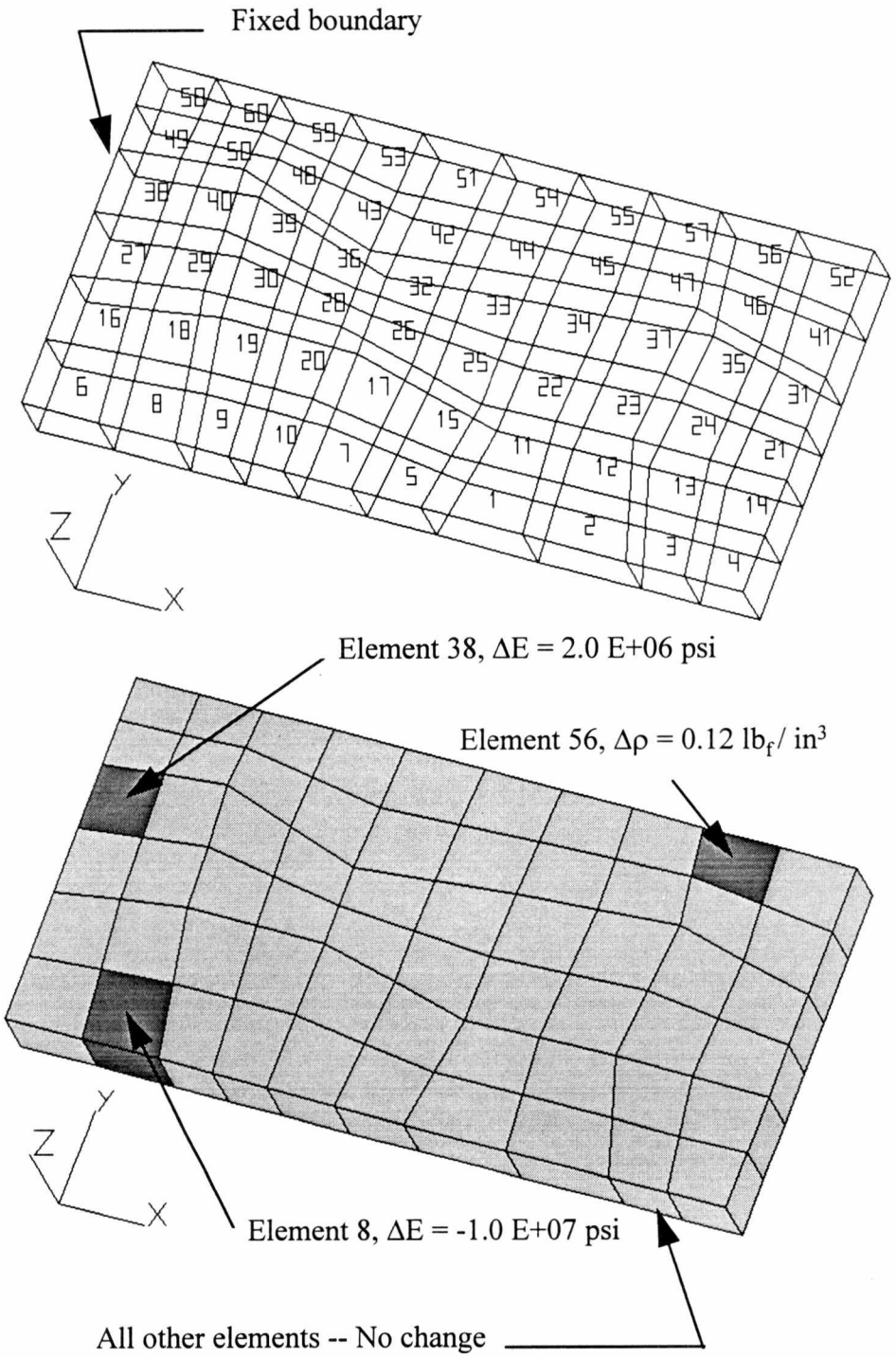


Figure 29. Adjustment technique demonstration model.

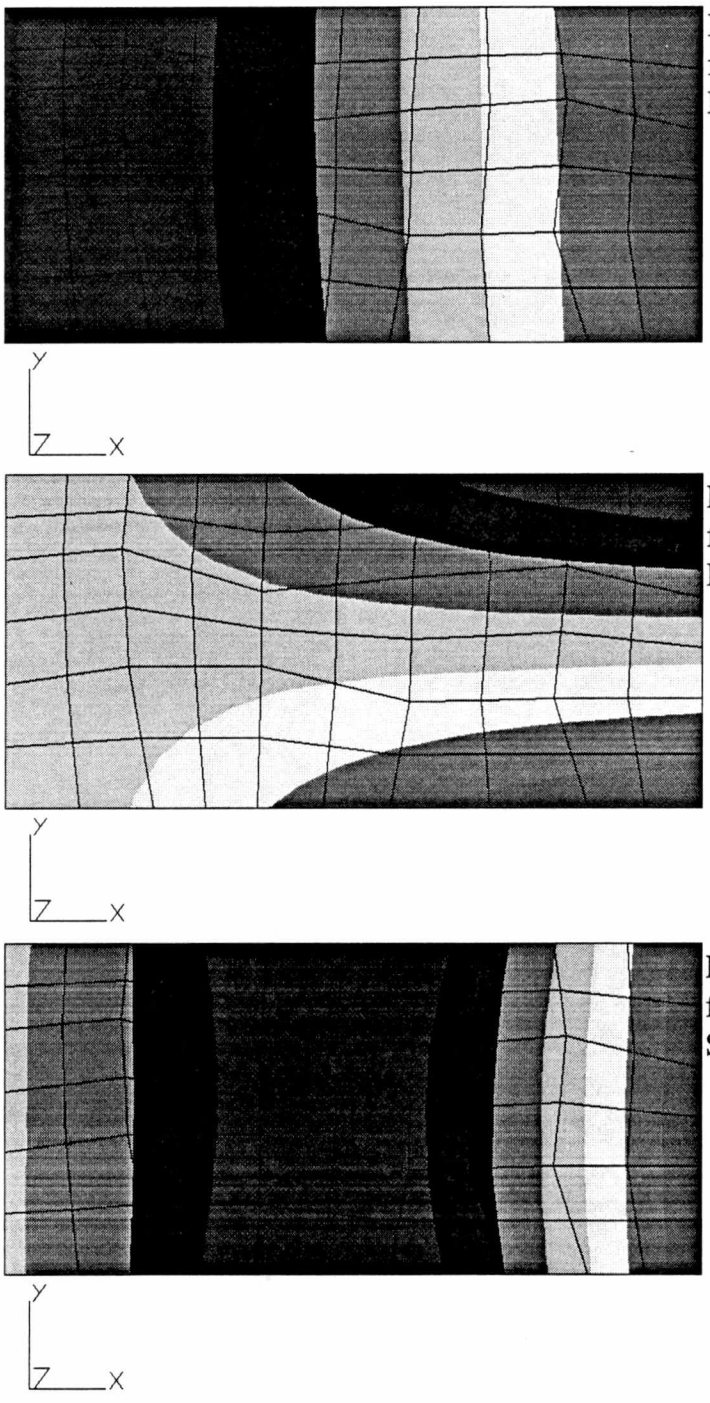
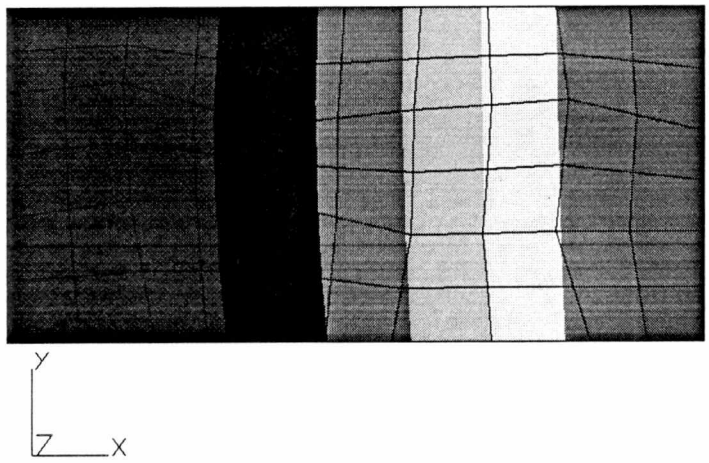
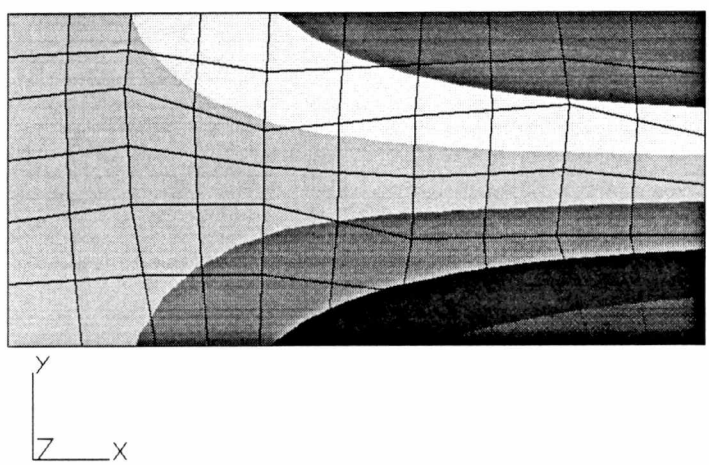


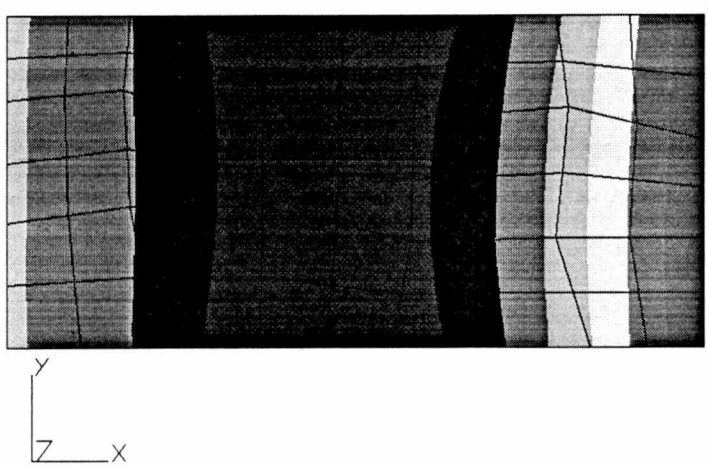
Figure 30. Baseline mode shapes and frequencies.



Mode 1
f=758 hz
First Bending



Mode 2
f=2593 hz
First Torsion



Mode 3
f=4797 hz
Second Bending

Figure 31. Perturbed mode shapes and frequencies.

Table 2. Comparison of input material properties vs. solution.

Element	Perturbed Values			Solution		
Number	E	ν	ρ	E	ν	ρ
8	20,000,000.0	0.30	0.28	19,999,999.9	0.299999	0.28000
10	30,000,000.0	0.30	0.28	30,000,000.0	0.300000	0.27997
38	32,000,000.0	0.30	0.28	32,000,000.0	0.299999	0.28000
56	30,000,000.0	0.30	0.40	30,000,000.0	0.300000	0.39999
59	30,000,000.0	0.30	0.28	30,000,000.0	0.300000	0.28000

Three modes used in solution
E-Young's Modulus, psi
ν - Poisson's ratio
ρ - Weight density, lbf/in^3

measured using a Guyan reduction scheme [96]. Another option is to employ an expansion technique like that documented by Berman [78]. In Berman's scheme, the stiffness and mass matrices are partitioned according to the measured degrees of freedom as

$$\mathbf{K}_A = \begin{pmatrix} \mathbf{K}_{TT} & \mathbf{K}_{TA} \\ \mathbf{K}_{TA}^T & \mathbf{K}_{AA} \end{pmatrix}, \ \mathbf{M}_A = \begin{pmatrix} \mathbf{M}_{TT} & \mathbf{M}_{TA} \\ \mathbf{M}_{TA}^T & \mathbf{M}_{AA} \end{pmatrix} \quad \leftrightarrow \quad \begin{Bmatrix} \vec{\varphi}_T \\ \vec{\varphi}_A \end{Bmatrix} \tag{30}$$

where subscript "*T*" stands for "test" and subscript "*A*" stands for "analysis". Considering the eigenproblem to be solved,

$$\left(\mathbf{K}_A - \Omega_t \mathbf{M}_A\right)\vec{\varphi}_t = 0 \tag{31}$$

and substituting the elements of (30) into (31), the results is

$$\left(\begin{pmatrix} \mathbf{K}_{TT} & \mathbf{K}_{TA} \\ \mathbf{K}_{TA}^T & \mathbf{K}_{AA} \end{pmatrix} - \Omega_t \begin{pmatrix} \mathbf{M}_{TT} & \mathbf{M}_{TA} \\ \mathbf{M}_{TA}^T & \mathbf{M}_{AA} \end{pmatrix}\right) \begin{Bmatrix} \vec{\varphi}_T \\ \vec{\varphi}_A \end{Bmatrix} = \vec{0}. \tag{32}$$

Taking the bottom partition of (32) and solving for $\vec{\varphi}_A$ yields

$$\vec{\varphi}_A = -\left(\mathbf{K}_{AA} - \Omega_i \mathbf{M}_{AA}\right)^{-1}\left(\mathbf{K}_{TA}^T - \Omega_i \mathbf{M}_{TA}^T\right)\vec{\varphi}_T. \tag{33}$$

This value along with the $\vec{\varphi}_T$ are rearranged into the original order of the degrees of freedom of $\mathbf{K}_A$ and $\mathbf{M}_A$ to produce the eigenvector, $\vec{\varphi}_i$, used in the present model adjustment technique. Since this is an extrapolation technique, there will obviously be some noise in the eigenvector data.

This method was used to generate eigenvectors from the experimental data for the $12.5 \times 4.0 \times 0.188$ inch plate presented in previous sections. The model used for application of the technique to the experimental results is shown in Figure 32. This model had fewer degrees of freedom than that used in the analytical assessments presented previously because the prototype computer implementation had memory limitations that would not permit larger models to be run. (The code was not optimized for operation on a personal computer.) Consequently, the model was stiffer than would normally be expected. This significantly affected the magnitude of the eigenvalues but did not appreciably affect the characteristic shape of the eigenvectors. Experimental frequencies were scaled in an attempt to account for this. Two modes were available.

Only four displacement values were reliably measured. Additionally, displacements at elements containing strain gages were determined by scaling the analytical eigenvectors to match the experimental stress values. This provided an additional six displacement values. To enrich the Z-displacement "data pool" further, a cubic polynomial was fit between the experimental data. Since ten data points were available, a polynomial with ten coefficients was computed. The resulting functions for the two modes tested were

$$\begin{aligned} Z_{\text{mode 1}} = {} & 1.442689E-05x^3y^3 - 9.67981E-04x^3 + 6.32291E-03y^3 - \\ & 6.705523E-04x^2y^2 + 1.981465E-02x^2 - 3.666706E-02y^2 + \\ & 7.418412E-03xy - 3.110381E-02x + 4.836951E-02y + 3.702897E-03 \end{aligned} \tag{34}$$

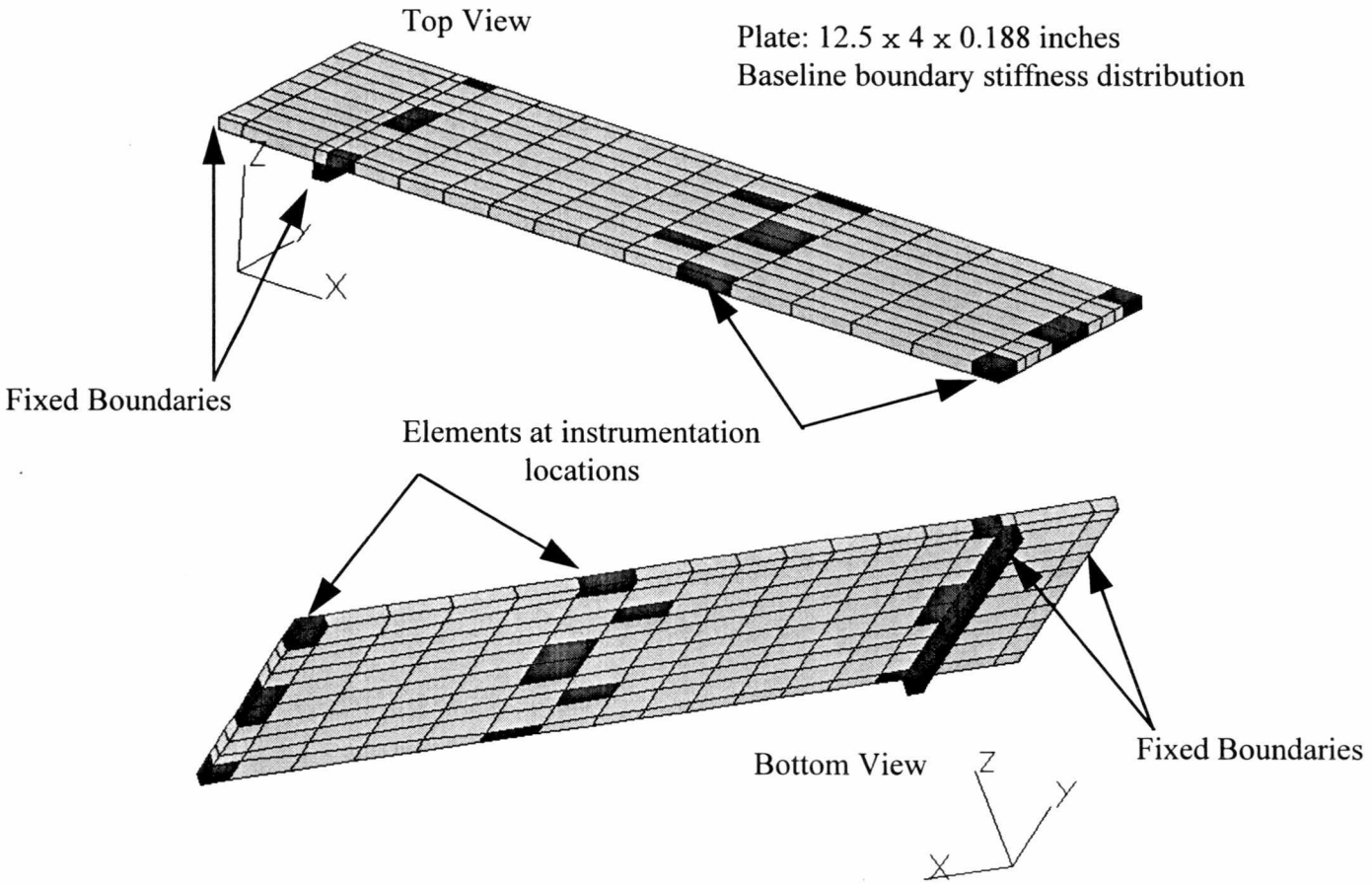


Figure 32. Model used with experimental data.

and

$$Z_{\text{mode 2}} = 2.154088E-05x^3y^3 - 6.371821E-03x^3 + 2.279781E-03y^3 - 1.126755E-03x^2y^2 + 1.73061E-01x^2 - 1.368952y^2 + 1.664756E-02xy - 1.115545x + 2.032003y + 5.183709E-02 \quad (35)$$

These functions were used to compute Z-displacements for each node of each cantilevered element and exactly reproduced experimental values at instrumentation locations. Displacements of nodes at elements aft of the boundary were assumed to be zero. Equation (33) was then used to compute X and Y-displacements for nodes of the cantilevered elements and all displacement components for the elements at the boundary. The resulting experimental displacement fields are shown in Figure 33. Note that the contour lines are curvy along the chord of the plate. This characteristic was not seen on any of the mode shapes that were photographed (cf. Appendix 2) and is likely a result of measurement bias in the experimental data. These two displacement fields were used in the model adjustment algorithm. The baseline eigenvectors are shown in Figure 34 for comparison.

It was assumed that differences between the experimental and analytical results were caused by mis-modeled boundary conditions and by the mass of the applied instrumentation. Consequently, adjustments to the stiffness of the elements at the boundary and to the mass of elements where instrumentation was applied were sought. The resulting adjustments are shown in Figures 35 and 36. As shown, the specified values of Young's Modulus at the boundary are much smaller than anticipated. This may be attributable to the introduction of the paper cushion which was put in place to help hold the blocks in place (see page 28). Adjustments to account for the weight of the accelerometers and mid-span strain gages were reasonable. These results were then included in the finite element formulation and new eigenvectors and eigenvalues were computed. The solution to the updated eigenproblem are presented in Figure 37 and as shown, tend to "smooth-out" the eigenvectors (cf. Figure 33). These results compare very well with the skewed node lines that were characteristic of the experimental node

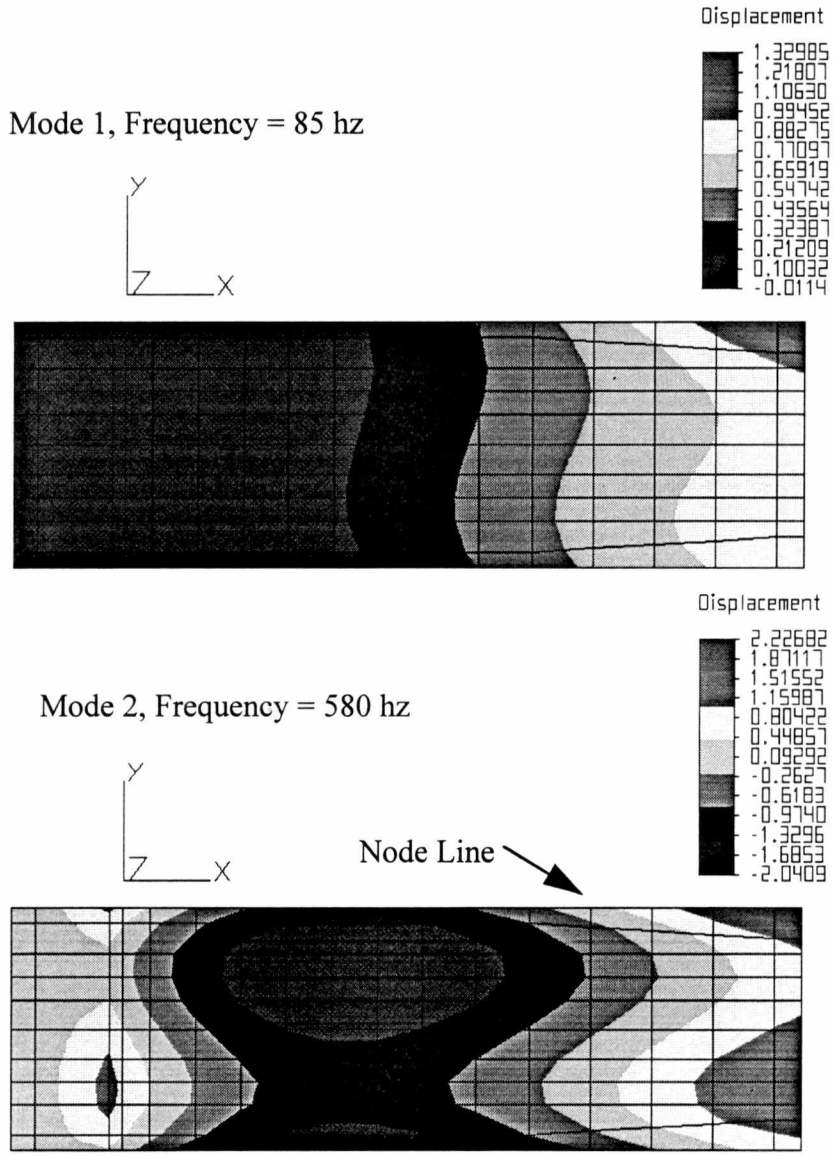


Figure 33. Experimental Z-displacement contours.

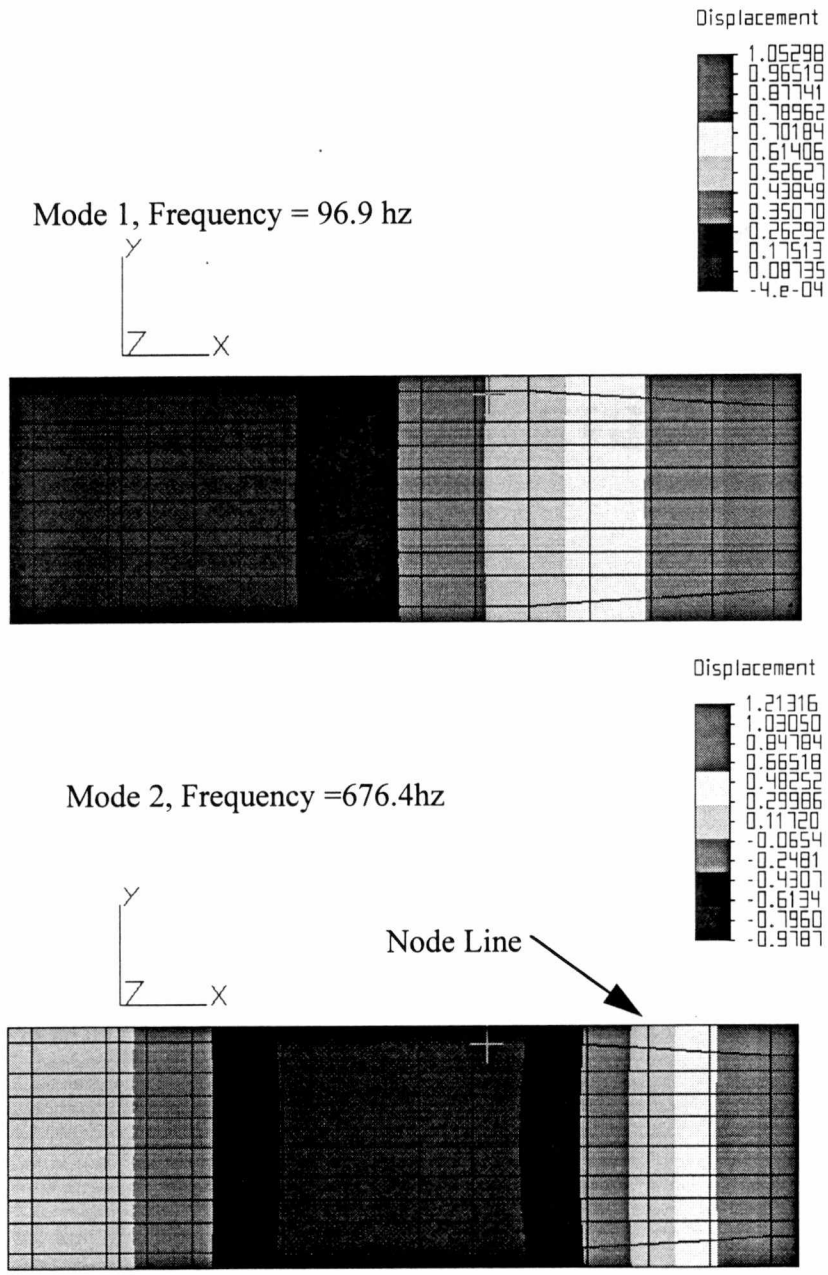


Figure 34. Baseline Z-displacement contours.

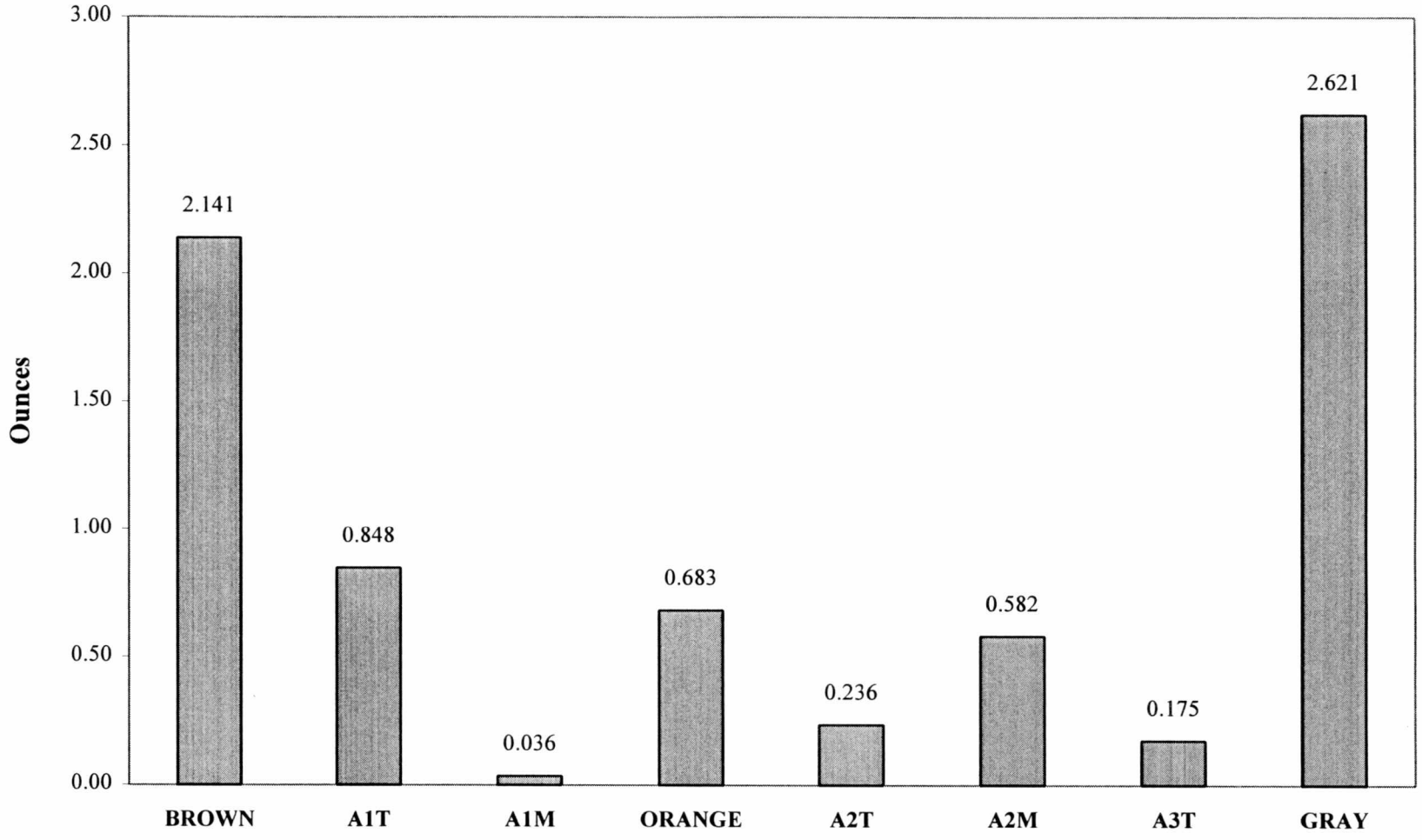


Figure 35. Computed weight of instrumentation.

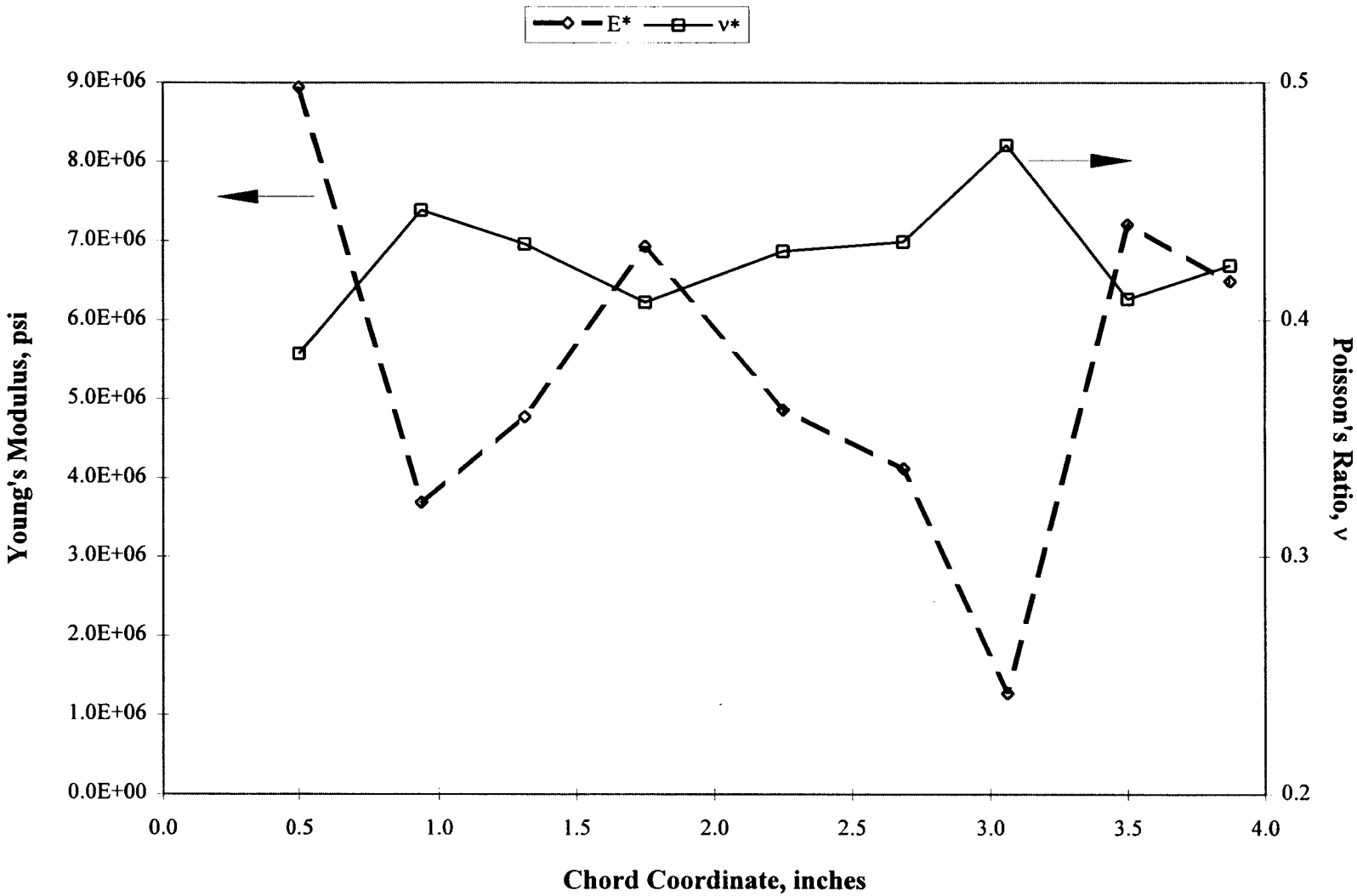


Figure 36. Computed stiffness parameters of boundary constraint elements.

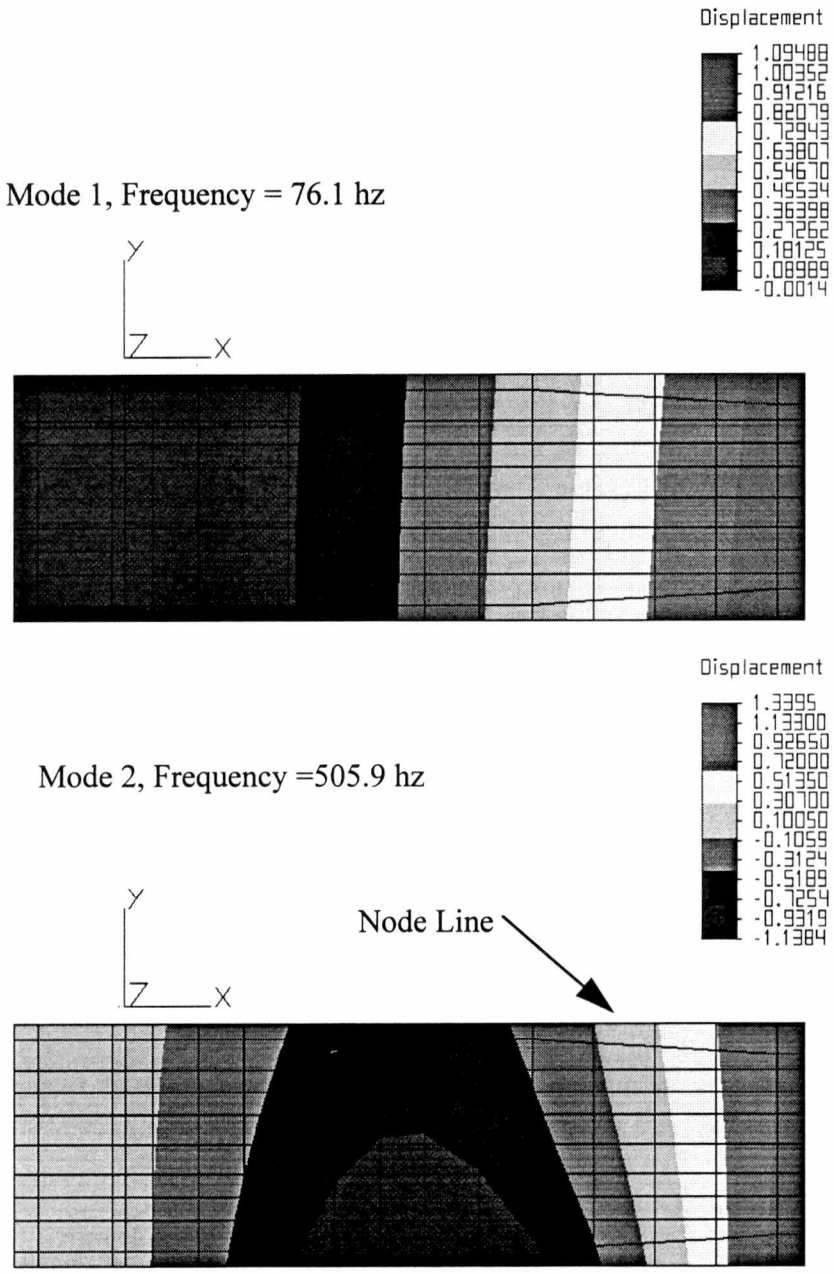


Figure 37. Z-displacement contours of adjusted model.

lines (cf. Figure 17). Modal frequencies with the adjustments were lower than the experimental values. During investigation of this result, it was found that the computed mass adjustments were very sensitive to the experimental modal frequencies used in the adjustment algorithm. Additional investigations were not pursued since values used for the experimental frequencies were scaled based on an artificially stiff analytical model. Future work is recommended that will permit use of more elements in the analytical model and bring about better agreement between the analytical and experimental modal frequencies.

8. CONCLUSIONS

The following conclusions are drawn as a result of this work:

- The stiffness, magnitude and distribution, of the surrounding structure under investigation can significantly affect the modal characteristics of the structure under evaluation. Variations in measured stresses as a function of stiffness distribution were as high as 30% when compared to stresses from the baseline stiffness distribution. Displacements at measurement locations varied by as much as 35% when compared to displacements from the baseline stiffness distribution. Finite element results were similar.
- The extent of the effect varies with the geometry of the component under investigation. Maximum variations occurred on the 12.5 × 4 × 0.188 inch plate.
- A new dynamic finite element model adjustment technique which uses *finite perturbation elements* has been developed that can accurately adjust an analytical structural model to better reflect experimental results. Application of the technique to a case with "perfect" numerical data produced exact computation of needed adjustments. The technique has the ability to focus adjustments to regions of the analytical model where modeling uncertainty is highest. Further, the technique can make adjustments to only the mass or stiffness or both. Lastly, the technique is extendible to other types of finite elements.
- The mass of experimental instrumentation can significantly affect the modal characteristics of a structure during modal test. Application of the model adjustment technique to the baseline analytical model of the 12.5 × 4 × 0.188 inch plate produced reasonable adjustments to the stiffness of the boundary and to the mass of elements where instrumentation was located which could account for differences between experimental and analytical results. This also highlights the diagnostic value of the present model adjustment technique. The adjustment algorithm successfully produced an analytical model that better reflects the actual displacement field and compensated for experimental measurement uncertainties.

9. RECOMMENDED FUTURE WORK

Several areas of future work are recommended to take advantage of the benefits of the present model adjustment technique.

- Streamline the present code that implements the algorithm to permit use of more elements.
- Incorporate "incompatible modes" to the formulation of the element mass and stiffness matrices as this has been shown to produce more realistic modal results with fewer elements. (Analytical results presented during the investigation of the boundary stiffness distributions used this formulation.)
- Extend the results to other types of isoparametric elements to permit greater flexibility in modeling.
- Continue development of the parabolic interpolation used in this work to reduce FFT amplitude attenuation.

LIST OF REFERENCES

[1] Manson, S.S., Meyer, A.J., Jr., Calvert, H.F., Hanson, M.P., "Factors AffectingVibration of Axial - Flow Compressor Blades," *Proceedings of the Society for Experimental Stress Analysis*, Vol. VII, No. 2, 1949, pp. 1-16.

[2] Hanson, M.P., Meyer, A.J., Jr., Manson, S.S., "A Method of Evaluating Loose-Blade Mounting as a Means of Suppressing Turbine and Compressor Blade Vibration," *Proceedings of the Society for Experimental Stress Analysis*, Vol. X, No. 2, 1953, pp.103-116.

[3] Danforth, C.E., Anderson, B.R., "Vibratory Stress Measurements in Multistage Compressor Blading," *Proceedings of the Society for Experimental Stress Analysis*, Vol. XIV, No. 1, 1955, pp. 21-34.

[4] Berger, R.A., Brunot, A.W., "Dynamic Stress Measurements in Gas Turbines," *Proceedings of the Society for Experimental Stress Analysis*, Vol. XII, No. 2, 1955, pp. 45-54.

[5] Baumberger, R., Hines, F., "Practical Reduction Formulas for Use on Bonded Wire Strain Gages in Two-Dimensional Stress Fields," *Proceedings of the Society for Experimental Stress Analysis*, Vol. II, No. 1, 1944, pp. 113-127.

[6] Kern, R.E., "The Stress Gage," *Proceedings of the Society for Experimental Stress Analysis*, Vol. IV, No. 1, 1946, pp. 124-129.

[7] Manson, S.S., Kemp, R.H., "High-Temperature Strain Gages and Their Application to Measurement of Vibratory Stresses in Turbosupercharger Buckets," *Proceedings of the Society for Experimental Stress Analysis*, Vol. V, No. 1, 1947, pp. 90-100.

[8] Day, E.E., "Characteristics of Electric Strain Gages at Elevated Temperatures," *Proceedings of the Society for Experimental Stress Analysis*, Vol. IX, No. 1, 1951, pp. 141-150.

[9] Edelman,S., Jones, E. Smith, E.R., "Some Developments in Vibration Measurement," *Journal of the Acoustical Society of America,* Vol. 27, No.4, July 1955, pp. 728-734.

[10] Hines, F.F., Weymouth, L.J., "Practical Aspects of Temperature Effects on Resistance Strain Gages," *Strain Gage Readings*, Vol IV, No. 1, April--May 1961, pp. 3-17.

[11] Ades, C.S., Lee, L.H.N., "Strain-gage Measurements in Regions of High Stress Gradient," *Experimental Mechanics*, June 1961, pp. 199-200.

[12] Brace, W.F., "Effect of Pressure on Electric-resistance Strain Gages," *Experimental Mechanics*, July 1964, pp.212-216.

[13] Milligan, R.V., "The Effects of High Pressure on Foil Strain Gages on Convex and Concave Surfaces," *Experimental Mechanics*, February 1965, pp. 59-64.

[14] Oi, K., "Transient Response of Bonded Strain Gages," *Experimental Mechanics*, September 1966, pp. 463-469.

[15] Troke, R.W., "Flat vs. Stacked Rosettes," *Experimental Mechanics*, May 1967, pp. 24A-28A.

[16] Mehrotra, C.L., Singh, A.N., "Strain Measurements in Regions of High Strain Gradients," *Experimental Mechanics*, August 1973, pp.345-347.

[17] Rosard, D.D., "Natural Frequencies of Twisted Cantilever Plates," *Journal of Applied Mechanics*, Vol. 20, June 1953, pp. 241-244.

[18] Carnegie, W., "Vibrations of Pre-Twisted Cantilever Blading," *Proceedings of the Institution of Mechanical Engineers*, Vol. 173, 1959, pp. 343-374.

[19] Isakson, G., Eisely, J.G., "Natural Frequencies in Coupled Bending and Torsion of Twisted Rotating and Non-Rotating Blades," CR-65, July 1964, NASA.

[20] Houbolt, J.C. Brooks, G. W., "differential Equations of Motion for Combined Flapwise Bending, Chordwise Bending, and Torsion of Twisted Nonuniform Rotor Blades," Rept. 1346, 1958, NACA.

[21] Anderson, R.G., Irons, B.M., Zienkiewicz, O.C., "Vibration and Stability of Plates using Finite Elements," *International Journal of Solids and Structures*, Vol. 4, October 1968, pp. 1031-1055.

[22] MacBain, J.C., "Vibratory Behavior of Twisted Cantilevered Plates," *Journal of Aircraft*, Vol. 12, No. 4, April 1975, pp. 343-349.

[23] Alderson, R.G., Peterson, M.R., Stockton, R.J., Tree, D.J., "Turbine Engine Components Stress-Simulation Program," AFAPL-TR-77-72, November 1977.

[24] Lyle, K.H., Leatherwood, J.D., Daniels, E.F., "Predicted and Measured Strain Responses of Isotropic Panels to Base Excitation," TM-4054, August 1988, NASA.

[25] Boày, C.G., "Free Vibration of Rectangular Isotropic Plates With and Without A Concentrated Mass," Technical Note, *Computers & Structures*, Vol. 48, No. 3, August 1993, pp. 529-533.

[26] Weiss, O., Moshaiov, A., "Vibration Analysis of Continuous Plate Structures Using Boundary Integrals," Computers & Structures, Vol. 47, No. 6, June 1993, pp. 971-976.

[27] Leissa, A., "Vibrational Aspects of Rotating Turbomacinery Blades," *Applied Mechanics Reviews*, Vol. 34, No. 5, May 1981, pp. 629-635.

[28] Dalley, J.W., Ripperger, E.A., "Experimental Values of Natural Frequencies for Skew and Rectangular Cantilever Plates," *Proceedings of the Society for Experimental Stress Analysis*, Vol. IX, No. 2, 1952, pp.51-66.

[29] Grinsted, B., "Nodal Pattern Analysis," *Proceeding of the Institution of Mechanical Engineers*, Vol. 166, No. 3, 1952, pp. 309-321.

[30] Chapman, G.M., Wang, X., "Interpretation of Experimental and Theoretical Data for Prediction of Mode Shapes of Vibrating Turbocharger Blades," *Journal of Vibration, Acoustics, Stress and Reliability in Design*, Vol. 110, January 1988, pp.53-58.

[31] Leissa, A., "Vibration of Plates," SP-160, 1969, NASA.

[32] O'Donnell, W.J., "The Additional Deflection of a Cantilever Due to the Elasticity of the Support," *Journal of Applied Mechanics*, Vol. 27, No. 1, March 1960, pp. 461-464.

[33] MacBain, J.C., Genin, J., "Natural Frequencies of a Beam Considering Support Characteristics," Journal of Sound and Vibration, Vol. 27, No. 2, 1973, pp. 197-206.

[34] Leissa, A.W., MacBain, J.C., Kielb, R.E., "Vibrations of Twisted Cantilevered Plates--Summary of Previous and Current Studies," *Journal of Sound and Vibration*, Vol. 96, No. 2, 1984, pp. 159-173.

[35] Kielb, R.E., Leissa, A.W., Macbain, J.C., "Vibrations of Twisted Cantilever Plates--A Comparison of Theoretical Results," I*nternational Journal for Numerical Methods in Engineering*, Vol. 21, 1985, pp.1365-1380.

[36] MacBain, J.C., Kielb, R.E., Leissa, A.W., "Vibrations of Twisted Cantilevered Plates--Experimental Investigation," *Journal of Engineering for Gas Turbines and Power,* Vol. 107, January 1985, pp. 187-196.

[37] Kielb, R.E., Leissa, A.W., MacBain, J.C., Carney, K.S., "Joint Research Effort on Vibrations of Twisted Plates," RP-1150, September 1985, NASA.

[38] Abell, E.E., Kielb, R.E., Henderson, P.J., "Structural Analysis of a Cooled, Directionally Solidified Turbine Blade," *Proceeding of the AIAA/ASME/SAE, 17th Structures, Structural Dynamics, and Materials Conference,* May 1976, pp.291-297.

[39] Kaza, K.R.V., Williams, M.H., Mehmed, O., Narayanan, G.V., "Aeroelastic Response of Metallic and Composite Propfan Models in Yawed Flow," TM-100964, July 1988, NASA.

[40] Wachter, J., Pfeiffer, R., Jarosch, J., "Some practical aspects of the interpretation of coupled LP-stage vibration," *IMechE*, C316/84, 1984, pp. 311-317.

[41] Brown, G.V., Kielb, R.E., Meyn, E.H., Morris, R.E., Posta, S.J., "Lewis Research Center Spin Rig and Its Use in Vibration Analysis of Rotating Systems," TP-2304, May 1984, NASA.

[42] Srinivasan, A.V., Cutts, D.G., "Aerodynamically Excited Vibrations on a Part-Span Shrouded Fan," *Journal of Engineering for Gas Turbines and Power*, Vol. 107, April 1985, pp. 399-407.

[43] Hasemann, H. Haupt, U., Jin, D., Seidel, U., Chen, J., Rautenberg, M., "Rotating Stall Flow and Dangerous Blade Excitation of Centrifugal Compressor Impeller--Part 2 Case Study of Blade Failure," *Proceedings of the International Gas Turbine and Aeroengine Congress and Exposition*, No. 91-GT-103, June 1991.

[44] Griffin, J.H. "Optimizing Instrumentation when Measuring Jet Engine Blade Vibration," *Proceedings of the International Gas Turbine and Aeroengine Congress and Exposition*, No. 91-GT-71, June 1991.

[45] Jeffers, J.D. II, Meece, C.E. Jr., "F100 Fan Stall Flutter Problem Review and Solution," *Journal of Aircraft*, Vol. 12, No. 4, pp. 350-359.

[46] Blakely, K., "Get the Model Right, Then Run the Analysis," *Machine Design*, October 24, 1991, pp. 109-114.

[47] Rizzo, A.R., "Estimating Errors in FE Analyses," *Mechanical Engineering*, May 1991, pp. 61-63.

[48] Larson, R.F., "Back to Basics Is Necessary for Viable FEA Modeling," *Plastics Engineering*, April 1992, pp. 29-33.

[49] Zienkiewicz, O.C., Zhu, J.Z., "A Simple Error Estimator and Adaptive Proceedure for Practical Engineering Analysis," *International Journal for Numerical Methods in Engineering*, Vol. 24, No. 3, 1987, pp. 337-357.

[50] Dow, J.O., Harwood, S.A., Jones, M.S., Stevenson, I., "Validation of a Finite Element Error Estimator," *AIAA Journal*, Vol. 29, No. 10, October 1991, pp. 1736-1742.

[51] Cook, R.D., "Error Estimators for Eigenvalues Computed from Discretized models of Vibrating Structures," Technical Notes *AIAA Journal*, Vol. 29, No. 9, September 1991, pp. 1527-1529.

[52] Sistla, R., "Error Analysis of Finite Element Results on Plates with Nonuniform Grids," *AIAA Journal*, Vol. 31, No. 6, June 1993, pp.1075-1076.

[53] Sistla, R., Thurston, G.A., "An Improved Error Analysis of Finite Element Solutions for Postbuckled Plates," *Proceedings of the 32nd AIAA/ASME/ASCE/AHS/ASC Structures, Structural Dynamics, and Materials Converence*, Paper No. AIAA-91-1003-CP, April 1991.

[54] Sistla, R., "Error Analysis of Finite Element Results on Plates wkth Nonuniform Grids," *Proceedings of the 33rd AIAA/ASME/ASCE/AHS/ASC Structures, Structural Dynamics, and Materials Converence*, No. AIAA-92-2353-CP, April 1992,pp. 479-489.

[55] Thurston, G.A., Sistla, R., "Elimination of Gibbs' Phenomena From Error Analysis of Finite Element Results," *Proceedings of the 31st AIAA/ASME/ASCE/AHS/ASC Structures, Structural Dynamics, and Materials Converence*, Paper No. AIAA-90-0932-CP, April 1990.

[56] Thurston, G.A., Reissner, J.E., Stein, P.A., Knight, N.F. Jr., "Error Analysis and Correction of Discrete Solutions from Finite Element Codes," *AIAA Journal*, Vol. 26, No. 4, April 1988, pp.446-453.

[57] Lin, R.M., Du, H., Ong, J.H., "Sensitivity Based Method for Structural Dynamic Model Improvement," *Computers & Structures*, Vol. 47, No. 3, May 1993, pp. 349-369.

[58] Ibrahim, R.A., "Structural Dynamics with Parameter Uncertainties," *Applied Mechanics Reviews*, Vol. 40, No. 3, 1987, pp. 309-328.

[59] Collins, J.D., Thomson, W.T., "The Eigenvalue Problem for Structural Systems with Statistical Properties," *AIAA Journal*, Vol.7, No.4, 1969, pp 642-648.

[60] Nelson, R.B., "Simplified Calculation of Eigenvector Derivatives," *AIAA Journal*, Vol. 14, No. 9, 1976, pp. 642-648.

[61] Chen, S-Y, Wei, F-S., "Systematic Approach for Eigensensitivity Analysis," Sistla, R., Thurston, G.A., "An Improved Error Analysis of Finite Element Solutions for Postbuckled Plates," *Proceedings of the 28th AIAA/ASME/ASCE/AHS/ASC Structures, Structural Dynamics, and Materials Converence*, No. 85-0635, April 1985.

[62] Peckner, D., "How to Use Probability Paper to Solve Materials Problems," *Materials in Design Engineering,* Vol. 52, No. 5, November 1960, pp.138-142.

[63] Perry, C.C., "Statistical Treatment of Experimental Data," *Experimental Mechanics*, April 1967, pp. 19A-25A.

[64] Neri, F., Patanè, S., Saitta, G., "Error-affected experimental data analysis: application to fitting procedures," *Measurement Science and Technology*, Vol. 1, No.10, October 1990, pp. 1007-1010.

[65] Dally, J.W., Riley, W.F., Experimental Stress Analysis, 3rd Ed., McGraw-Hill, New York, New York, 1991.

[66] Ewins, D.J., Modal Testing: Theory and Practice, John Wiley & Sons Inc., New York, New York, 1984.

[67] Beckwith, T.G., Buck, N.L., Mechanical Measurements, Addison-Wesley Publishing Company, Inc., Reading, Massachusetts, 1961.

[68] Perry, C.C., Lissner, H.R., The Strain Gage Primer, 2nd Ed., McGraw-Hill Book Company, Inc., New York, New York, 1962.

[69] Adibi, M.M., "Minimization of Uncertainties in Analog Measurements for Use in State Estimation," *IEEE Transactions on Power Systems*, Vol. 5, No. 3, August 1990, pp. 902-910.

[70] Adibi, M.M., "On Estimation of Uncertainties in Analog Measurements," *IEEE Transactions on Power Systems*, Vol. 5, No. 4, November 1990, pp. 1222-1230.

[71] Gutenberger, P.J., "A Study of the Variability of Strain Gage Results in a Round-Robin Study," *Experimental Techniques*, November/December 1991, pp. 8-9.

[72] Soucy, Y., Deering, D.W., "Effects of Data Acquisition Conditions on Modal Testing of a Simple Structure," *Experimental Techniques*, October 1989, pp. 35-39.

[73] Fessler, H., "The Importance of Attending to Details in Experimental Stress Analysis," *Experimental Mechanics*, Vol. 32, No. 1, March 1992, pp. 42-48.

[74] Nichol, K.L., "Strain Gage Placement Considerations for Dynamic Data Analysis," *Proceedings of the 32nd AIAA/ASME/ASCE/AHS/ASC Structures, Structural Dynamics, and Materials Converence*, No. 91-1250, April 1991.

[75] Wei, F-S., "Mass and Stiffness Interaction Effects in Analytical Model Modification," *Technical Notes AIAA Journal*, Vol. 28, No. 9, September 1990, pp.1686-1687.

[76] Wei, F-S., "Analytical Dynamic Model Improvement Using Vibration Test Data," *Technical Notes AIAA Journal*, Vol. 28, No. 1, January 1990, pp.175-177.

[77] Kabe, A.M., "Stiffness Matrix Adjustment Using Mode Data," *AIAA Journal*, Vol. 23, Sept 1985, pp. 1431-1436.

[78] Berman, A., Wei, F-S, "Automated Dynamic Analytical Model Improvement," CR-3452, July 1981, NASA.

[79] Wei, F-S., "Stiffness Matrix Correction from Incomplete Test Data," *AIAA Journal*, Vol. 18, No. 10, October 1980, pp.1274-1275.

[80] Berman, A., Nagy, E.J., "Improvement of a Large Analytical Model Using Test Data," *AIAA Journal*, Vol. 21, No. 8, August 1983, pp. 1168-1173.

[81] Berman, A., "Mass Matrix Correction Using an Incomplete Set of Measured Modes," Technical Notes, *AIAA Journal*, Vol. 17, No. 10, October 1979, pp. 1147-1148.

[82] Baruch, M., Bar-Itzhack, I.Y., "Optimal Weighted Orthogonalization of Measured Modes," *AIAA Journal*, Vol. 16, April 1978, pp 346-351.

[83] Berman, A., Flannelly, W.G., "The Theory of Incomplete Models of Dynamic Structures," *Proceedings of the 11th AIAA/ASME Structural Dynamics, and Materials Converence*, April 1970, pp.183-192.

[84] Berman, A., Fuh, J-S, "Automated Dynamic Analytical Model improvement for Damped Structures", CR-177945, September 1985, NASA .

[85] Tong, M., Liang, Z., Lee, G.C., "Correction Criteria of Finite Element Modeling in Structural Dynamics", *Journal of Engineering Mechanics*, Vol. 118, No.4, April 1992, pp.663-682.

[86] R.J. Glaser, C.P. Kuo, B.K. Wada, "Improvement of Structural Models Using Covariance Analysis and Nonlinear Generalized Least Squares," *AIAA Journal*, Vol. 30, No. 1, January 1992, pp. 226-233.

[87] "Metallic Materials and Elements for Aerospace Vehicle Structures", Military Standardization Handbook, Mil-HDBK-5D, June 1983.

[88] Brigham, E.O., The Fast Fourier Transform , Prentice Hall, Englewood Cliffs, New Jersey, 1974, pp. 140-146.

[89] Thompson, W.T., Theory of Vibration with Applications, 2nd Ed., Prentice Hall, Englewood Cliffs, New Jersey, 1981, pp. 197-201.

[90] Lim, T.W., "Submatrix Approach to Stiffness Matrix Correction Using Modal Test Data," *AIAA Journal*, Vol. 28, No. 6, June 1990, pp. 1123-1130.

[91] Farhat, C., Hemez, F.M., "Updating Finite element Dynamic Models Using an Element-by-Element Sensitivity Methodology," *AIAA Journal*, Vol. 31, No. 9, September 1993, pp. 1702-1711.

[92] Hemez, F.M., Farhat, C. , "Bypassing Numerical Difficulties Associated with Updating Simultaneously Mass and Stiffness Matrices," *AIAA Journal*, Vol. 33, No. 3, March 1995, pp. 539-546

[93] Golub, G.H., Van Loan, C.F., Matrix Computations, 2nd edition, The Johns Hopkins University Press, Baltimore, Maryland, 1990, p.427.

[94] Chandruppatla, T.R., Belegundu, A.D., Introduction to Finite Elements in Engineering, Prentice Hall, Englewood Cliffs, New Jersey, 1991, pp.104.

[95] Chandruppatla, T.R., Belegundu, A.D., Introduction to Finite Elements in Engineering, Prentice Hall, Englewood Cliffs, New Jersey, 1991, p. 262.

[96] Guyan, R.J., "Reduction of Stiffness and Mass Matrices," *AIAA Journal*, Vol. 3, No. 2, 1965, pp. 380-385.

APPENDICES

APPENDIX 1

Table A1-1. Tabulation of normalized displacement data.

Experimental & Finite Element Normalized Accelerometer Data, Mils Pk/Mil @ A3T												
2nd Bending			A1T		A2T		A1M		A2M		Avg Freq	Freq
CD	Plate I.D.	Repeat?	EXP	FEM	EXP	FEM	EXP	FEM	EXP	FEM	EXP	FEM
1	1200	P	0.8823	1.0000	0.8396	1.0118	0.0019	0.8898	1.0317	0.8898	129.50	125.55
2	1200	P	1.0370	1.0633	0.9081	1.0438	0.0021	0.9023	1.1894	0.9337	129.77	125.42
3	1200	P	0.8832	0.9712	0.8414	0.9972	0.8700	0.8842	1.0296	0.8699	129.94	125.35
4	1200	P	0.9240	1.0261	0.8573	1.0250	0.8829	0.8949	1.0719	0.9078	130.39	125.45
5	1200	P	1.0062	1.0000	0.8941	1.0118	0.7776	0.8899	1.1538	0.8899	129.86	125.39
6	1200	P	0.6922	1.0001	0.6294	1.0118	0.7679	0.8898	1.1003	0.8898	129.30	125.41
3rd Bending			A1T		A2T		A1M		A2M		Avg Freq	Freq
CD	Plate I.D.	Repeat?	EXP	FEM	EXP	FEM	EXP	FEM	EXP	FEM	EXP	FEM
1	1200	P	0.8389	1.0000	0.8333	1.0691	0.0025	0.5345	0.5736	0.5345	365.44	352.96
2	1200	P	0.8706	1.0156	0.8535	1.0773	0.0025	0.5312	0.6009	0.5414	367.07	352.59
3	1200	P	0.8438	0.9930	0.8396	1.0651	0.5352	0.5312	0.5698	0.5267	365.67	352.38
4	1200	P	0.8571	1.0062	0.8465	1.0723	0.5358	0.5325	0.5788	0.5365	365.76	352.71
5	1200	P	0.6496	1.0000	0.6395	1.0689	0.4097	0.5314	0.5785	0.5314	365.11	352.48
6	1200	P	0.6448	1.0000	0.6389	1.0690	0.4115	0.5322	0.5738	0.5322	365.23	352.60
5	1200	R	0.6505		0.6412		0.4118		0.5815		365.3400	
1st Bending			A1T		A2T		A1M		A2M		Avg Freq	Freq
CD	Plate I.D.	Repeat?	EXP	FEM	EXP	FEM	EXP	FEM	EXP	FEM	EXP	FEM
1	1288	P	0.8505	1.0000	0.8031	1.0004	0.3110	0.2877	0.1303	0.2877	36.82	37.47
2	1288	P	0.8333	0.9992	0.7912	1.0000	0.3078	0.2882	0.0804	0.2888	36.82	37.36
3	1288	P	0.8386	1.0004	0.7959	1.0006	0.2783	0.2892	0.0908	0.2889	36.47	37.32
4	1288	P	0.8356	0.9997	0.7965	1.0003	0.3154	0.2882	0.0829	0.2885	36.53	37.39
5	1288	P	0.8402	1.0000	0.8021	1.0004	0.3119	0.2887	0.1294	0.2887	36.62	37.36
6	1288	P	0.8359	1.0000	0.7990	1.0004	0.3117	0.2886	0.1294	0.2886	36.61	37.35
2nd Bending			A1T		A2T		A1M		A2M		Avg Freq	Freq
CD	Plate I.D.	Repeat?	EXP	FEM	EXP	FEM	EXP	FEM	EXP	FEM	EXP	FEM
1	1288	P	1.3418	1.0001	1.0359	1.0115	1.0043	-0.8906	1.4111	-0.8907	253.36	233.78
2	1288	P	1.1313	1.2122	0.9414	1.1187	0.9506	-0.9325	0.6648	-1.0380	253.91	233.08
3	1288	P	1.4172	0.9215	1.0729	0.9717	0.8295	-0.8754	0.8255	-0.8364	251.78	232.84
4	1288	P	1.4151	1.0778	1.0712	1.0508	1.0216	-0.9060	0.8203	-0.9446	252.67	233.33
5	1288	P	0.8846	1.0000	0.8303	1.0114	0.8865	-0.8908	0.9924	-0.8908	252.08	233.02
6	1288	P	1.0089	1.0002	0.8874	1.0115	0.9188	-0.8907	1.1115	-0.8908	252.77	233.14
1st Bending			A1T		A2T		A1M		A2M		Avg Freq	Freq
CD	Plate I.D.	Repeat?	EXP	FEM	EXP	FEM	EXP	FEM	EXP	FEM	EXP	FEM
1	8100	P	0.8713	1.0000	0.8312	1.0017	0.2812	0.2858	0.1352	0.2858	42.95	43.58
2	8100	P	0.8589	0.9993	0.8191	1.0013	0.2887	0.2859	0.1371	0.2865	42.68	43.52
3	8100	P	0.8524	1.0003	0.8107	1.0018	0.2864	0.2867	0.1320	0.2865	42.68	43.49
4	8100	P	0.8604	0.9997	0.8211	1.0015	0.2929	0.2860	0.1359	0.2863	42.60	43.53
5	8100	P	0.8515	1.0000	0.8157	1.0017	0.2874	0.2864	0.1320	0.2864	42.68	43.51
6	8100	P	0.8515	1.0000	0.8160	1.0017	0.2922	0.2863	0.1360	0.2863	42.60	43.51
5	8100	R	0.8360		0.8009		0.2904		0.1337		42.60	

Table A1-1 (concluded). Tabulation of normalized displacement data.

2nd Bending			A1T		A2T		A1M		A2M		Avg Freq	Freq
CD	Plate I.D.	Repeat?	EXP	FEM	EXP	FEM	EXP	FEM	EXP	FEM	EXP	FEM
1	8100	P	0.8498	1.0000	0.8501	1.0363	0.9032	-0.8999	0.9570	-0.8999	270.76	271.45
2	8100	P	0.8590	0.9907	0.8515	1.0314	0.9097	-0.8966	0.9686	-0.8949	270.27	271.05
3	8100	P	0.8377	1.0043	0.8368	1.0384	0.9022	-0.9016	0.9571	-0.9024	269.69	270.81
4	8100	P	0.8678	0.9962	0.8566	1.0342	0.9119	-0.8985	0.9743	-0.8978	270.55	271.17
5	8100	P	0.8561	1.0000	0.8525	1.0362	0.9070	-0.9001	0.9645	-0.9001	269.70	270.92
6	8100	P	0.8568	1.0000	0.8522	1.0362	0.9072	-0.8998	0.9656	-0.8998	270.15	271.05
4	8100	R	0.8651		0.8545		0.9122		0.9730		270.79	
3rd Bending			A1T		A2T		A1M		A2M		Avg Freq	Freq
CD	Plate I.D.	Repeat?	EXP	FEM	EXP	FEM	EXP	FEM	EXP	FEM	EXP	FEM
1	8100	P	0.8271	1.0000	1.0149	1.2383	0.5748	0.5621	0.5251	0.5621	758.58	762.05
2	8100	P	0.8405	0.9759	1.0070	1.2226	0.5622	0.5601	0.5425	0.5431	754.76	760.91
3	8100	P	0.7928	1.0111	0.9732	1.2437	0.5640	0.5552	0.5030	0.5631	753.96	760.22
4	8100	P	0.8655	0.9903	1.0242	1.2318	0.5636	0.5602	0.5611	0.5534	756.56	761.29
5	8100	P	0.8310	1.0000	1.0004	1.2370	0.5571	0.5571	0.5281	0.5571	753.48	760.51
6	8100	P	0.8364	1.0000	1.0047	1.2377	0.5631	0.5584	0.5412	0.5584	755.06	760.97
3	8100	R	0.7933		0.9720		0.5627		0.5021		753.23	
2nd Bending			A1T		A2T		A1M		A2M		Avg Freq	Freq
CD	Plate I.D.	Repeat?	EXP	FEM	EXP	FEM	EXP	FEM	EXP	FEM	EXP	FEM
1	8188	P	0.7928	1.0000	0.8074	1.0353	0.8614	-0.9012	0.8865	-0.9012	540.61	502.81
2	8188	P	0.7900	0.9746	0.8008	1.0219	0.8661	-0.8923	0.8939	-0.8873	536.93	500.72
3	8188	P	0.7885	1.0106	0.8040	1.0405	0.8603	-0.9052	0.8847	-0.9072	535.04	499.85
4	8188	P	0.8039	0.9903	0.8116	1.0301	0.8685	-0.8977	0.8965	-0.8958	536.65	501.49
5	8188	P	0.7584	1.0000	0.7907	1.0351	0.8470	-0.9015	0.8596	-0.9015	530.01	500.36
6	8188	P	0.7978	1.0000	0.0260	1.0351	0.8607	-0.9010	0.8831	-0.9010	535.52	500.93
2	8188	R	0.7927		0.8030		0.8671		0.8962		537.18	
5	8188	R	0.7584		0.7900		0.8482		0.8612		531.10	
3rd Bending			A1T		A2T		A1M		A2M		Avg Freq	Freq
CD	Plate I.D.	Repeat?	EXP	FEM	EXP	FEM	EXP	FEM	EXP	FEM	EXP	FEM
1	8188	P	0.7716	1.0000	0.9837	1.2339	0.5468	0.5346	0.5385	0.5346	1556.31	1350.00
2	8188	P	0.7901	0.9792	0.9911	1.2189	0.5359	0.5267	0.5488	0.5120	1549.51	1313.40
3	8188	P	0.7667	1.0102	0.9802	1.2367	0.5283	0.5187	0.5134	0.5258	1544.52	1289.10
4	8188	P	0.8207	0.9987	1.0216	1.2320	0.5381	0.5283	0.5629	0.5275	1553.00	1340.30
5	8188	P	0.7056	0.9999	0.9419	1.2307	0.5218	0.5220	0.4494	0.5220	1536.98	1288.80
6	8188	P	0.7861	1.0001	0.0188	1.2323	0.5235	0.5252	0.5202	0.5252	1546.01	1340.40
4	8188	R	0.8197		1.0191		0.5374		0.5620		1552.10	

Notes:
1. CD-Constraint Distribution Number
2. P/R-Primary/Repeat
3. Plate I.D.'s as per Figure 9
4. FEM-Finite Element Model
5. Frequencies in cycles/second
6. Accelerometer designations as in Figure 7
7. Units for displacement data are mils-peak/mil @ A3T

Table A1-2. Tabulation of stress data.

Combined Experimental & Finite Element Strain Gage Data, Clamping Line Gages

2nd Bending-1200			BLUE							RED							BLACK						
Stress Component (Psi/Mil Pk)--->			Sx		Sy		Txy		Freq	Sx		Sy		Txy		Freq	Sx		Sy		Txy		Freq
CD	Plate I.D.	Repeat?	EXP	FEM	EXP	FEM	EXP	FEM	EXP	EXP	FEM	EXP	FEM	EXP	FEM	EXP	EXP	FEM	EXP	FEM	EXP	FEM	EXP
1	1200	P	73.3	72.15	10.7	8.52	6.7	-5.00	129.50	69.9	77.81	21.2	23.16	9.5	0.00	129.50	71.4	72.15	11.8	8.52	7.5	5.00	129.50
2	1200	P	76.0	75.41	10.6	8.81	4.3	-4.40	129.77	78.6	80.06	23.7	23.98	11.2	0.45	129.77	82.2	72.96	13.8	8.53	8.9	5.76	129.77
3	1200	P	71.3	69.87	9.6	7.86	6.6	-5.02	129.94	69.3	76.36	21.9	22.92	9.3	-0.11	129.94	70.3	71.23	12.1	8.25	8.3	4.46	129.94
4	1200	P	74.2	73.74	11.2	8.98	6.5	-4.83	130.39	71.8	78.46	22.2	23.22	9.9	0.09	130.39	74.6	72.47	13.1	8.55	9.3	5.34	130.39
5	1200	P	74.4	71.55	10.7	8.05	5.0	-4.74	129.86	74.4	77.97	20.2	23.97	10.2	0.00	129.86	78.9	71.55	12.5	8.05	8.7	4.74	129.87
6	1200	P	72.9	72.16	11.2	8.77	7.6	-5.09	129.29	71.4	76.90	20.7	22.25	10.8	0.00	129.30	74.6	72.16	12.0	8.77	9.4	5.09	129.29
3rd Bending			BLUE							RED							BLACK						
Stress Component (Psi/Mil Pk)--->			Sx		Sy		Txy		Freq	Sx		Sy		Txy		Freq	Sx		Sy		Txy		Freq
CD	Plate I.D.	Repeat?	EXP	FEM	EXP	FEM	EXP	FEM	EXP	EXP	FEM	EXP	FEM	EXP	FEM	EXP	EXP	FEM	EXP	FEM	EXP	FEM	EXP
1	1200	P	217.7	218.83	34.9	29.12	8.3	3.22	365.45	192.6	219.57	59.9	66.81	2.7	0.00	365.46	209.4	218.83	36.7	29.12	8.3	-3.22	365.45
2	1200	P	224.2	218.15	35.0	28.68	7.1	1.92	367.06	202.7	220.07	62.6	67.51	4.7	-0.34	367.06	213.5	220.17	38.1	29.20	9.5	-4.05	367.06
3	1200	P	209.6	215.21	31.0	27.56	8.5	2.93	365.68	191.2	216.96	61.9	66.77	2.6	-0.18	365.68	204.8	215.13	38.1	28.14	9.7	-2.16	365.68
4	1200	P	220.8	219.21	36.7	29.97	8.4	2.94	365.76	192.7	218.74	60.7	66.13	3.7	0.21	365.77	211.5	219.17	39.3	29.20	11.4	-3.65	365.76
5	1200	P	215.5	215.96	35.3	27.56	29.5	2.33	365.10	189.8	219.42	52.2	69.43	25.8	0.00	365.10	205.4	215.96	33.7	27.56	30.5	-2.33	365.10
5	1200	R	215.4		35.1		28.5		365.35	190.2		52.7		25.1		365.35	205.1		33.4		29.4		365.35
6	1200	P	214.8	218.36	37.0	29.90	30.0	3.52	365.24	189.5	216.16	56.1	63.68	25.3	0.00	365.24	206.1	218.37	35.2	29.90	30.0	-3.53	365.24
1st Bending			BLUE							RED							BLACK						
Stress Component (Psi/Mil Pk)--->			Sx		Sy		Txy		Freq	Sx		Sy		Txy		Freq	Sx		Sy		Txy		Freq
CD	Plate I.D.	Repeat?	EXP	FEM	EXP	FEM	EXP	FEM	EXP	EXP	FEM	EXP	FEM	EXP	FEM	EXP	EXP	FEM	EXP	FEM	EXP	FEM	EXP
1	1288	P	19.1	19.34	2.5	1.16	1.3	2.96	36.82	18.3	23.78	4.7	6.64	1.5	0.00	36.82	19.1	19.34	2.6	1.16	0.7	-2.96	36.82
2	1288	P	18.7	19.16	2.2	1.12	0.8	2.78	36.82	18.3	23.70	4.8	6.66	1.4	-0.07	36.82	18.7	19.50	2.3	1.18	0.3	-3.07	36.82
3	1288	P	19.1	19.25	2.4	1.08	1.7	2.90	36.47	17.9	23.68	4.9	6.70	1.7	0.01	36.47	18.7	19.23	2.5	1.13	0.6	-2.82	36.47
4	1288	P	19.0	19.42	2.4	1.23	1.4	2.95	36.51	18.2	23.56	5.6	6.50	1.6	-0.01	36.52	18.6	19.44	2.4	1.18	0.5	-3.03	36.52
5	1288	P	18.9	19.18	2.1	1.06	1.5	2.83	36.61	17.5	23.98	3.6	7.02	1.3	0.00	36.61	20.1	19.18	6.0	1.06	1.6	-2.83	36.61
6	1288	P	18.9	19.48	2.2	1.26	1.5	3.02	36.61	17.3	23.26	3.8	6.22	1.4	0.00	36.61	19.3	19.48	2.7	1.26	0.8	-3.03	36.61
2nd Bending			BLUE							RED							BLACK						
Stress Component (Psi/Mil Pk)--->			Sx		Sy		Txy		Freq	Sx		Sy		Txy		Freq	Sx		Sy		Txy		Freq
CD	Plate I.D.	Repeat?	EXP	FEM	EXP	FEM	EXP	FEM	EXP	EXP	FEM	EXP	FEM	EXP	FEM	EXP	EXP	FEM	EXP	FEM	EXP	FEM	EXP
1	1288	P	163.1	-130.43	20.9	-9.62	6.8	-8.71	253.35	166.2	-141.73	44.0	-41.81	24.3	0.00	253.35	209.6	-130.43	33.2	-9.62	30.2	8.71	253.36
2	1288	P	154.0	-150.53	18.3	-11.55	2.6	-5.01	253.90	152.1	-155.52	41.8	-46.49	20.3	3.61	253.90	180.4	-135.26	25.3	-9.59	21.7	13.39	253.90
3	1288	P	164.4	-119.71	20.9	-8.36	13.7	-8.96	251.78	168.4	-134.68	49.0	-40.52	28.1	-1.19	251.78	213.7	-126.28	32.5	-9.47	32.2	6.13	251.78
4	1288	P	165.8	-139.01	20.9	-10.87	9.4	-7.75	252.66	172.7	-145.30	55.3	-42.42	27.1	1.12	252.66	216.4	-132.20	32.5	-9.68	31.5	10.53	252.66
5	1288	P	144.2	-127.85	16.1	-8.99	1.8	-7.62	252.07	122.1	-142.38	25.8	-44.49	14.7	0.00	252.08	152.1	-127.85	45.6	-8.99	25.3	7.61	252.08
6	1288	P	150.3	-130.63	17.5	-10.28	2.1	-9.06	252.78	132.2	-137.55	29.7	-38.81	18.5	0.00	252.77	166.4	-130.63	27.5	-10.28	23.0	9.07	252.77
	Standard Deviation		8.8		2.1		4.8		0.8	20.9		11.3		5.2		0.8	27.3		7.1		4.6		0.8
1st Bending			BLUE							RED							BLACK						
Stress Component (Psi/Mil Pk)--->			Sx		Sy		Txy		Freq	Sx		Sy		Txy		Freq	Sx		Sy		Txy		Freq
CD	Plate I.D.	Repeat?	EXP	FEM	EXP	FEM	EXP	FEM	EXP	EXP	FEM	EXP	FEM	EXP	FEM	EXP	EXP	FEM	EXP	FEM	EXP	FEM	EXP
1	8100	P	22.3	22.33	3.8	2.87	0.4	3.23	42.96	23.8	28.08	7.1	8.17	2.4	0.00	42.96	21.2	22.33	3.9	2.87	1.2	-3.23	42.96
2	8100	P	21.9	22.19	3.3	2.78	0.4	3.16	42.68	23.4	28.04	6.6	8.19	2.2	-0.04	42.68	21.0	22.39	3.3	2.88	0.4	-3.28	42.68
3	8100	P	22.7	22.20	3.8	2.71	0.9	3.20	42.68	23.5	28.01	7.3	8.18	2.2	0.00	42.68	21.3	22.22	3.8	2.77	1.2	-3.18	42.68
4	8100	P	21.8	22.39	3.2	2.96	0.4	3.24	42.60	23.4	27.96	7.1	8.10	1.9	0.00	42.60	21.0	22.36	3.6	2.88	1.2	-3.26	42.60
5	8100	P	22.1	22.18	3.8	2.70	0.5	3.17	42.68	23.1	28.20	6.0	8.40	2.1	0.00	42.68	20.9	22.18	3.3	2.70	0.8	-3.17	42.68
6	8100	P	21.0	22.39	3.3	2.96	1.0	3.27	42.60	23.2	27.75	6.7	7.89	2.3	0.00	42.60	20.8	22.39	3.5	2.96	0.9	-3.27	42.60
5	8100	R	22.0		3.8		0.7		42.60	23.2		6.1		2.0		42.60	20.8		3.3		0.6		42.60

Table A1-2 (continued). Tabulation of stress data.

2nd Bending			BLUE							RED							BLACK						
Stress Component (Psi/Mil Pt)--->			Sx		Sy		Txy		Freq	Sx		Sy		Txy		Freq	Sx		Sy		Txy		Freq
CD	Plate I.D.	Repeat?	EXP	FEM	EXP	FEM	EXP	FEM	EXP	EXP	FEM	EXP	FEM	EXP	FEM	EXP	EXP	FEM	EXP	FEM	EXP	FEM	EXP
1	8100	P	152.0	-162.07	28.8	-24.60	14.2	-6.41	270.76	138.4	-164.64	42.1	-49.30	18.1	0.00	270.76	145.9	-162.08	30.3	-24.60	22.2	6.41	270.76
2	8100	P	148.5	-158.89	25.3	-23.67	13.9	-5.85	270.27	137.0	-163.22	39.8	-49.22	17.5	0.19	270.27	146.4	-162.00	24.2	-24.57	17.3	6.63	270.27
3	8100	P	154.0	-160.58	29.3	-23.45	11.1	-6.02	269.69	134.3	-163.87	43.3	-49.45	16.4	0.04	269.69	143.5	-160.10	29.2	-23.76	22.9	5.92	269.69
4	8100	P	149.1	-161.60	24.5	-25.08	14.6	-6.47	270.56	138.6	-163.26	43.5	-48.70	15.3	-0.04	270.56	149.9	-161.95	27.5	-24.61	23.4	6.56	270.56
5	8100	P	149.8	-159.97	31.4	-23.30	13.9	-5.81	269.69	135.9	-164.87	36.5	-50.87	16.5	0.00	269.69	143.1	-159.98	25.0	-23.30	20.8	5.81	269.69
6	8100	P	150.7	-162.00	30.9	-25.13	11.7	-6.68	270.15	137.3	-162.08	41.6	-47.37	18.9	0.00	270.15	146.8	-162.01	27.3	-25.13	21.6	6.69	270.15
4	8100	R	150.2		25.5		14.3		270.79	138.8		43.5		15.1		270.79	149.9		27.5		23.1		270.79
3rd Bending			BLUE							RED							BLACK						
Stress Component (Psi/Mil Pt)--->			Sx		Sy		Txy		Freq	Sx		Sy		Txy		Freq	Sx		Sy		Txy		Freq
CD	Plate I.D.	Repeat?	EXP	FEM	EXP	FEM	EXP	FEM	EXP	EXP	FEM	EXP	FEM	EXP	FEM	EXP	EXP	FEM	EXP	FEM	EXP	FEM	EXP
1	8100	P	422.5	509.95	86.0	84.53	10.9	-1.07	758.58	367.3	490.73	112.0	146.73	7.3	0.00	758.57	409.5	509.96	90.4	84.53	22.8	1.07	758.58
2	8100	P	399.4	489.76	71.6	80.17	9.3	-2.88	754.76	357.2	480.70	102.3	145.05	10.0	-0.46	754.76	410.0	507.87	66.5	83.99	15.5	0.40	754.76
3	8100	P	414.2	504.57	84.8	80.76	4.9	-2.83	753.98	341.9	486.48	112.7	146.92	7.2	-0.27	753.96	387.8	499.64	85.6	81.46	19.5	3.01	753.96
4	8100	P	410.1	504.23	73.4	85.64	10.5	-0.74	756.57	368.2	483.55	115.5	143.90	10.1	0.28	756.56	432.7	508.19	81.5	84.31	21.9	0.57	756.55
5	8100	P	402.3	499.78	95.8	79.80	11.0	-3.48	753.48	352.2	488.85	91.4	151.71	12.4	-0.01	753.48	395.4	499.79	69.5	79.79	17.4	3.48	753.47
6	8100	P	412.8	507.82	99.7	86.18	8.6	-0.05	755.06	361.6	480.25	109.6	139.31	7.9	0.00	755.06	413.0	507.87	79.6	86.17	19.1	0.04	755.06
3	8100	R	410.0		82.4		6.4		753.20	340.3		111.0		7.2		753.18	385.5		86.2		19.1		753.25
2nd Bending			BLUE							RED							BLACK						
Stress Component (Psi/Mil Pt)--->			Sx		Sy		Txy		Freq	Sx		Sy		Txy		Freq	Sx		Sy		Txy		Freq
CD	Plate I.D.	Repeat?	EXP	FEM	EXP	FEM	EXP	FEM	EXP	EXP	FEM	EXP	FEM	EXP	FEM	EXP	EXP	FEM	EXP	FEM	EXP	FEM	EXP
1	8188	P	273.7	-288.61	51.6	-31.13	28.2	-10.10	540.63	245.6	-294.71	75.5	-87.65	28.3	0.00	540.63	261.2	-288.63	49.6	-31.13	43.4	10.10	540.63
2	8188	P	260.7	-273.65	43.3	-28.96	23.3	-7.27	536.59	240.9	-287.62	73.7	-86.66	27.4	1.94	536.60	257.2	-287.97	40.9	-31.17	38.6	11.07	536.59
3	8188	P	263.5	-282.42	46.8	-29.27	27.1	-8.19	534.71	231.5	-291.17	79.9	-88.26	23.6	-0.77	534.65	253.5	-280.33	45.8	-29.67	38.3	7.79	534.70
4	8188	P	263.1	-286.32	42.5	-31.90	26.8	-10.26	536.63	241.3	-288.04	76.5	-85.13	25.8	0.73	536.60	263.7	-288.16	48.3	-31.24	37.1	10.72	536.61
5	8188	P	259.9	-279.71	43.7	-28.68	29.6	-7.42	530.02	214.8	-295.63	72.7	-92.74	24.8	0.00	530.01	224.3	-279.72	27.6	-28.68	42.6	7.42	530.02
6	8188	P	255.6	-288.50	30.0	-32.51	27.3	-11.08	535.52	227.6	-283.22	59.9	-81.25	22.8	0.00	535.48	252.7	-288.54	41.3	-32.51	35.1	11.09	535.49
2	8188	R	264.4		46.0		23.7		536.90	245.3		76.9		27.4		536.90	261.3		43.9		39.6		536.91
5	8188	R	261.5		44.2		29.6		531.10	219.3		73.8		24.5		531.11	225.7		27.9		42.9		531.11
3rd Bending			BLUE							RED							BLACK						
Stress Component (Psi/Mil Pt)--->			Sx		Sy		Txy		Freq	Sx		Sy		Txy		Freq	Sx		Sy		Txy		Freq
CD	Plate I.D.	Repeat?	EXP	FEM	EXP	FEM	EXP	FEM	EXP	EXP	FEM	EXP	FEM	EXP	FEM	EXP	EXP	FEM	EXP	FEM	EXP	FEM	EXP
1	8188	P	903.2	873.76	180.2	102.70	17.5	-9.85	1556.29	793.7	839.29	243.2	249.29	14.1	0.00	1556.30	888.8	873.77	174.8	102.70	46.8	9.84	1556.31
2	8188	P	866.4	893.13	160.2	99.94	17.5	-8.76	1549.50	794.7	814.13	247.1	243.36	14.5	7.58	1549.50	897.9	785.47	148.3	97.35	41.0	18.68	1549.48
3	8188	P	854.6	809.02	158.5	93.71	15.7	-21.22	1544.49	734.2	813.17	256.3	247.22	16.5	-2.99	1544.52	853.8	854.84	157.2	98.35	37.4	14.88	1544.51
4	8188	P	877.2	912.79	151.2	108.49	19.3	-2.06	1553.02	795.8	816.51	246.8	239.81	18.9	4.74	1552.99	930.6	823.38	174.3	100.03	44.4	13.91	1553.00
5	8188	P	856.6	828.65	156.0	93.38	19.0	-20.12	1536.96	661.1	830.31	234.2	264.44	17.5	-0.03	1536.97	721.9	828.88	85.8	93.39	33.2	20.11	1537.01
6	8188	P	834.8	864.88	111.6	106.75	24.3	-6.17	1546.01	727.3	792.39	186.2	224.28	19.6	0.04	1546.01	864.3	864.41	144.5	106.71	36.8	6.21	1546.01
4	8188	R	875.6		151.8		20.1		1552.10	795.8		245.2		19.9		1552.11	927.6		174.1		45.1		1552.11

Table A1-2 (continued). Tabulation of stress data.

Combined Experimental & Finite Element Strain Gage Data, Mid Span Gages

2nd Bending			BROWN							ORANGE							GRAY						
Stress Component (Psi/Mil Pt)--->			Sx		Sy		Txy		Freq	Sx		Sy		Txy		Freq	Sx		Sy		Txy		Freq
CD	Plate I.D.	Repeat?	EXP	FEM	EXP	FEM	EXP	FEM	EXP	EXP	FEM	EXP	FEM	EXP	FEM	EXP	EXP	FEM	EXP	FEM	EXP	FEM	EXP
1	1200	P	64.3	63.71	1.5	1.08	4.3	-1.48	129.51	60.3	62.45	3.7	4.52	2.1	0.00	129.51	59.2	63.71	1.4	1.08	3.3	1.48	129.48
2	1200	P	69.8	65.90	1.5	1.15	6.8	-0.86	129.73	66.4	64.34	4.1	4.65	1.2	0.68	129.76	66.1	65.35	1.5	1.07	2.5	2.19	129.79
3	1200	P	63.5	62.52	1.4	1.04	4.3	-1.77	129.97	59.5	61.42	3.6	4.43	2.1	-0.31	129.95	58.3	62.77	1.5	1.08	3.2	1.16	129.92
4	1200	P	65.3	64.58	1.5	1.11	5.0	-1.23	130.39	61.4	63.20	3.8	4.57	1.9	0.28	130.38	60.5	64.36	1.5	1.07	3.0	1.77	130.39
5	1200	P	67.8	63.59	1.5	1.07	6.3	-1.49	129.85	64.2	62.34	4.0	4.50	1.5	0.00	129.87	63.7	63.59	1.5	1.07	2.7	1.49	129.87
6	1200	P	65.3	63.61	1.4	1.08	18.0	-1.48	129.30	61.6	62.36	3.8	4.51	6.9	0.00	129.29	60.8	63.61	1.6	1.08	7.4	1.48	129.29
3rd Bending			BROWN							ORANGE							GRAY						
Stress Component (Psi/Mil Pt)--->			Sx		Sy		Txy		Freq	Sx		Sy		Txy		Freq	Sx		Sy		Txy		Freq
CD	Plate I.D.	Repeat?	EXP	FEM	EXP	FEM	EXP	FEM	EXP	EXP	FEM	EXP	FEM	EXP	FEM	EXP	EXP	FEM	EXP	FEM	EXP	FEM	EXP
1	1200	P	186.3	165.08	14.2	5.62	18.6	24.96	365.46	166.6	158.99	23.8	20.80	3.8	0.00	365.43	172.7	165.08	6.7	5.62	16.9	-24.96	365.42
2	1200	P	189.7	166.21	14.5	5.64	17.3	25.74	367.08	169.2	160.28	24.3	20.97	3.1	0.66	367.07	175.3	166.63	6.7	5.69	18.1	-24.44	367.10
3	1200	P	182.9	164.69	14.0	5.61	17.6	24.48	365.65	163.8	158.52	23.6	20.75	4.0	-0.29	365.66	169.5	164.49	6.6	5.59	16.1	-25.07	365.64
4	1200	P	184.4	165.54	14.1	5.63	16.8	25.25	365.77	164.8	159.52	23.5	20.87	3.8	0.26	365.75	170.5	165.71	6.3	5.65	16.6	-24.73	365.75
5	1200	P	185.5	165.15	14.2	5.62	53.8	24.88	365.11	165.9	159.06	23.8	20.83	22.9	0.00	365.11	171.4	165.15	6.4	5.62	6.0	-24.88	365.14
5	1200	R	184.8		14.0		53.5		365.34	165.1		23.7		22.2		365.34	171.0		6.3		5.1		365.31
6	1200	P	184.1	165.12	14.1	5.62	53.4	24.89	365.22	164.5	159.04	23.5	20.80	22.6	0.00	365.23	170.2	165.13	6.3	5.62	5.8	-24.89	365.20
1st Bending			BROWN							ORANGE							GRAY						
Stress Component (Psi/Mil Pt)--->			Sx		Sy		Txy		Freq	Sx		Sy		Txy		Freq	Sx		Sy		Txy		Freq
CD	Plate I.D.	Repeat?	EXP	FEM	EXP	FEM	EXP	FEM	EXP	EXP	FEM	EXP	FEM	EXP	FEM	EXP	EXP	FEM	EXP	FEM	EXP	FEM	EXP
1	1288	P	4.3	5.38	0.1	-0.03	0.6	-0.63	36.82	4.3	5.41	0.2	-0.14	0.2	0.00	36.83	4.1	5.38	0.3	-0.03	0.5	0.63	36.82
2	1288	P	4.3	5.35	0.1	-0.03	0.6	-0.62	36.81	4.2	5.38	0.2	-0.14	0.2	0.00	36.81	4.0	5.35	0.3	-0.03	0.5	0.62	36.82
3	1288	P	4.3	5.34	0.1	-0.03	0.6	-0.62	36.47	4.2	5.38	0.2	-0.14	0.2	0.00	36.47	4.0	5.34	0.3	-0.03	0.5	0.62	36.47
4	1288	P	4.3	5.36	0.1	-0.03	0.6	-0.63	36.56	4.2	5.39	0.2	-0.14	0.2	0.00	36.54	4.0	5.36	0.3	-0.03	0.5	0.63	36.53
5	1288	P	4.3	5.35	0.1	-0.03	0.6	-0.62	36.62	4.2	5.38	0.2	-0.13	0.2	0.00	36.63	4.0	5.35	0.3	-0.03	0.5	0.62	36.62
6	1288	P	4.3	5.35	0.1	-0.03	0.6	-0.62	36.60	4.2	5.38	0.2	-0.14	0.2	0.00	36.61	4.0	5.35	0.3	-0.03	0.5	0.62	36.61
2nd Bending			BROWN							ORANGE							GRAY						
Stress Component (Psi/Mil Pt)--->			Sx		Sy		Txy		Freq	Sx		Sy		Txy		Freq	Sx		Sy		Txy		Freq
CD	Plate I.D.	Repeat?	EXP	FEM	EXP	FEM	EXP	FEM	EXP	EXP	FEM	EXP	FEM	EXP	FEM	EXP	EXP	FEM	EXP	FEM	EXP	FEM	EXP
1	1288	P	155.4	118.37	0.9	1.74	19.2	-2.76	253.31	152.3	115.95	9.4	8.10	0.4	0.00	253.40	156.6	118.37	2.6	1.74	0.6	2.76	253.38
2	1288	P	142.1	132.10	1.3	2.14	13.3	0.91	253.94	137.5	127.71	8.4	8.89	1.6	4.27	253.89	139.8	128.62	2.6	1.68	1.4	7.05	253.91
3	1288	P	159.2	112.42	0.7	1.57	21.1	-4.15	251.83	156.9	110.77	9.8	7.70	1.3	-1.58	251.79	161.9	113.71	2.5	1.74	1.5	1.21	251.74
4	1288	P	159.9	123.28	0.7	1.89	21.2	-1.41	252.71	157.5	120.14	10.0	8.38	1.3	1.57	252.68	162.5	122.00	2.5	1.71	1.5	4.34	252.65
5	1288	P	123.2	117.82	1.4	1.72	5.9	-2.79	252.07	117.2	115.42	7.1	8.02	3.8	0.00	252.08	116.8	117.82	2.9	1.72	3.6	2.79	252.09
6	1288	P	132.4	117.93	1.4	1.73	9.6	-2.76	252.73	127.0	115.52	7.9	8.06	2.6	0.00	252.78	128.0	117.92	2.7	1.73	2.3	2.77	252.76
	Standard Deviation		15.3		0.3		6.5		0.8	16.9		1.2		1.2		0.8	19.2		0.2		1.0		0.8
1st Bending			BROWN							ORANGE							GRAY						
Stress Component (Psi/Mil Pt)--->			Sx		Sy		Txy		Freq	Sx		Sy		Txy		Freq	Sx		Sy		Txy		Freq
CD	Plate I.D.	Repeat?	EXP	FEM	EXP	FEM	EXP	FEM	EXP	EXP	FEM	EXP	FEM	EXP	FEM	EXP	EXP	FEM	EXP	FEM	EXP	FEM	EXP
1	8100	P	5.5	6.35	0.2	-0.03	0.9	-0.87	42.93	5.4	6.34	0.2	-0.08	0.1	0.00	42.93	5.2	6.35	0.5	-0.03	0.7	0.87	42.94
2	8100	P	5.4	6.33	0.2	-0.03	0.9	-0.86	42.67	5.3	6.32	0.2	-0.08	0.1	0.00	42.68	5.1	6.33	0.5	-0.03	0.7	0.86	42.68
3	8100	P	5.4	6.33	0.2	-0.03	0.9	-0.86	42.69	5.4	6.32	0.3	-0.08	0.2	0.00	42.69	5.1	6.32	0.5	-0.03	0.7	0.86	42.68
4	8100	P	5.4	6.33	0.2	-0.03	0.9	-0.87	42.59	5.3	6.33	0.2	-0.09	0.2	0.00	42.59	5.1	6.34	0.5	-0.03	0.7	0.86	42.59
5	8100	P	5.4	6.33	0.2	-0.03	0.9	-0.86	42.67	5.3	6.32	0.2	-0.08	0.2	0.00	42.67	5.1	6.33	0.4	-0.03	0.7	0.86	42.68
6	8100	P	5.3	6.33	0.2	-0.03	0.9	-0.87	42.60	5.3	6.32	0.2	-0.09	0.2	0.00	42.60	5.1	6.33	0.4	-0.03	0.7	0.87	42.60
5	8100	R	5.4		0.2		0.9		42.60	5.3		0.2		0.2		42.60	5.1		0.4		0.7		42.60

Table A1-2 (concluded). Tabulation of stress data.

2nd Bending			BROWN							ORANGE							GRAY						
Stress Component (Psi/Mil Pk)--->			Sx		Sy		Txy		Freq	Sx		Sy		Txy		Freq	Sx		Sy		Txy		Freq
CD	Plate I.D.	Repeat?	EXP	FEM	EXP	FEM	EXP	FEM	EXP	EXP	FEM	EXP	FEM	EXP	FEM	EXP	EXP	FEM	EXP	FEM	EXP	FEM	EXP
1	8100	P	134.1	140.14	3.8	3.78	5.5	-2.60	270.76	124.8	135.97	11.7	14.18	2.4	0.00	270.76	126.3	140.14	1.0	3.78	3.7	2.60	270.78
2	8100	P	134.5	139.08	3.7	3.74	5.7	-2.86	270.26	125.5	135.05	11.7	14.06	1.9	-0.27	270.27	126.9	139.29	1.1	3.77	3.1	2.35	270.26
3	8100	P	134.0	140.01	4.7	3.77	5.1	-2.53	269.67	124.4	135.81	11.6	14.11	3.5	0.13	269.68	125.7	139.91	1.1	3.76	3.9	2.76	269.73
4	8100	P	135.1	139.62	3.7	3.77	6.2	-2.70	270.56	126.3	135.51	11.8	14.14	3.1	-0.11	270.56	128.1	139.71	1.1	3.78	3.7	2.49	270.53
5	8100	P	133.6	139.74	3.7	3.76	5.6	-2.64	269.68	124.7	135.59	11.5	14.07	3.2	0.00	269.69	126.4	139.74	1.1	3.76	3.8	2.64	269.76
6	8100	P	134.1	139.85	3.9	3.78	5.6	-2.59	270.14	125.0	135.69	11.6	14.17	3.2	0.00	270.15	126.5	139.85	1.1	3.78	3.8	2.59	270.15
4	8100	R	135.5		3.8		5.9		270.79	126.5		11.9		3.0		270.79	128.3		1.1		3.6		270.78
3rd Bending			BROWN							ORANGE							GRAY						
Stress Component (Psi/Mil Pk)--->			Sx		Sy		Txy		Freq	Sx		Sy		Txy		Freq	Sx		Sy		Txy		Freq
CD	Plate I.D.	Repeat?	EXP	FEM	EXP	FEM	EXP	FEM	EXP	EXP	FEM	EXP	FEM	EXP	FEM	EXP	EXP	FEM	EXP	FEM	EXP	FEM	EXP
1	8100	P	424.7	383.21	42.3	17.28	45.7	70.19	758.59	371.3	360.52	48.9	39.46	6.3	0.00	758.57	408.9	388.21	32.5	17.28	49.1	-70.19	758.59
2	8100	P	433.4	380.91	43.1	17.44	50.6	67.94	754.76	375.6	356.30	49.4	39.17	4.9	-1.32	754.75	408.1	376.48	31.1	16.73	51.9	-70.20	754.76
3	8100	P	418.8	384.50	41.7	17.26	53.3	70.71	753.96	368.8	362.73	48.6	40.13	6.7	0.61	753.97	406.4	386.51	31.1	17.58	46.3	-69.65	753.96
4	8100	P	444.1	382.30	44.7	17.33	48.1	69.14	756.56	382.8	358.84	50.5	39.23	3.8	-0.53	756.56	415.8	380.50	32.4	17.04	50.9	-70.06	756.55
5	8100	P	431.0	383.37	42.9	17.34	49.3	69.91	753.46	375.0	360.71	50.4	39.99	5.5	0.00	753.50	405.9	383.37	30.4	17.34	49.9	-69.91	753.46
6	8100	P	433.5	383.28	43.6	17.25	50.5	69.81	755.06	375.7	360.61	49.9	39.34	5.2	0.00	755.07	411.4	383.27	31.2	17.25	50.1	-69.82	755.05
3	8100	R	418.1		42.0		53.2		753.22	367.8		48.7		6.5		753.28	406.3		32.3		45.9		753.23
2nd Bending			BROWN							ORANGE							GRAY						
Stress Component (Psi/Mil Pk)--->			Sx		Sy		Txy		Freq	Sx		Sy		Txy		Freq	Sx		Sy		Txy		Freq
CD	Plate I.D.	Repeat?	EXP	FEM	EXP	FEM	EXP	FEM	EXP	EXP	FEM	EXP	FEM	EXP	FEM	EXP	EXP	FEM	EXP	FEM	EXP	FEM	EXP
1	8188	P	254.2	258.90	6.8	6.27	5.5	-5.06	540.62	237.1	250.84	21.0	25.43	9.1	0.00	540.64	236.4	258.90	5.9	6.27	2.5	5.06	540.55
2	8188	P	251.0	253.61	0.6	6.05	4.7	-6.33	538.22	235.2	246.19	19.5	24.86	8.5	-1.33	536.54	236.3	254.54	5.1	6.20	2.1	3.83	537.05
3	8188	P	250.7	258.23	7.2	6.22	5.1	-4.73	535.16	234.1	250.07	21.2	25.14	9.0	0.56	534.71	234.8	257.85	4.4	6.17	2.5	5.77	536.34
4	8188	P	254.9	256.51	8.1	6.18	6.4	-5.52	536.87	238.8	248.69	22.9	25.24	8.7	-0.51	536.66	239.7	256.87	2.8	6.24	2.2	4.57	536.54
5	8188	P	242.2	257.04	6.1	6.17	3.4	-5.24	530.00	225.5	249.10	19.7	24.99	10.0	0.00	530.01	225.5	257.04	4.2	6.17	4.1	5.24	530.00
6	8188	P	250.9	257.53	6.9	6.24	5.4	-5.05	535.75	234.5	249.50	21.4	25.37	9.2	0.00	535.56	235.4	257.53	3.1	6.24	3.1	5.05	535.30
2	8188	R	255.0		8.0		4.9		537.20	239.2		22.9		8.8		536.99	240.0		0.8		2.1		538.16
5	8188	R	243.6		6.2		3.3		531.09	226.8		20.0		10.0		531.12	226.9		4.2		4.0		531.07
3rd Bending			BROWN							ORANGE							GRAY						
Stress Component (Psi/Mil Pk)--->			Sx		Sy		Txy		Freq	Sx		Sy		Txy		Freq	Sx		Sy		Txy		Freq
CD	Plate I.D.	Repeat?	EXP	FEM	EXP	FEM	EXP	FEM	EXP	EXP	FEM	EXP	FEM	EXP	FEM	EXP	EXP	FEM	EXP	FEM	EXP	FEM	EXP
1	8188	P	806.6	720.91	84.6	28.61	122.2	123.89	1556.32	711.6	675.74	94.4	74.30	9.6	0.00	1556.33	762.1	720.90	64.1	28.61	129.4	-123.89	1556.33
2	8188	P	828.8	732.17	87.9	28.68	128.8	121.43	1549.50	728.9	669.05	97.1	74.33	9.8	6.03	1549.54	771.9	695.09	64.9	28.05	134.1	-121.19	1549.50
3	8188	P	800.2	718.11	82.7	28.73	121.5	122.93	1544.51	711.5	679.68	93.3	76.43	11.2	-1.72	1544.52	761.3	731.65	62.1	29.08	126.4	-122.44	1544.53
4	8188	P	841.0	729.31	89.3	28.45	118.2	123.71	1553.00	735.2	675.47	96.1	74.14	8.5	4.56	1553.01	774.0	711.67	64.9	28.63	134.6	-121.77	1553.00
5	8188	P	753.5	721.22	78.7	28.81	118.0	122.53	1537.00	684.0	676.19	90.7	76.33	16.5	-0.01	1536.97	741.5	721.23	60.9	28.81	112.7	-122.55	1536.97
6	8188	P	810.7	721.01	82.9	28.50	118.4	122.28	1546.01	717.3	675.98	95.1	73.94	10.8	0.03	1546.01	763.3	720.93	61.9	28.51	125.3	-122.25	1546.01
4	8188	R	841.9		87.7		119.6		1552.11	734.7		96.5		8.3		1552.11	773.4		66.0		135.5		1552.08

Notes:
1. CD-Constraint Distribution Number
2. P/R-Primary/Repeat
3. Sx-Stress in span-wise direction (psi/mil @ A3T)
4. Sy-Stress in chord-wise direction (psi/mil @ A3T)
5. Txy-In-plane shear stress (psi/mil @ A3T)
6. Plate I.D.'s as per Figure 9
7. Colors refer to rosette locations specified in Figure 8

APPENDIX 2

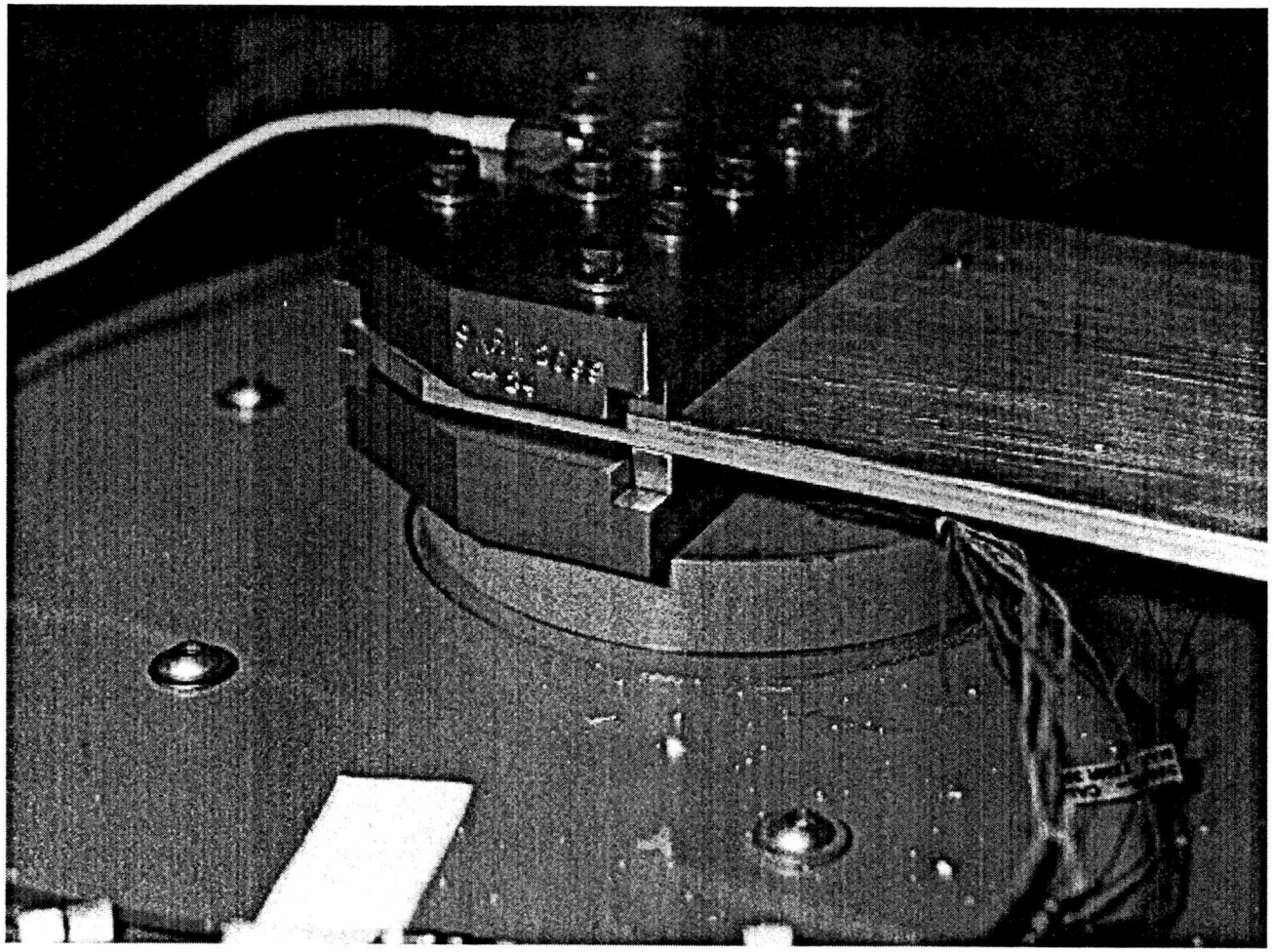


Figure A2-1. Plate clamping.

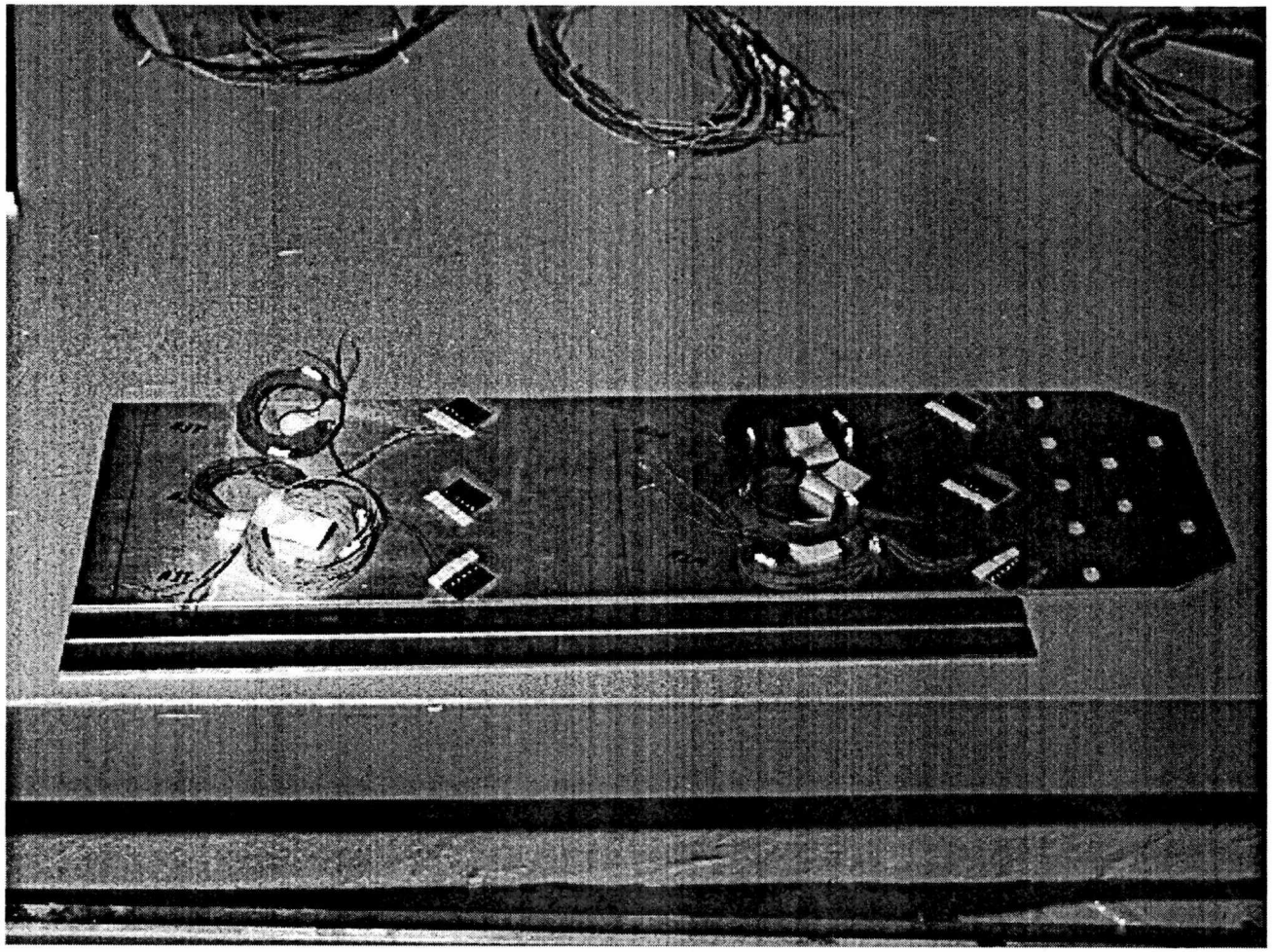


Figure A2-2. 12.5 x 4 x 0.100 inch plate.

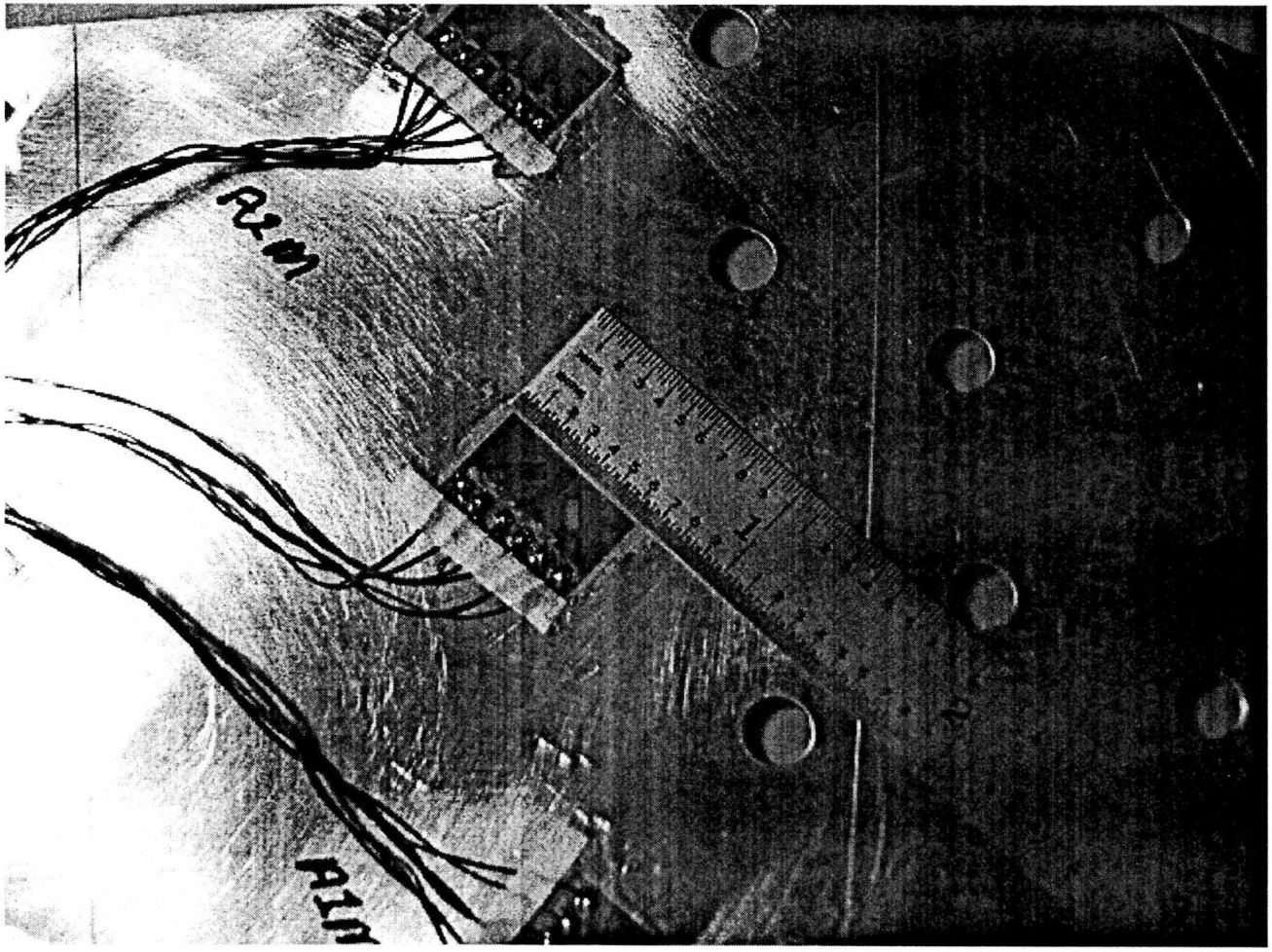


Figure A2-3. Strain gage rosette close up.

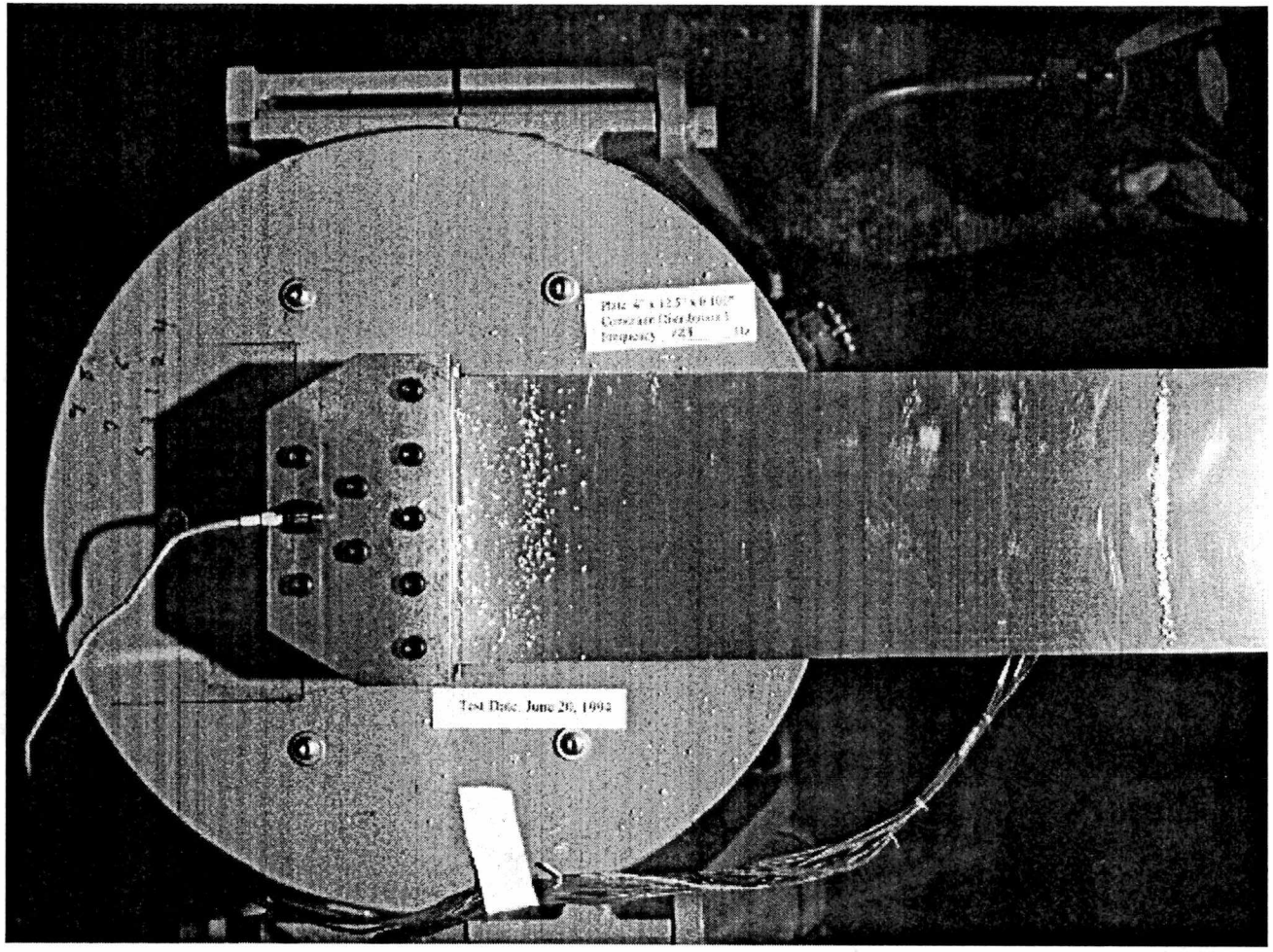


Figure A2-4. Second bending of 12.5 x 4 x 0.100 inch plate with stiffness distribution 1.

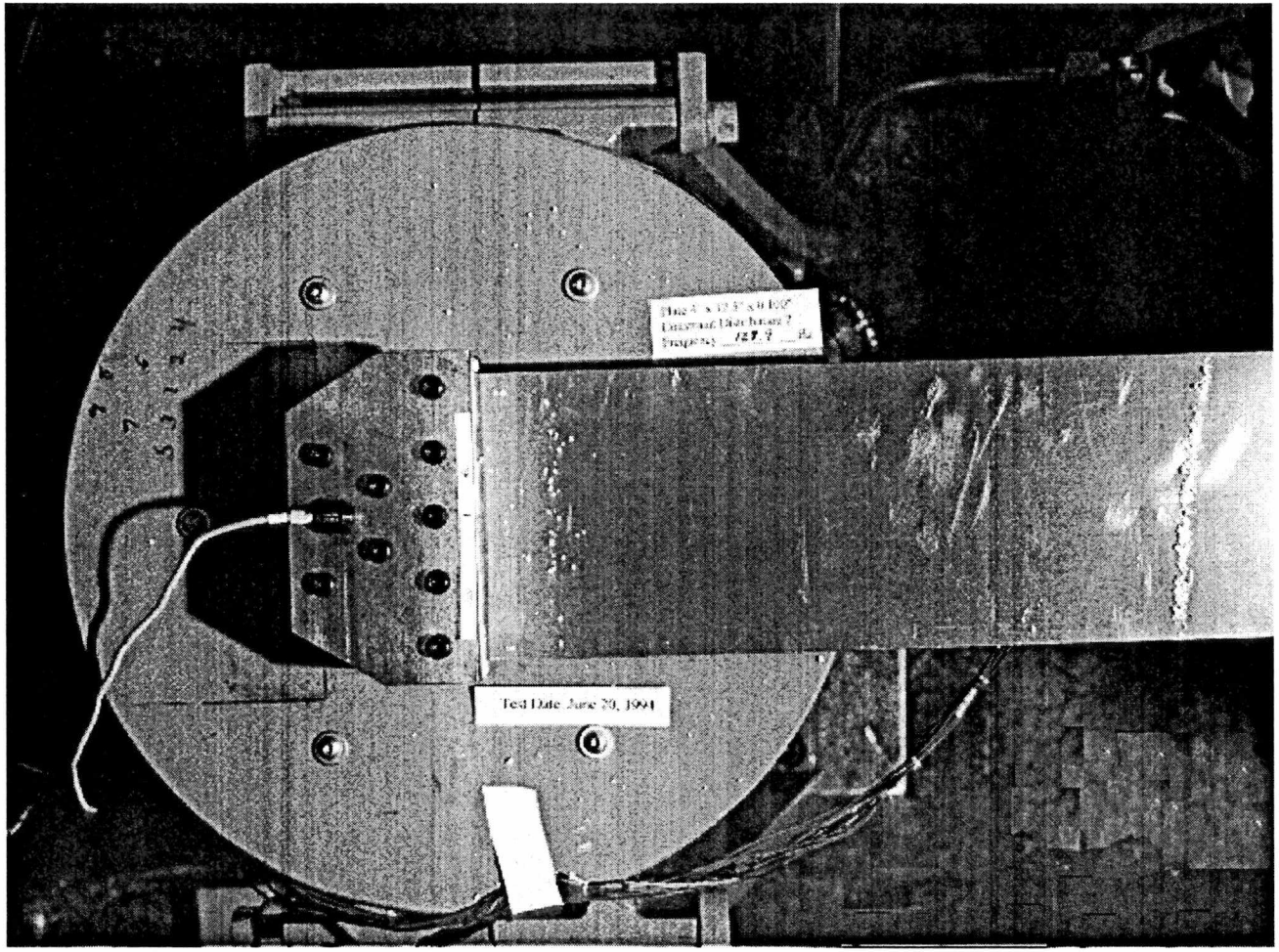


Figure A2-5. Second bending of 12.5 x 4 x 0.100 inch plate with stiffness distribution 2.

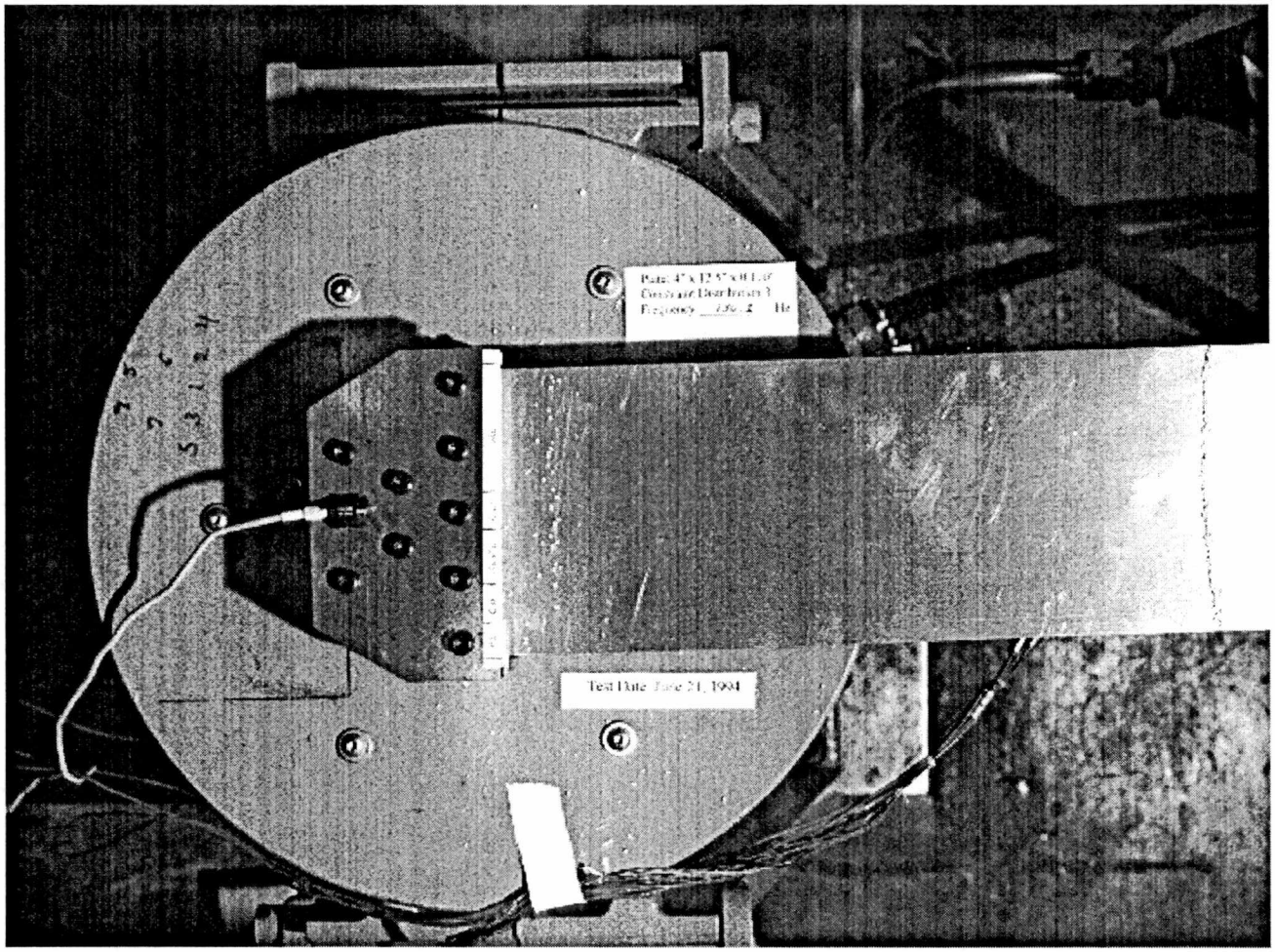


Figure A2-6. Second bending of 12.5 x 4 x 0.100 inch plate with stiffness distribution 3.

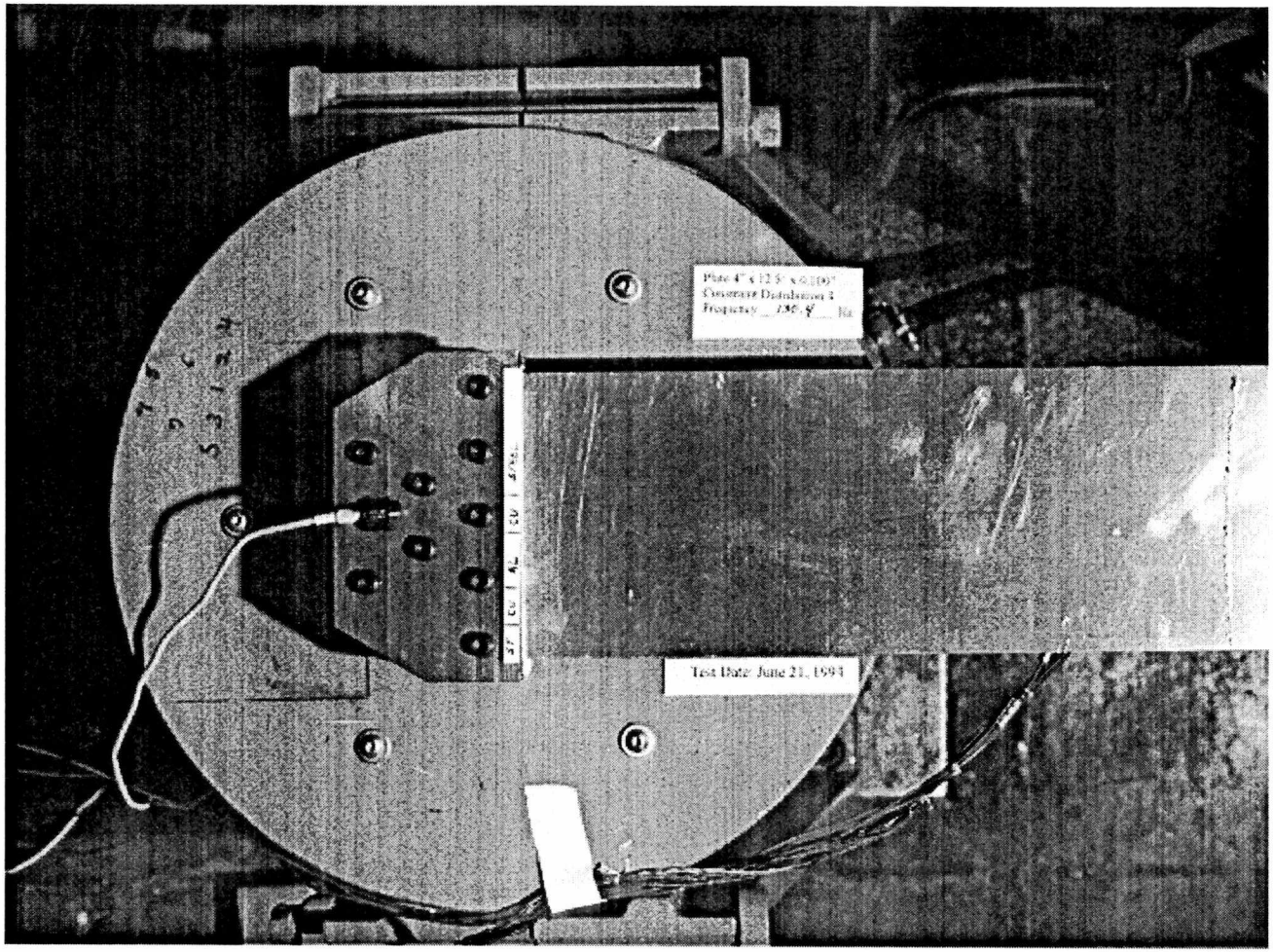


Figure A2-7. Second bending of 12.5 x 4 x 0.100 inch plate with stiffness distribution 4.

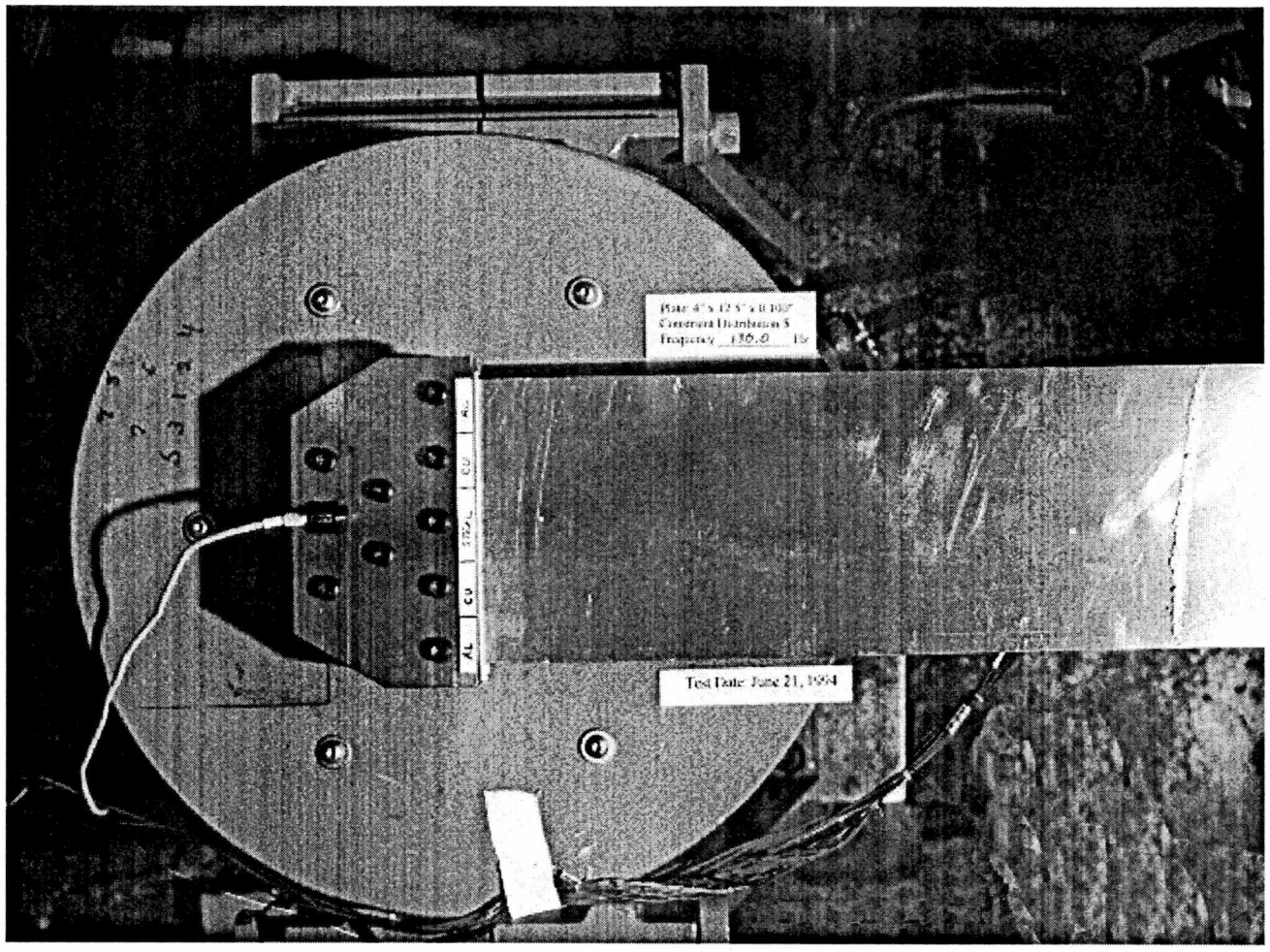


Figure A2-8. Second bending of 12.5 x 4 x 0.100 inch plate with stiffness distribution 5.

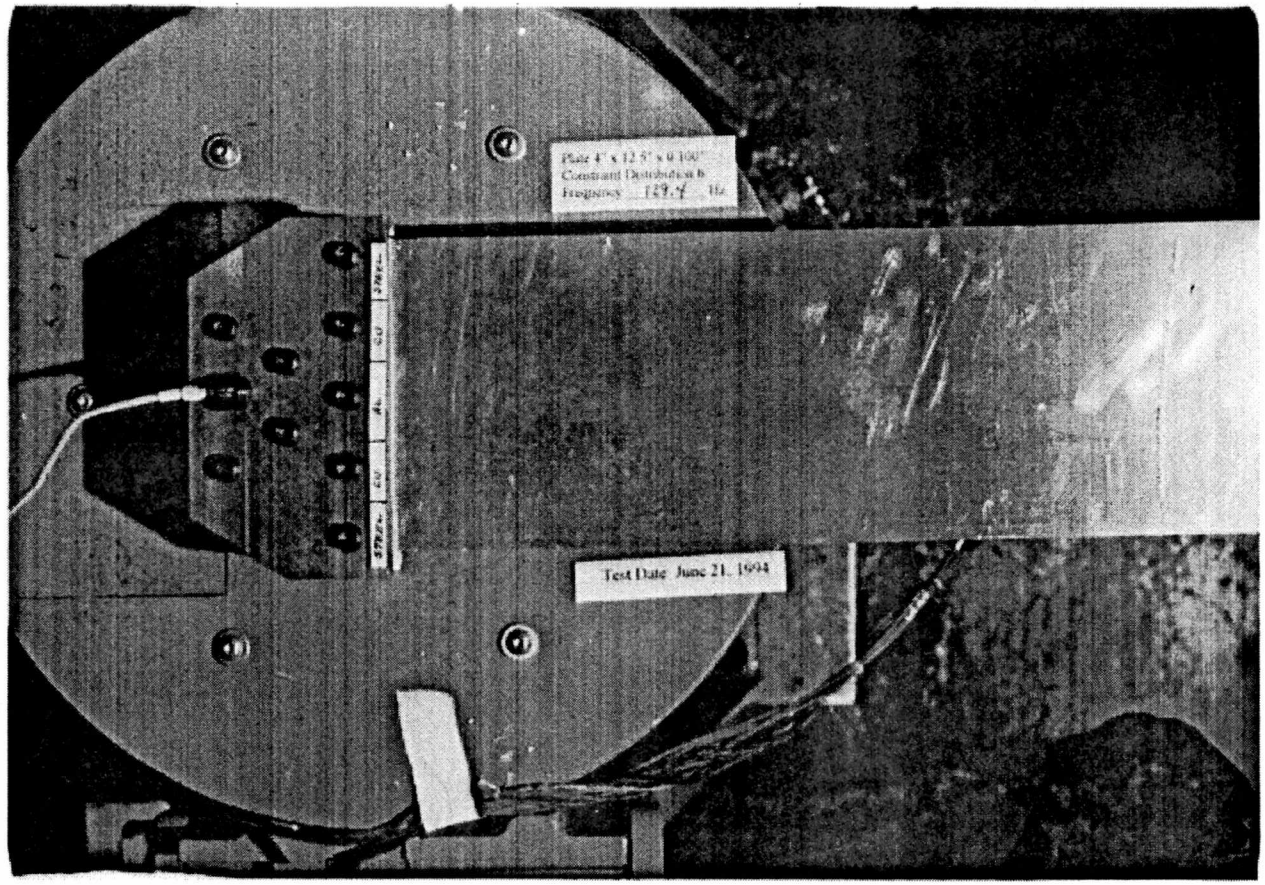


Figure A2-9. Second bending of 12.5 x 4 x 0.100 inch plate with stiffiness distribution 6.

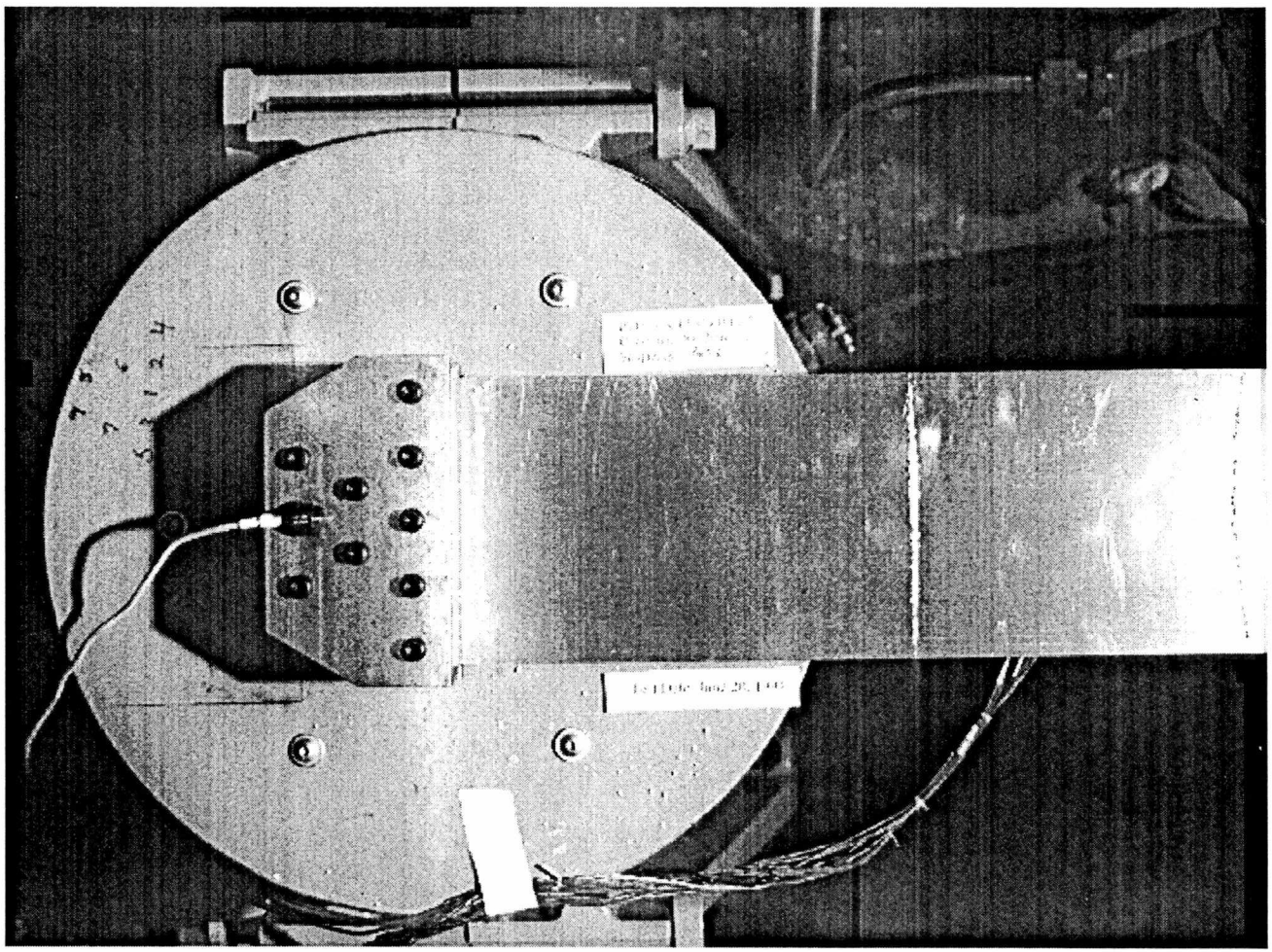


Figure A2-10. Third bending of 12.5 x 4 x 0.100 inch plate with stiffness distribution 1.

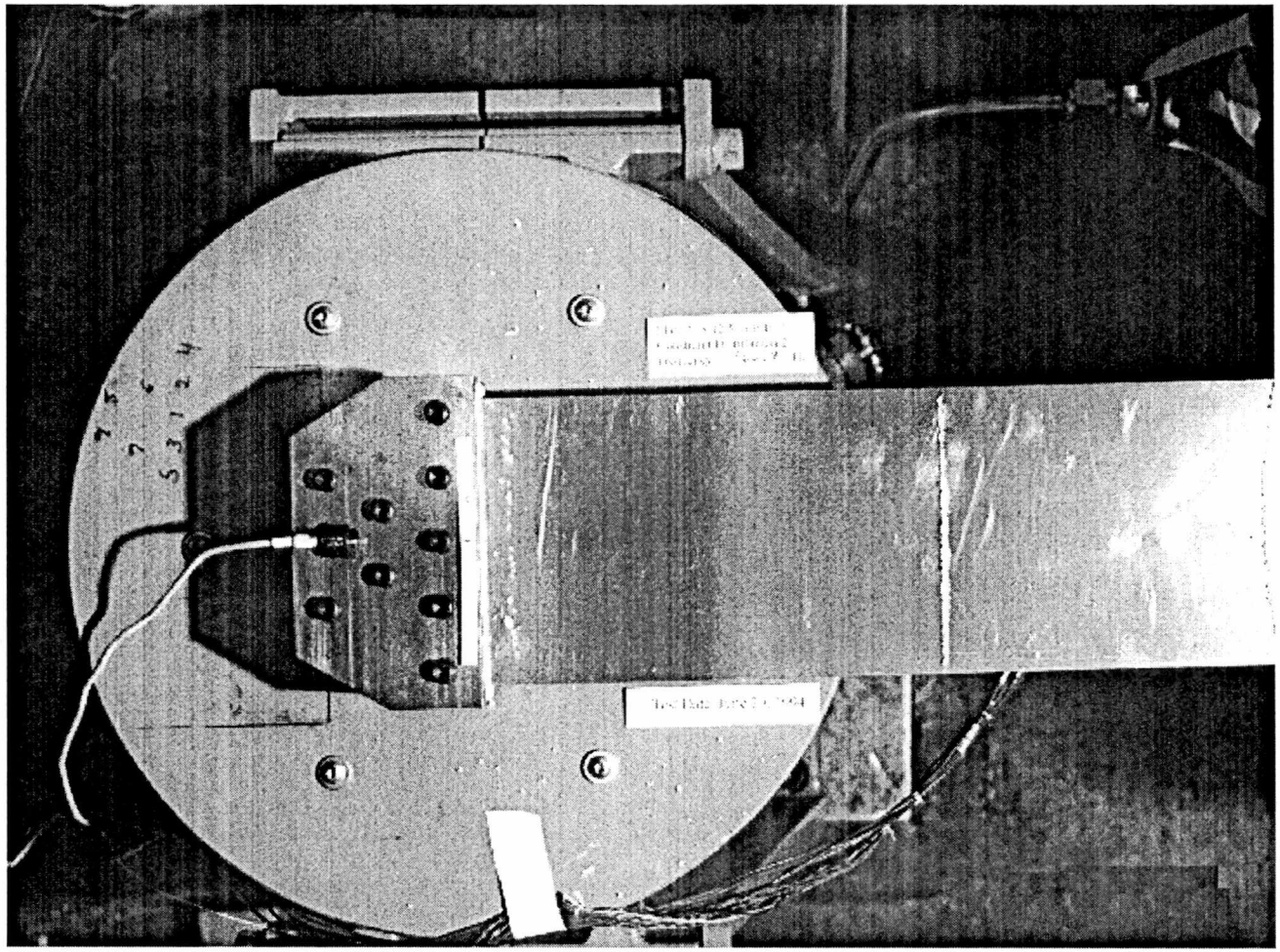


Figure A2-11. Third bending of 12.5 x 4 x 0.100 inch plate with stiffness distribution 2.

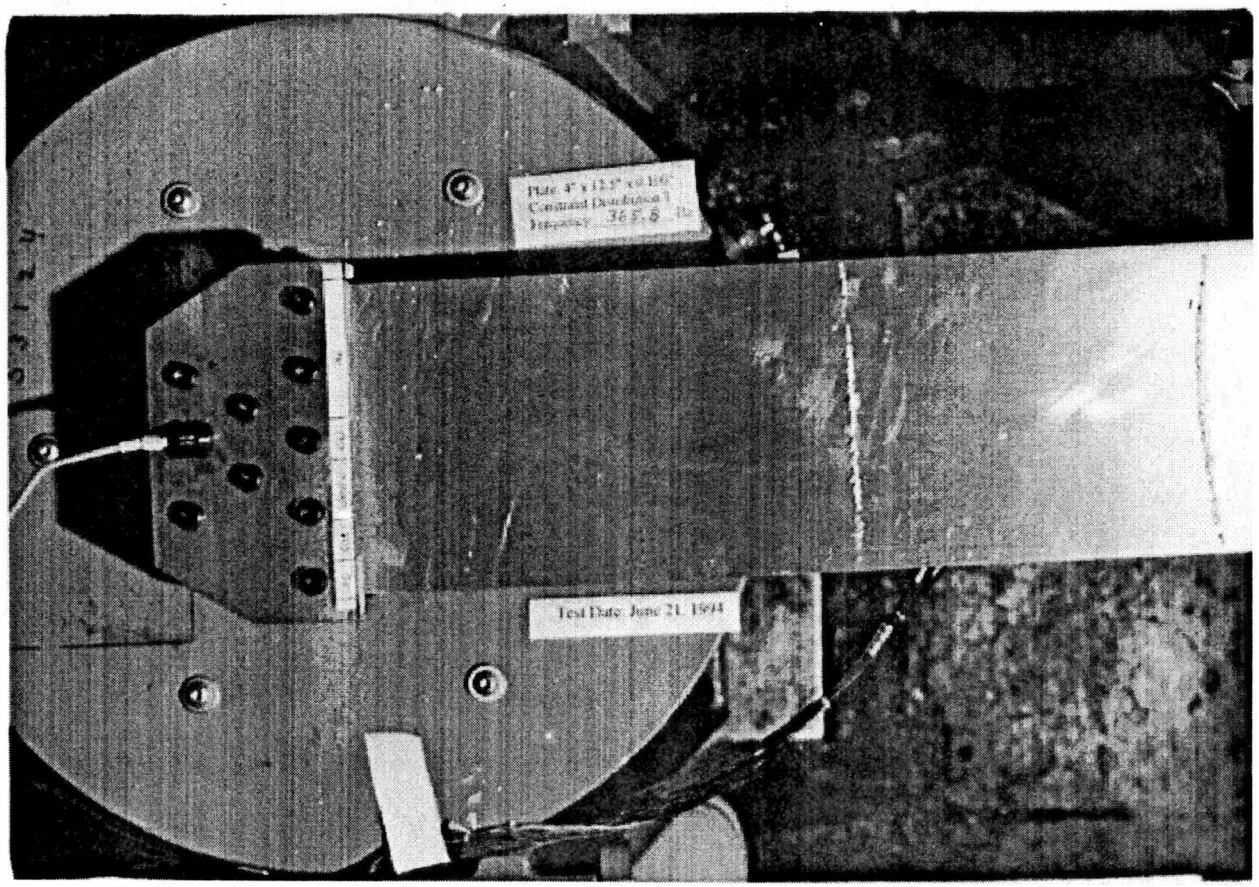


Figure A2-12. Third bending of 12.5 x 4 x 0.100 inch plate with stiffness distribution 3.

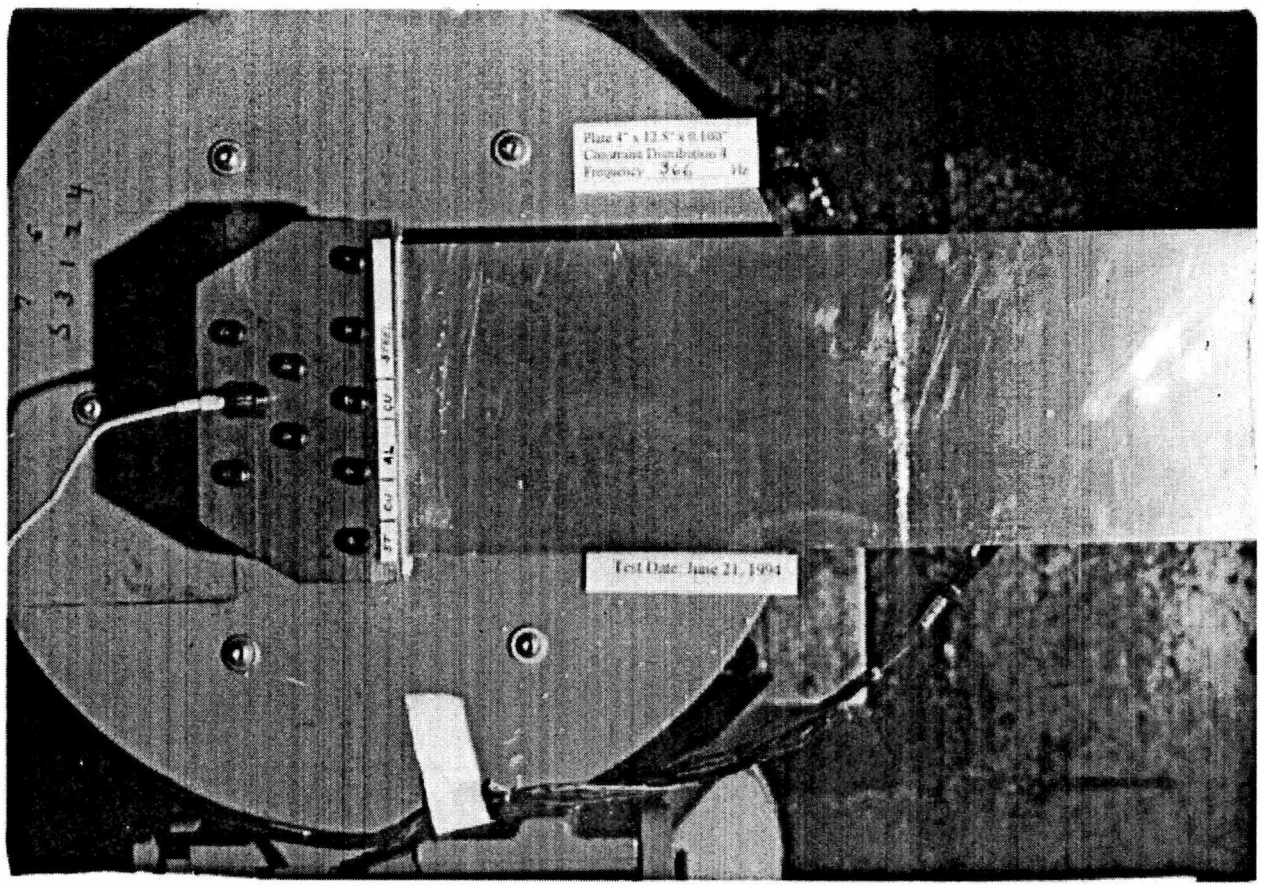


Figure A2-13. Third bending of 12.5 x 4 x 0.100 inch plate with stiffiness distribution 4.

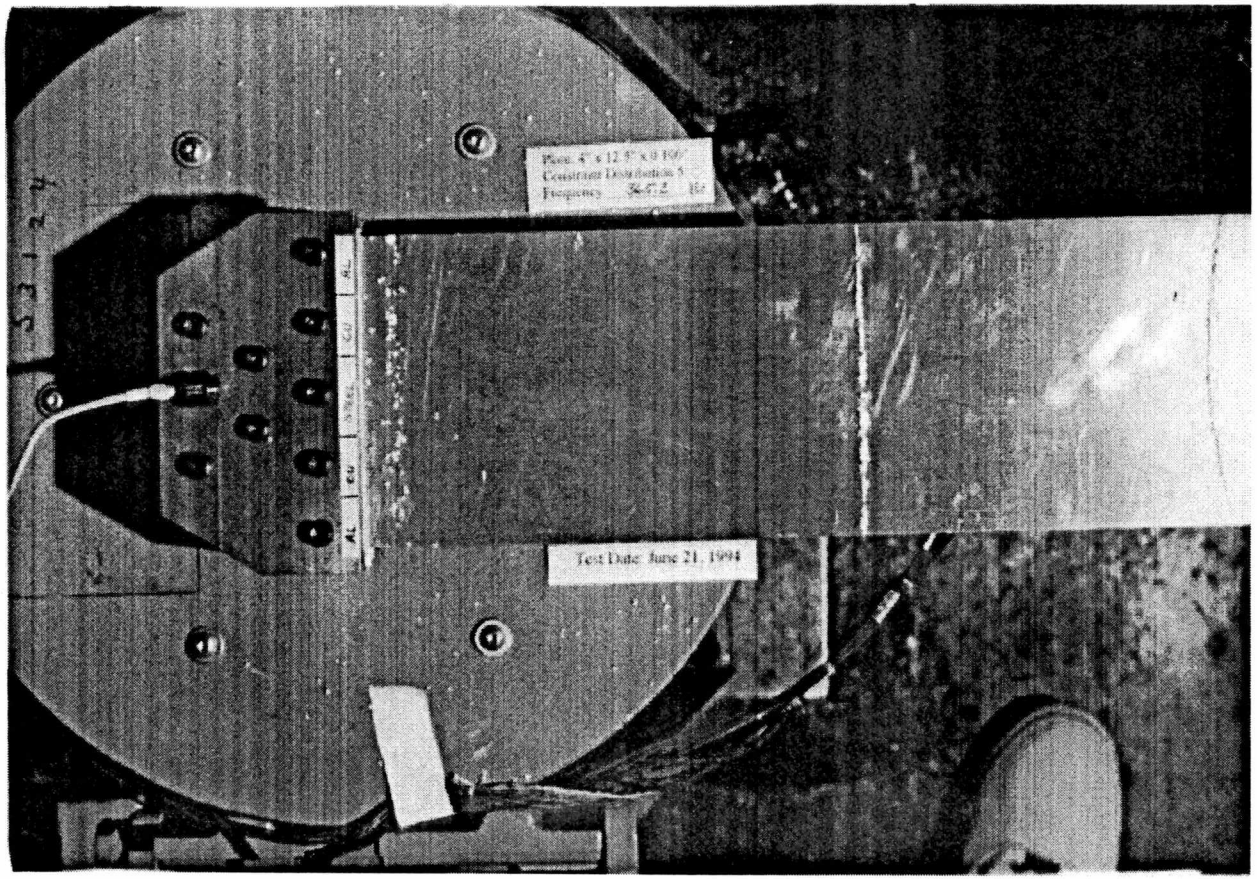


Figure A2-14. Third bending of 12.5 x 4 x 0.100 inch plate with stiffness distribution 5.

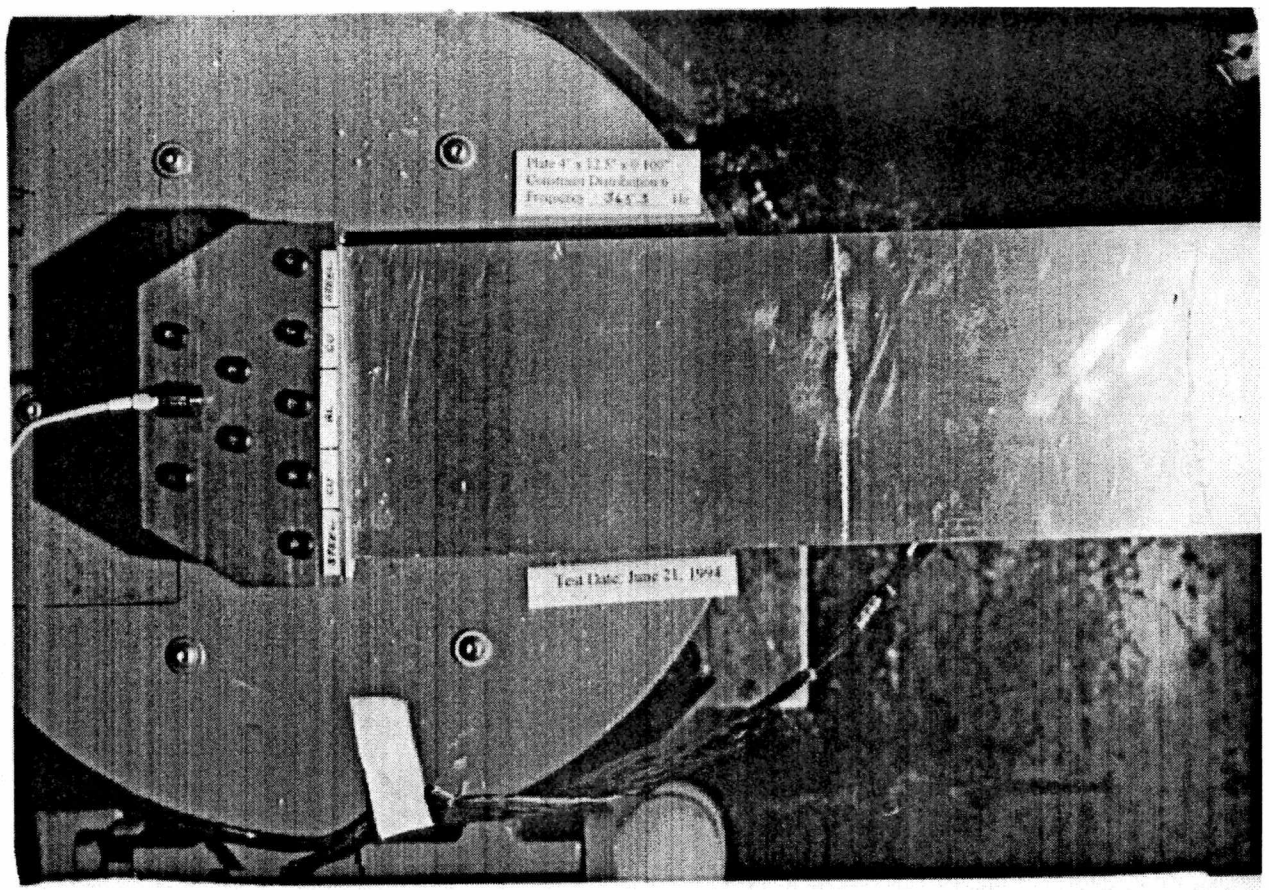


Figure A2-15. Third bending of 12.5 x 4 x 0.100 inch plate with stiffness distribution 6.

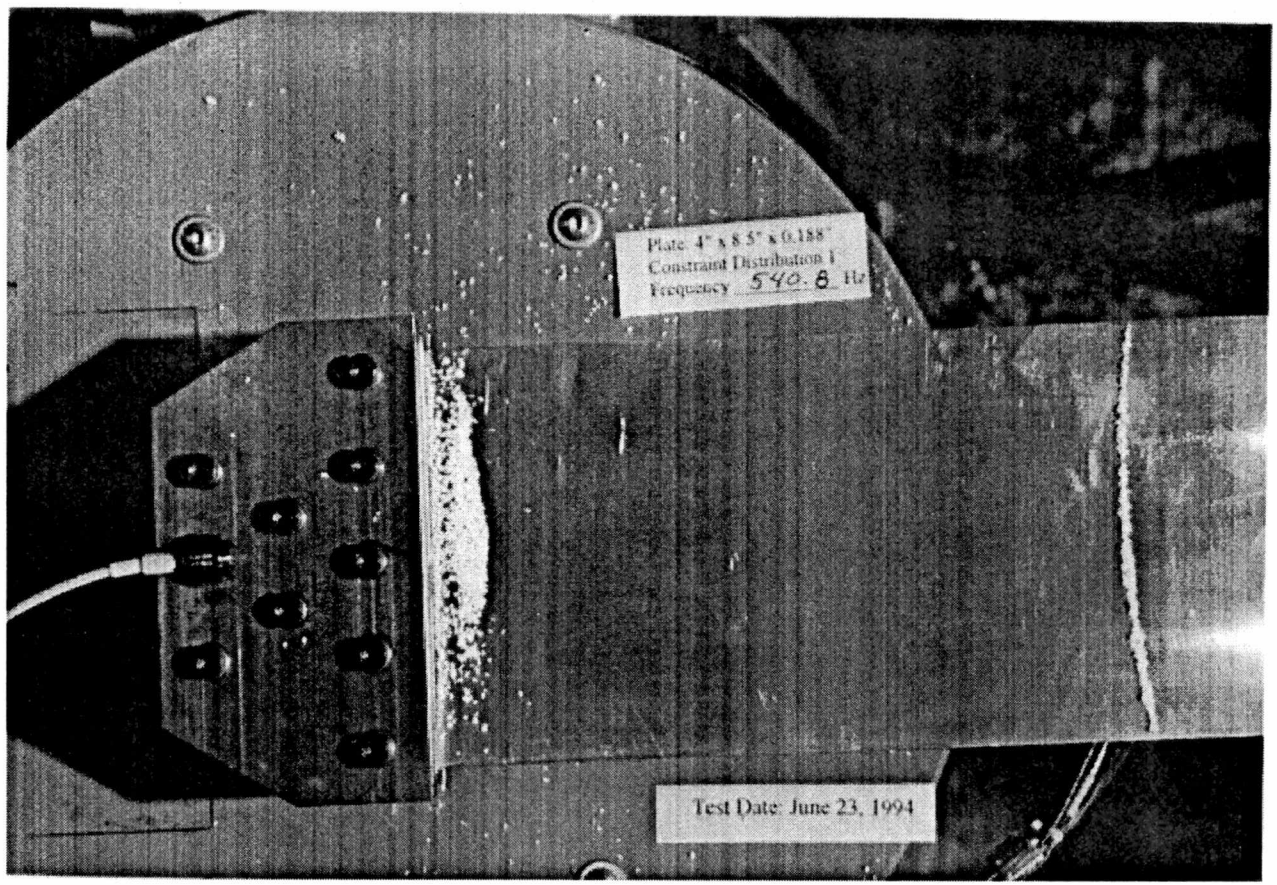


Figure A2-16. Second bending of 8.5 x 4 x 0.188 inch plate with stiffness distribution 1.

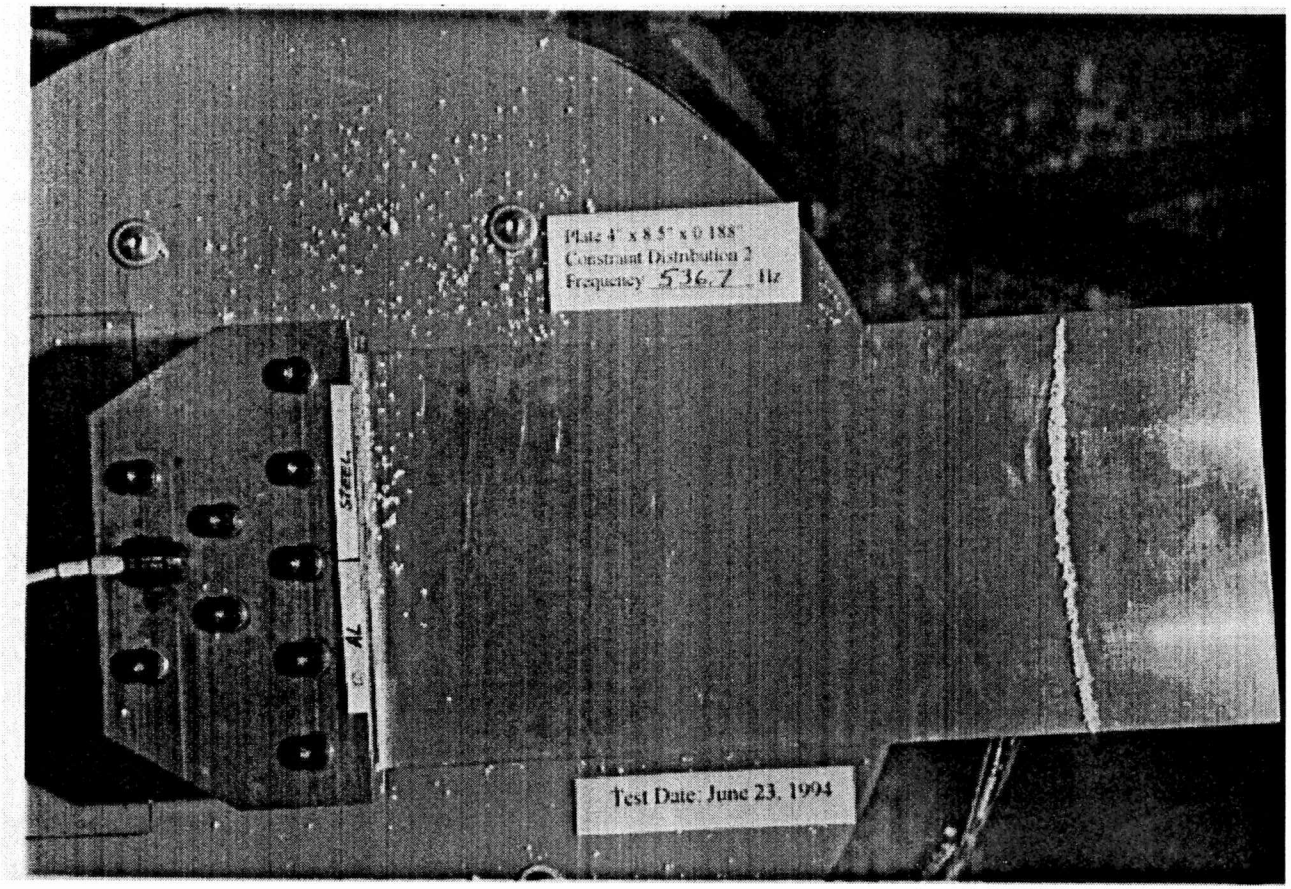


Figure A2-17. Second bending of 8.5 x 4 x 0.188 inch plate with stiffness distribution 2.

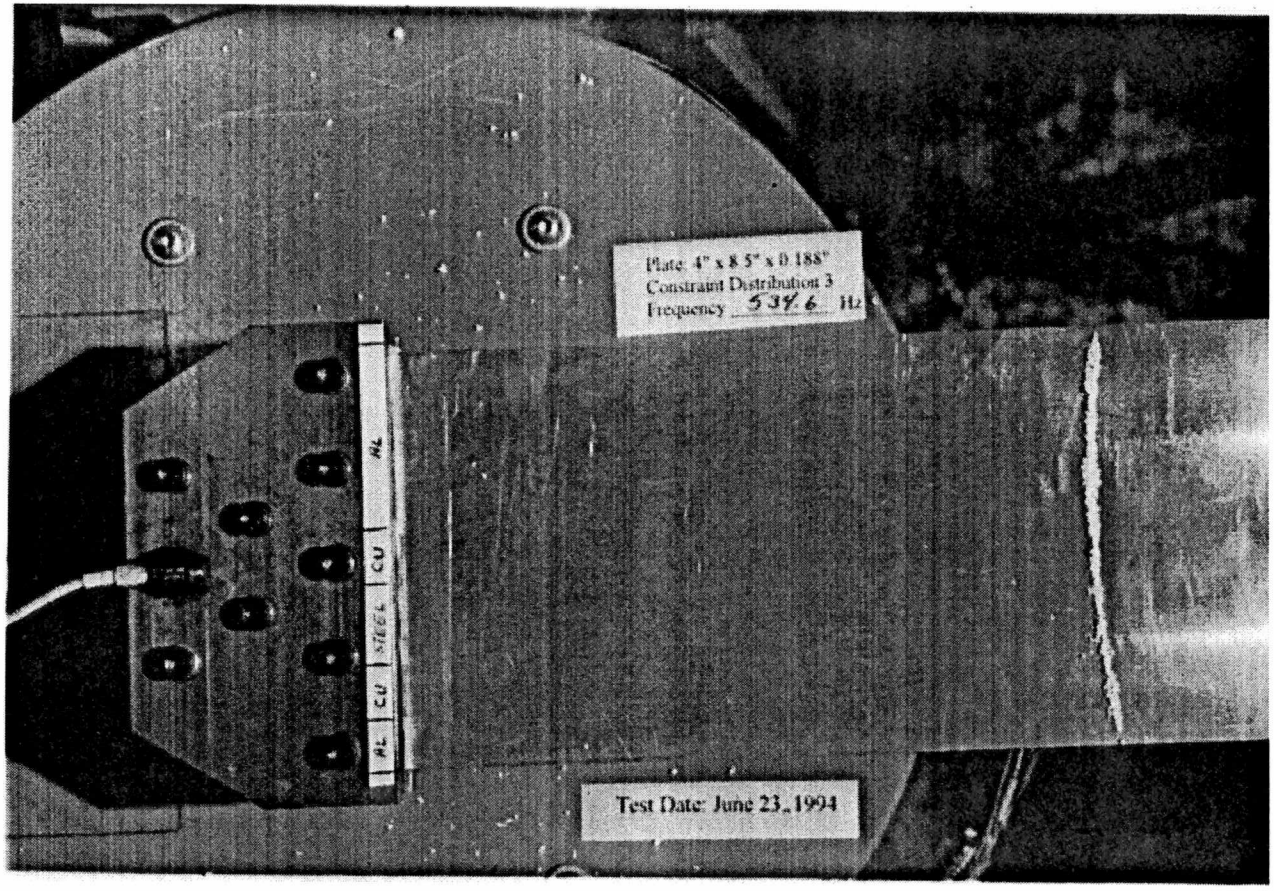


Figure A2-18. Second bending of 8.5 x 4 x 0.188 inch plate with stiffness distribution 3.

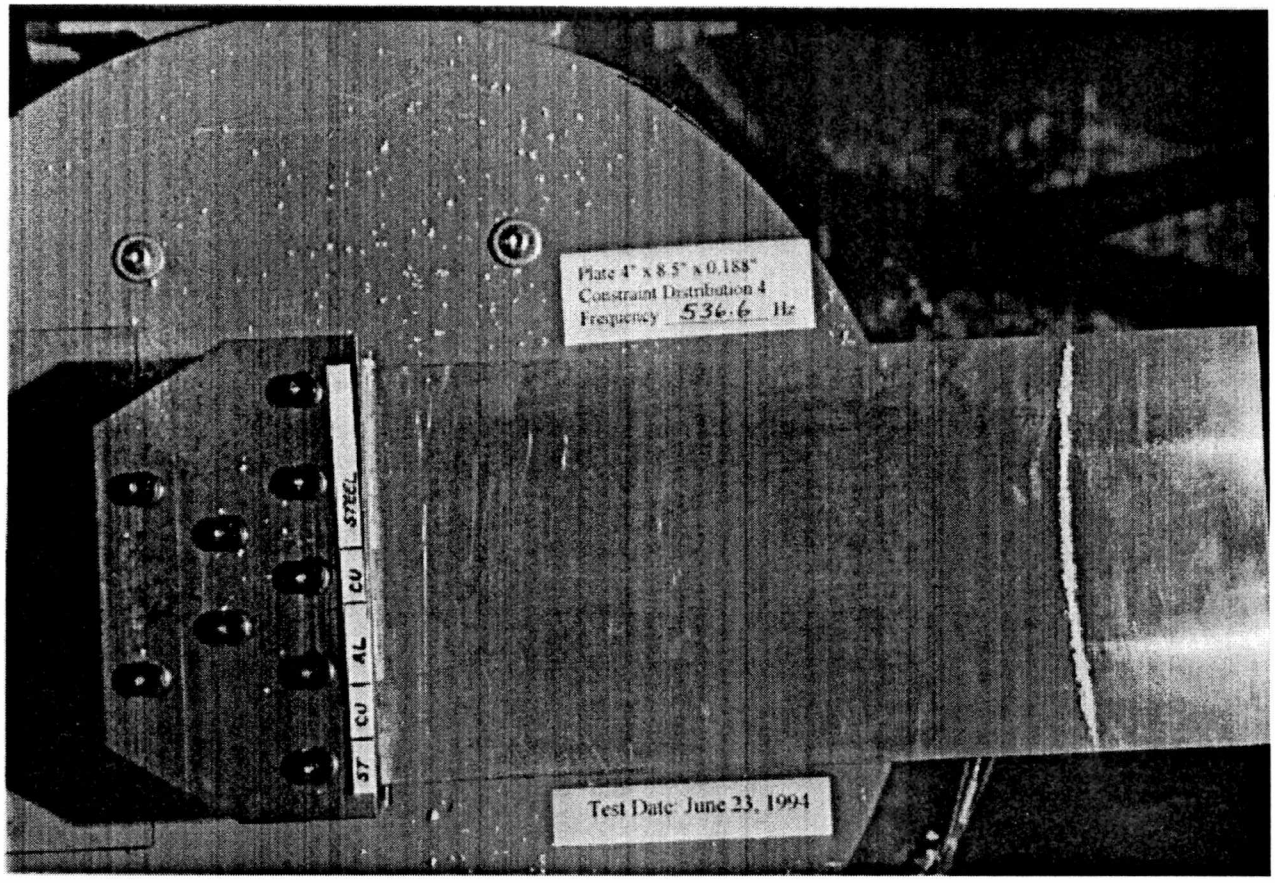


Figure A2-19. Second bending of 8.5 x 4 x 0.188 inch plate with stiffness distribution 4.

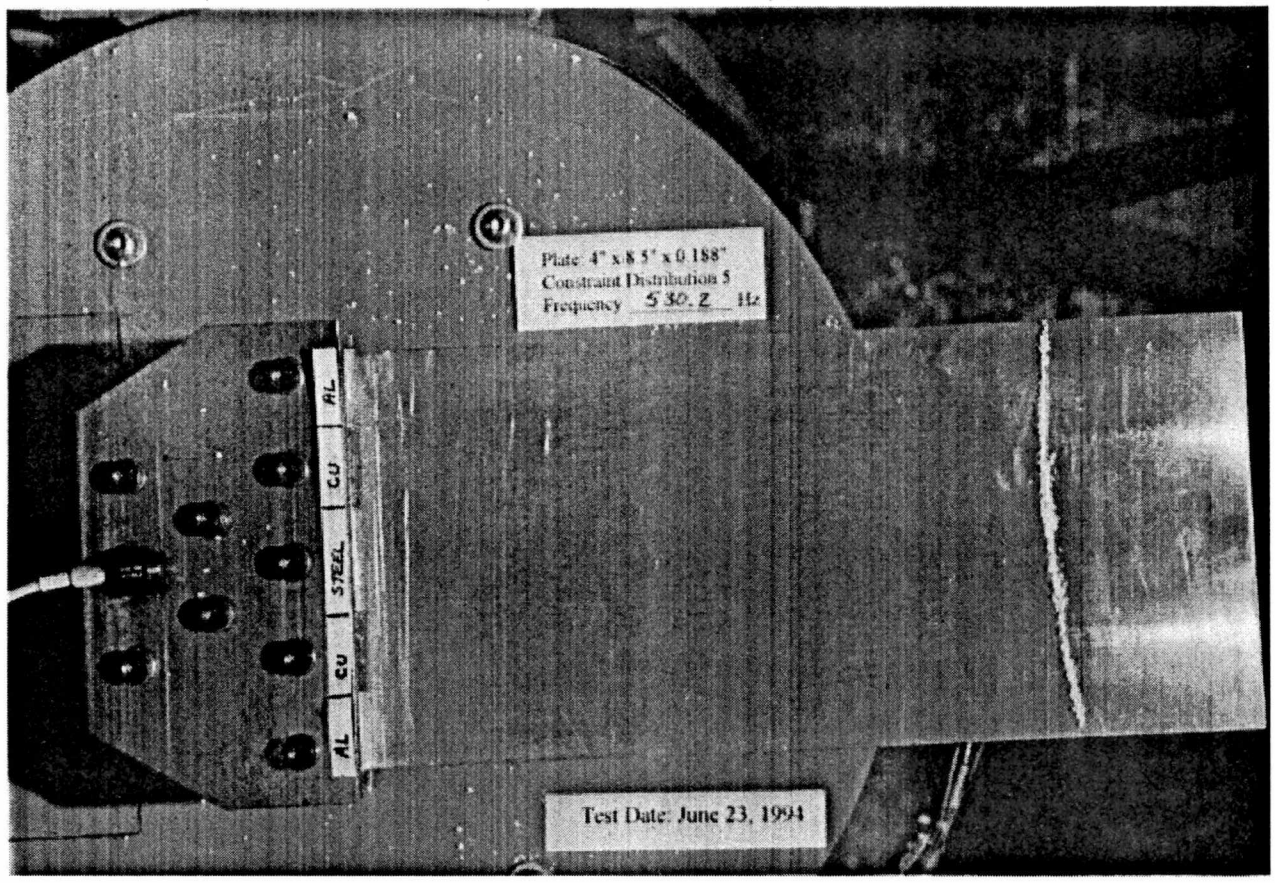


Figure A2-20. Second bending of 8.5 x 4 x 0.188 inch plate with stiffness distribution 5.

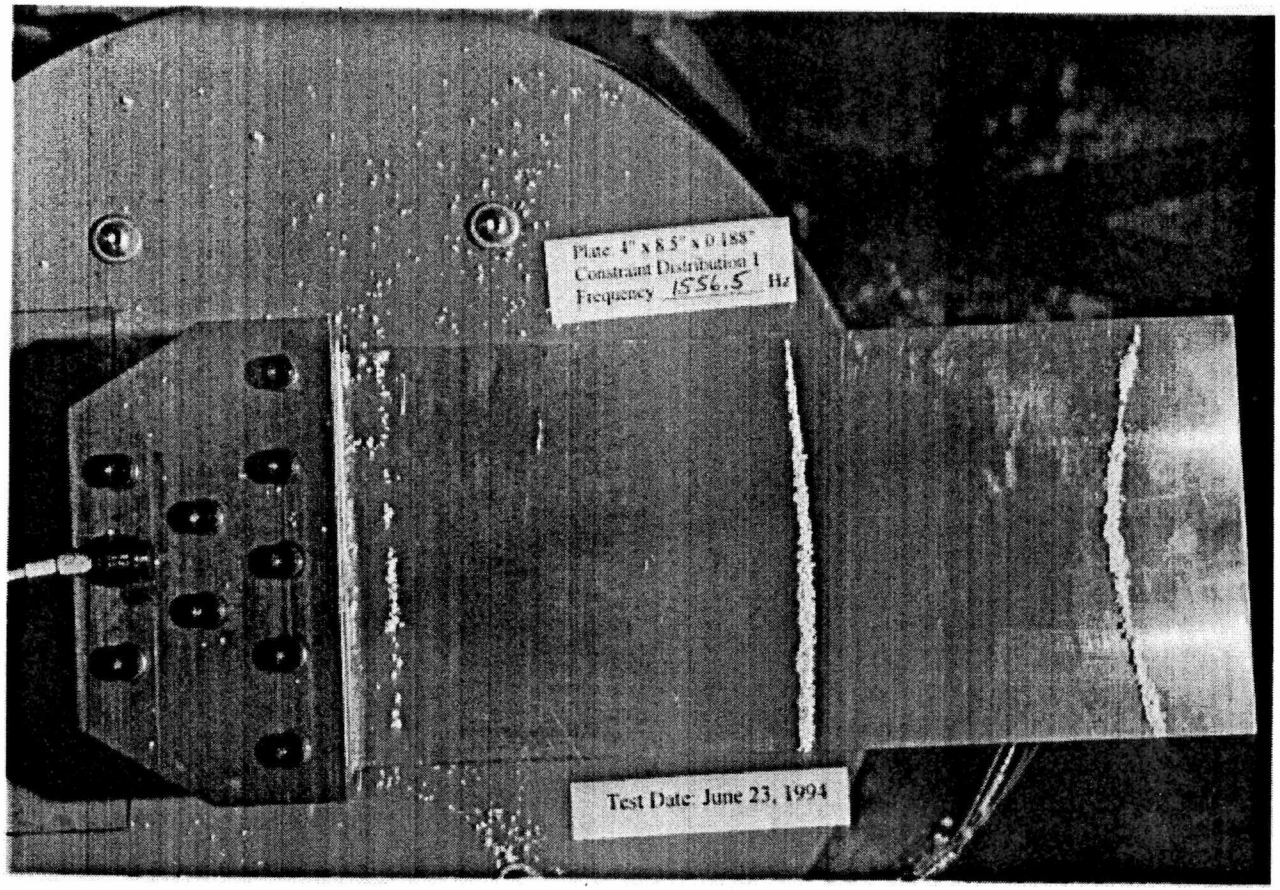


Figure A2-21. Third bending of 8.5 x 4 x 0.188 inch plate with stiffness distribution 1.

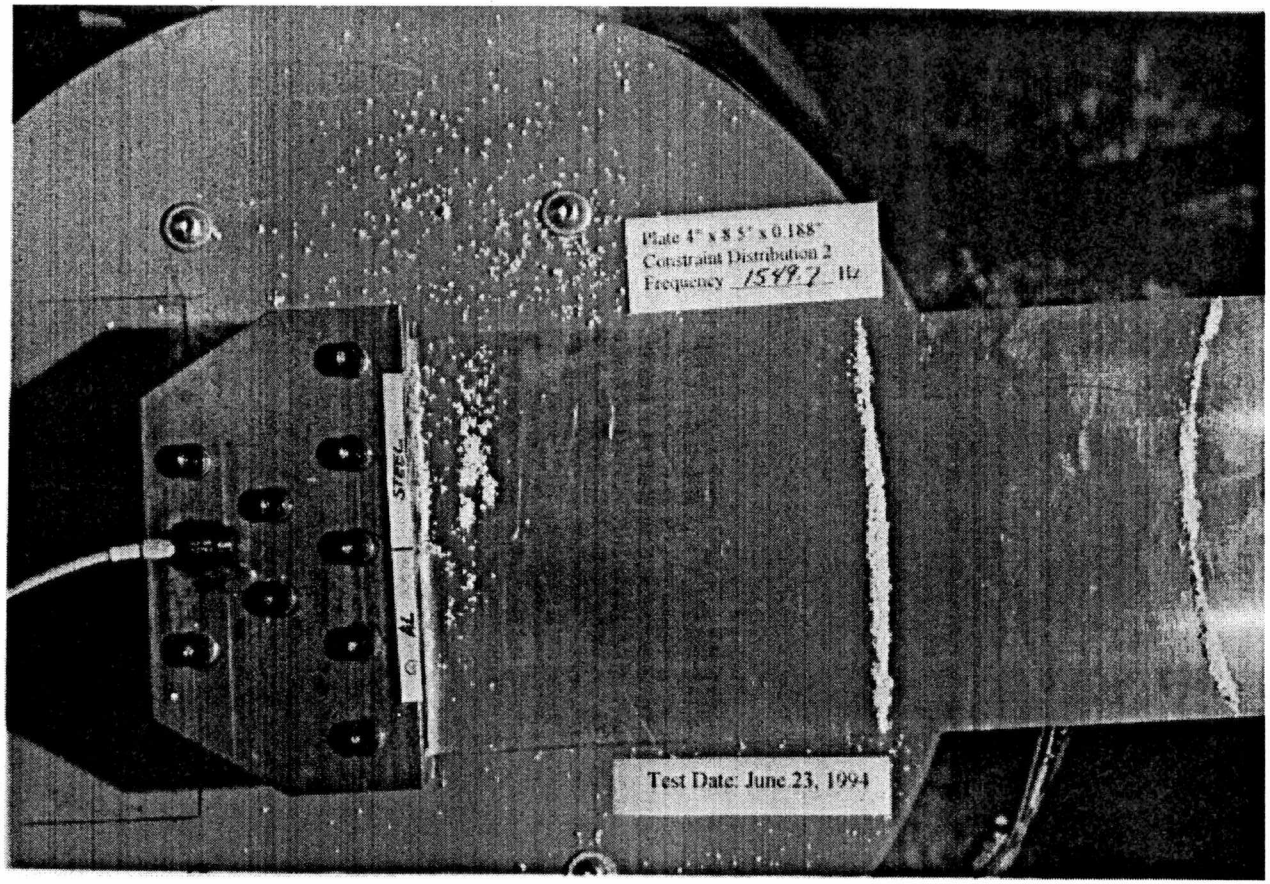


Figure A2-22. Third bending of 8.5 x 4 x 0.188 inch plate with stiffness distribution 2.

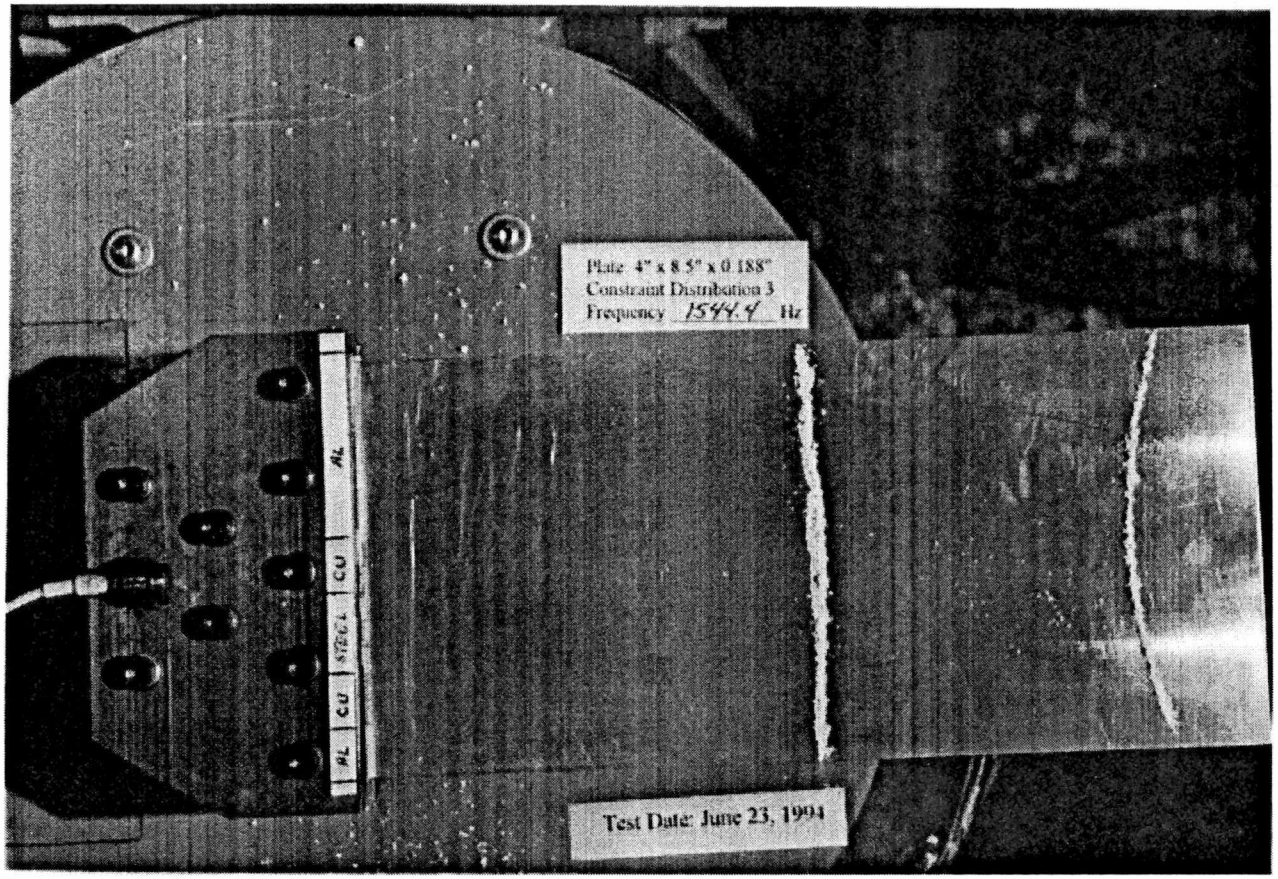


Figure A2-23. Third bending of 8.5 x 4 x 0.188 inch plate with stiffness distribution 3.

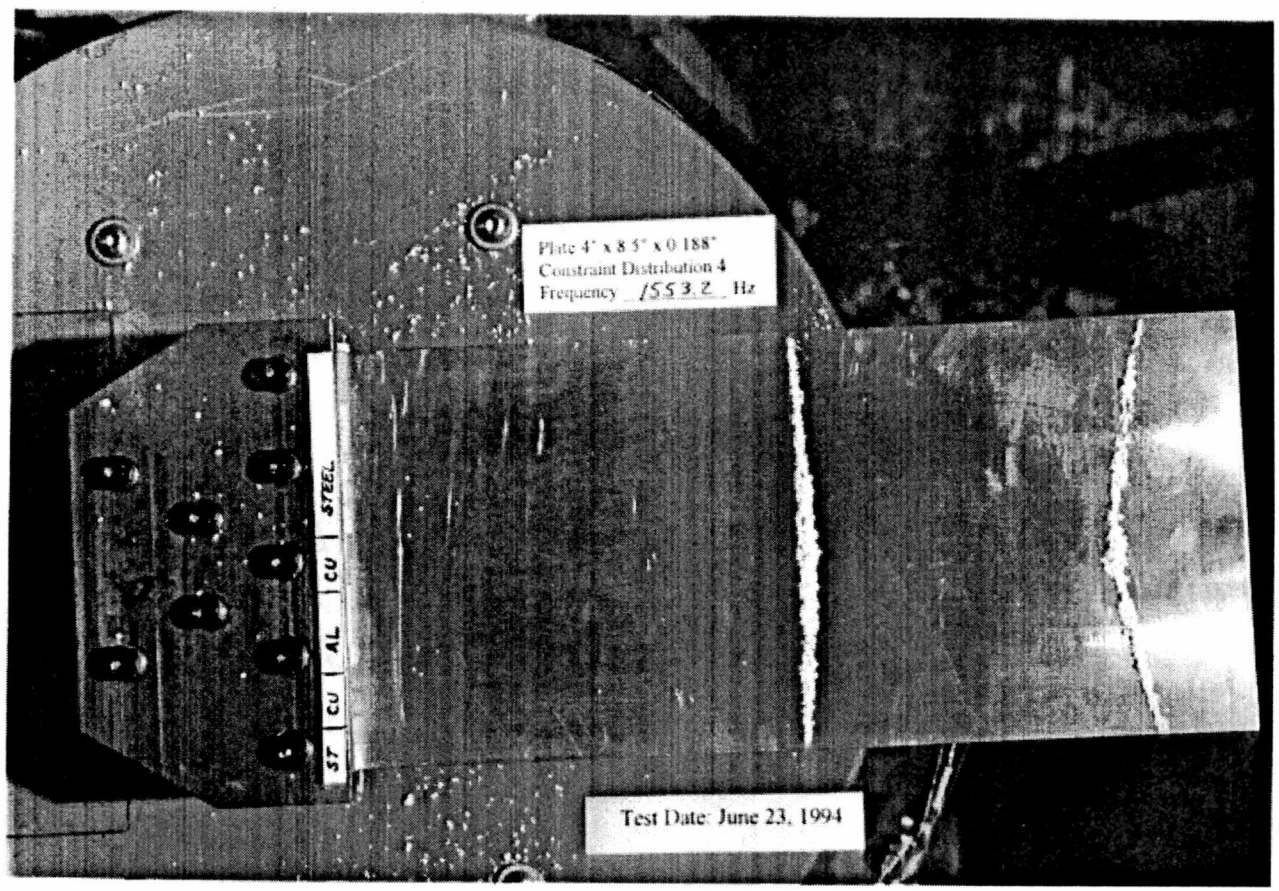


Figure A2-24. Third bending of 8.5 x 4 x 0.188 inch plate with stiffness distribution 4.

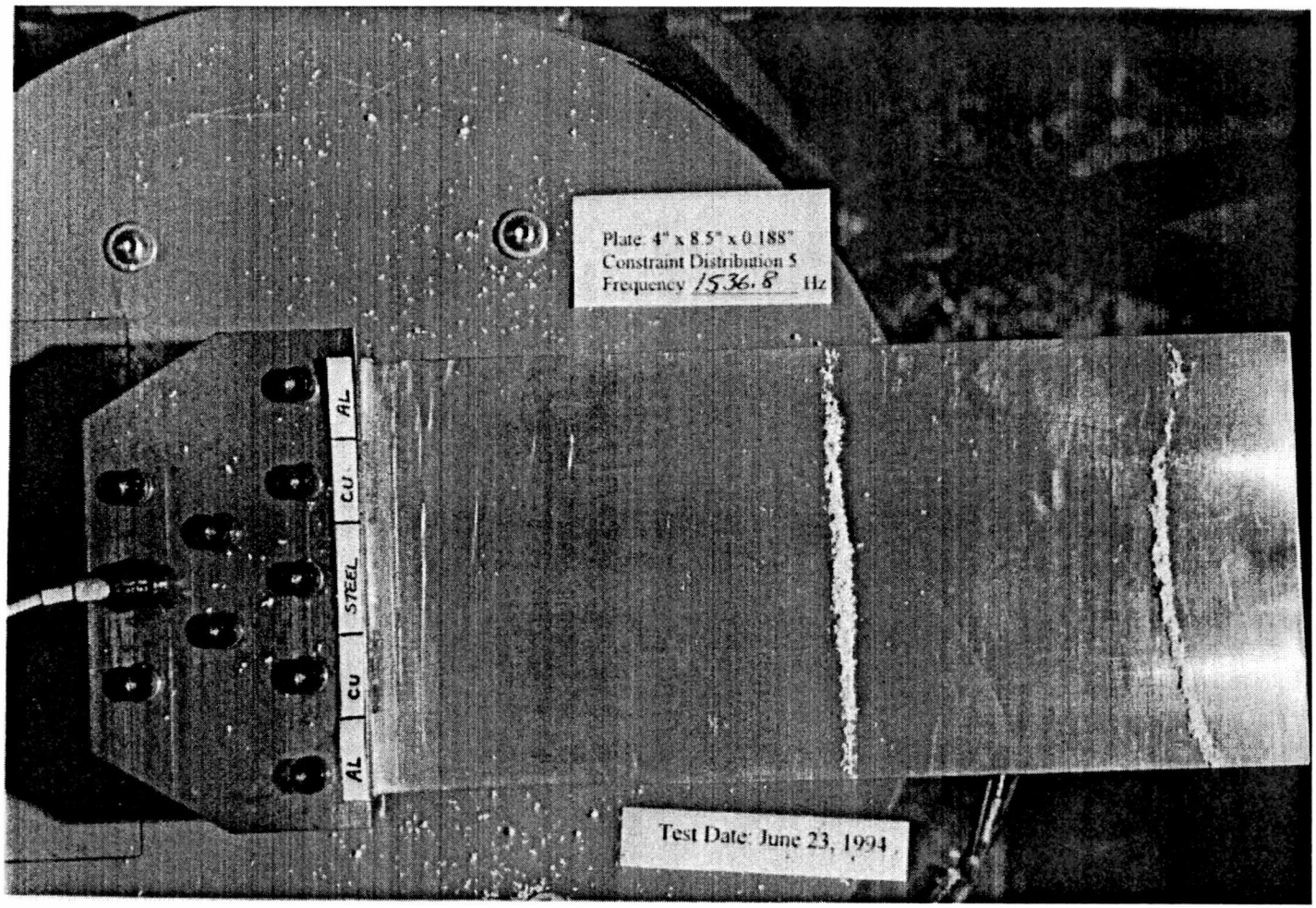


Figure A2-25. Third bending of 8.5 x 4 x 0.188 inch plate with stiffness distribution 5.

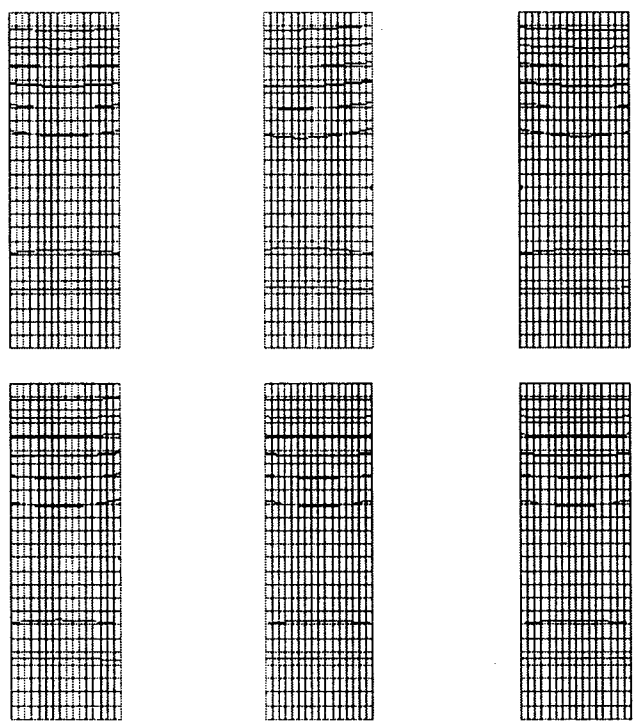
APPENDIX 3

Plate: 12.5" x 4" x 0.100"
Second Bending Mode

Constraint Distribution 1
Frequency 125.55 Hz

Constraint Distribution 2
Frequency 125.42 Hz

Constraint Distribution 3
Frequency 125.35 Hz



Constraint Distribution 4
Frequency 125.45 Hz

Constraint Distribution 5
Frequency 125.39 Hz

Constraint Distribution 6
Frequency 125.41 Hz

Figure A3-1. Analytical second bending mode shapes of 12.5 x 4 x 0.100 inch plate.

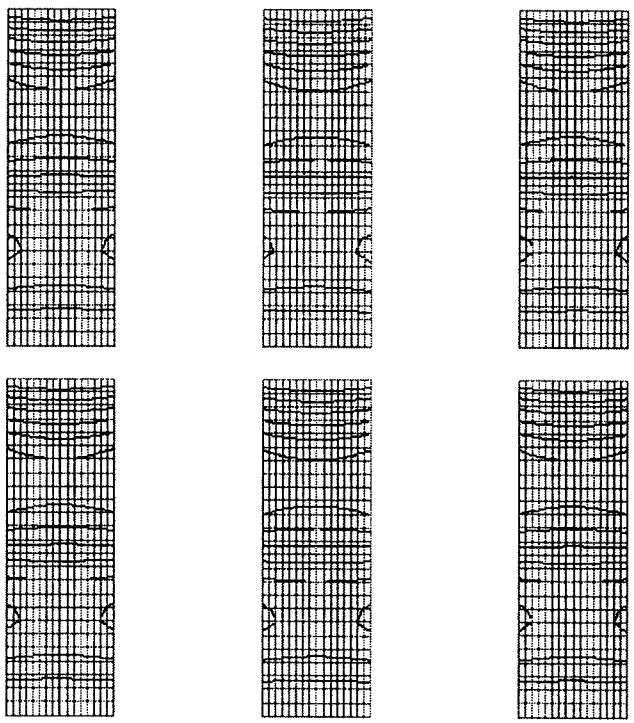
Plate: 12.5" x 4" x 0.100"

Third Bending Mode

Constraint Distribution 1
Frequency 352.96 Hz

Constraint Distribution 2
Frequency 352.59 Hz

Constraint Distribution 3
Frequency 352.38 Hz



Constraint Distribution 4
Frequency 352.71 Hz

Constraint Distribution 5
Frequency 352.48 Hz

Constraint Distribution 6
Frequency 352.60 Hz

Figure A3-2. Analytical third bending mode shapes of 12.5 x 4 x 0.100 inch plate.

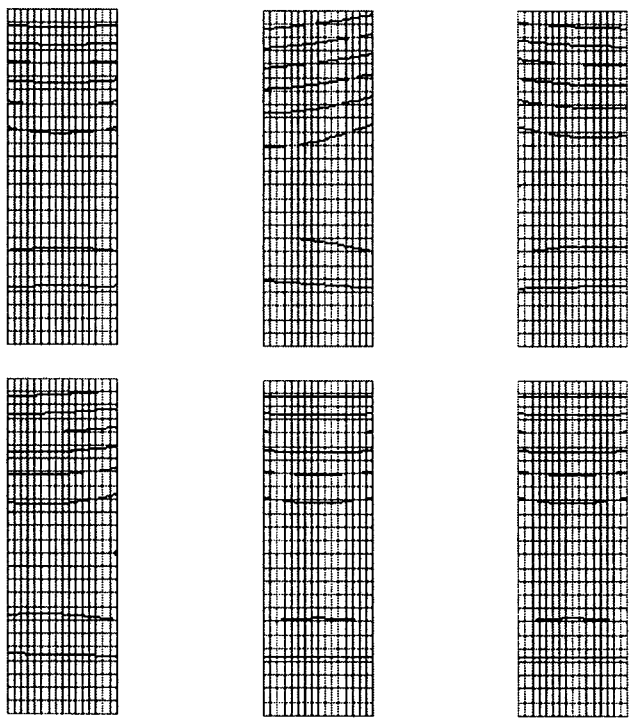
Plate: 12.5" x 4" x 0.188"

Second Bending Mode

Constraint Distribution 1
Frequency 233.78 Hz

Constraint Distribution 2
Frequency 233.08 Hz

Constraint Distribution 3
Frequency 232.84 Hz



Constraint Distribution 4
Frequency 233.33 Hz

Constraint Distribution 5
Frequency 233.02 Hz

Constraint Distribution 6
Frequency 233.14 Hz

Figure A3-3. Analytical second bending mode shapes of 12.5 x 4 x 0.188 inch plate.

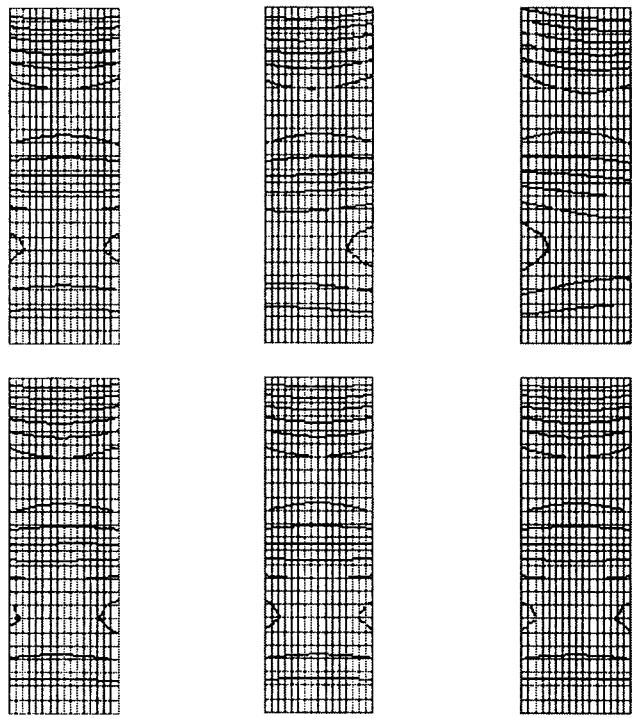
Plate: 12.5" x 4" x 0.188"

Third Bending Mode

Constraint Distribution 1
Frequency 655.91 Hz

Constraint Distribution 2
Frequency 653.55 Hz

Constraint Distribution 3
Frequency 652.69 Hz



Constraint Distribution 4
Frequency 654.69 Hz

Constraint Distribution 5
Frequency 653.67 Hz

Constraint Distribution 6
Frequency 654.22 Hz

Figure A3-4. Analytical third bending mode shapes of 12.5 x 4 x 0.188 inch plate.

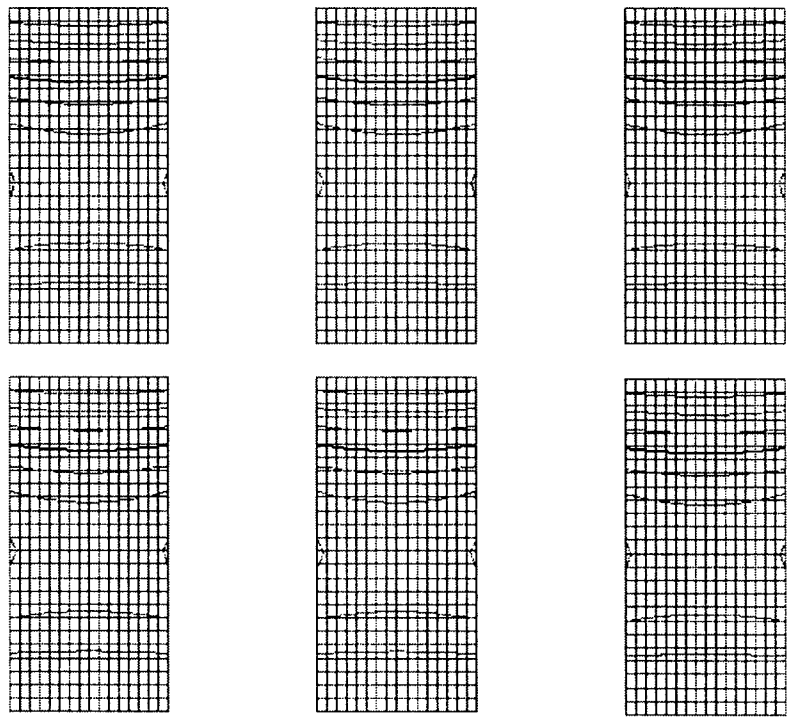
Plate: 8.5" x 4" x 0.100"

Second Bending Mode

Constraint Distribution 1
Frequency 271.45 Hz

Constraint Distribution 2
Frequency 271.05 Hz

Constraint Distribution 3
Frequency 270.81 Hz



Constraint Distribution 4
Frequency 271.17 Hz

Constraint Distribution 5
Frequency 270.92 Hz

Constraint Distribution 6
Frequency 271.05 Hz

Figure A3-5. Analytical second bending mode shapes of 8.5 x 4 x 0.100 inch plate.

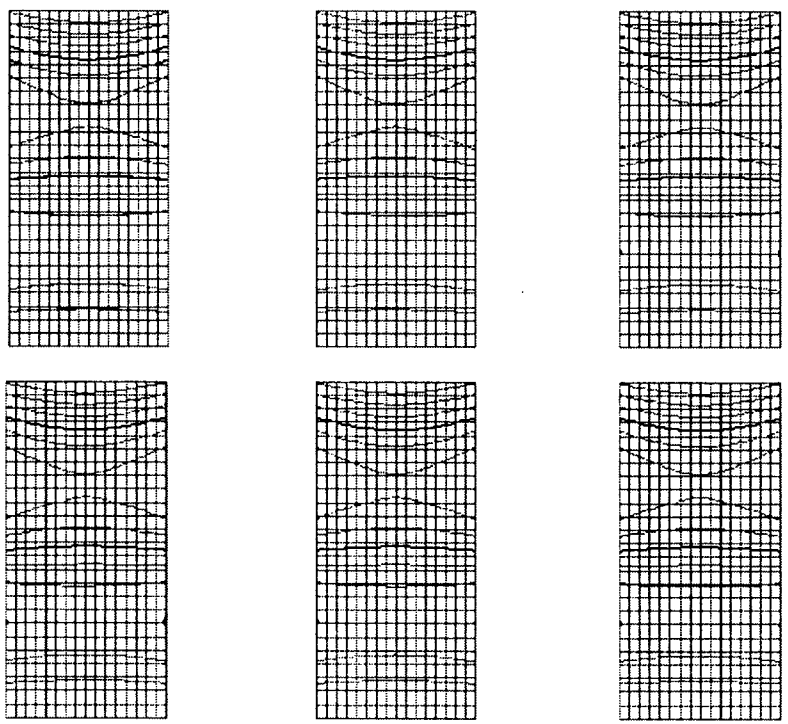
Plate: 8.5" x 4" x 0.100"

Third Bending Mode

Constraint Distribution 1
Frequency 762.05 Hz

Constraint Distribution 2
Frequency 760.91 Hz

Constraint Distribution 3
Frequency 760.22 Hz



Constraint Distribution 4
Frequency 761.29 Hz

Constraint Distribution 5
Frequency 760.51 Hz

Constraint Distribution 6
Frequency 760.97 Hz

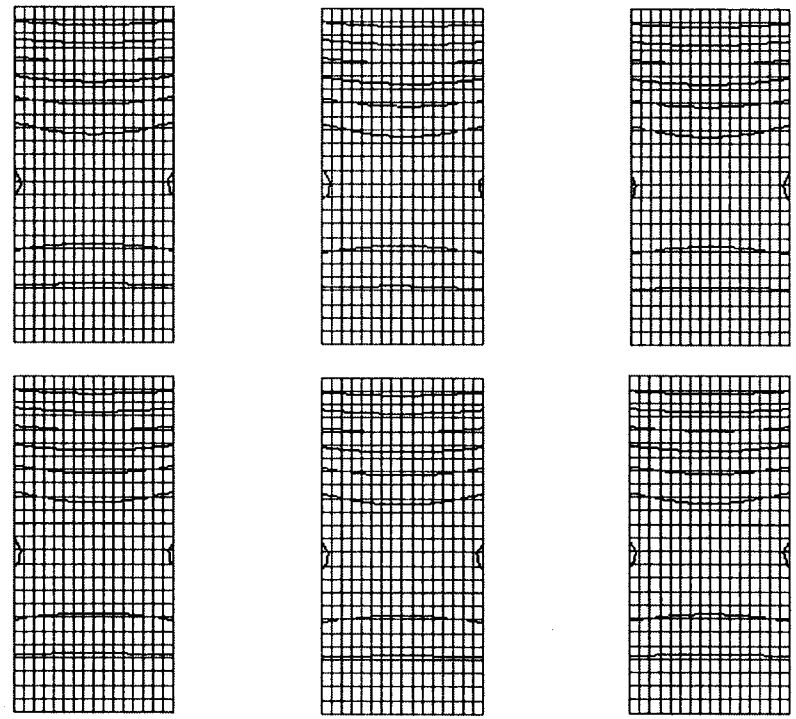
Figure A3-6. Analytical third bending mode shapes of 8.5 x 4 x 0.100 inch plate.

Plate: 8.5" x 4" x 0.188"
Second Bending Mode

Constraint Distribution 1
Frequency 502.81 Hz

Constraint Distribution 2
Frequency 500.72 Hz

Constraint Distribution 3
Frequency 499.85 Hz



Constraint Distribution 4
Frequency 501.49 Hz

Constraint Distribution 5
Frequency 500.4 Hz

Constraint Distribution 6
Frequency 500.93 Hz

Figure A3-7. Analytical second bending mode shapes of 8.5 x 4 x 0.188 inch plate.

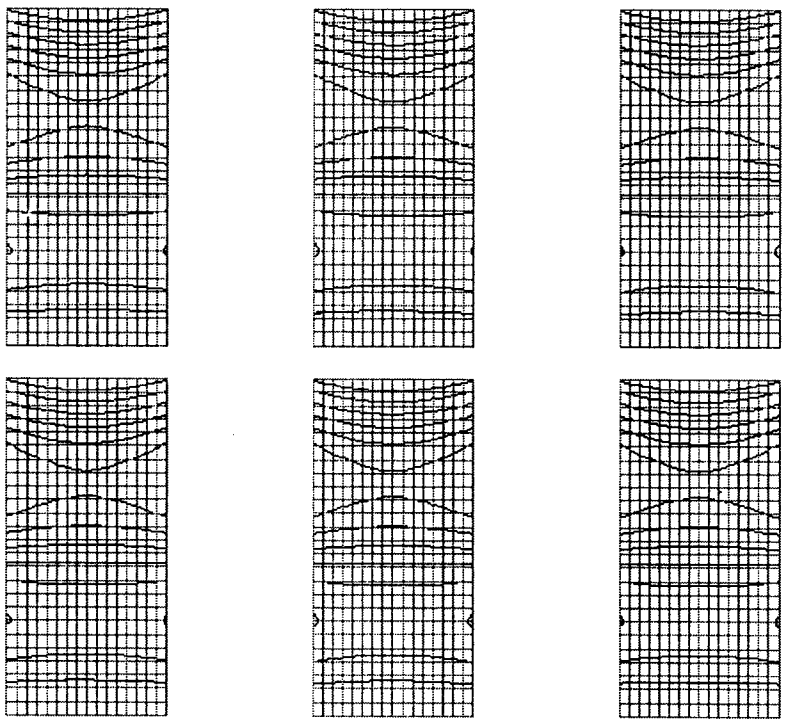
Plate: 8.5" x 4" x 0.188"

Third Bending Mode

Constraint Distribution 1
Frequency 1405.78 Hz

Constraint Distribution 2
Frequency 1400.30 Hz

Constraint Distribution 3
Frequency 1397.40 Hz



Constraint Distribution 4
Frequency 1402.30 Hz

Constraint Distribution 5
Frequency 1398.70 Hz

Constraint Distribution 6
Frequency 1400.70 Hz

Figure A3-8. Analytical third bending mode shapes of 8.5 x 4 x 0.188 inch plate.

VITA

Kurt Lancaster Nichol was born in Jacksonville, North Carolina, on January 30, 1961. He attended elementary school in Colonie, New York and was graduated from H.E. McCracken High School in Bluffton, South Carolina in 1979. The following August, he entered Embry-Riddle Aeronautical University in Daytona Beach, Florida, and in May 1983 he received a Bachelor of Science degree in aeronautical engineering.

After graduation, he began employment with Pratt & Whitney Aircraft, a division of United Technologies, in West Palm Beach, Florida as a turbine engine structural analyst. While employed there he received two United States Patents for inventions in the field of turbine engine rotor dynamics. In August 1987, he began employment with Sverdrup Technology, Inc., at the Arnold Engineering Development Center near Tullahoma, Tennessee. That same year he began graduate studies at the University of Tennessee Space Institute and was awarded a Master of Science degree in mechanical engineering in May, 1991. He continued his studies there and, in December 1995, was awarded a Doctor of Philosophy degree in engineering science and mechanics.

Kurt Nichol has been officially recognized by the AIAA, the United States Air Force, Sverdrup Technology, and United Technologies for significant contributions to the field of turbine engine structural analysis.

Kurt is steadfastly committed to the service of Jesus Christ at the First Baptist Church in Manchester, Tennessee where he serves as deacon and director of discipleship training. Kurt is married to the former Linda Lee Briggs and has one son, Samuel James.